Solar Neutrino Physics: historical evolution, present status and perspectives

Lino Miramonti†

Dipartimento di Fisica dell'Universita' di Milano and
Istituto Nazionale di Fisica Nucleare di Milano

Franco Reseghetti‡ §

Istituto Nazionale di Fisica Nucleare di Milano

Abstract. Solar neutrino physics is an exciting and difficult field of research for physicists, where astrophysics, elementary particle and nuclear physics meet.
The Sun produces the energy that life has been using on Earth for many years, about 10^9 y, emits a lot of particles: protons, electrons, ions, electromagnetic quanta... among them neutrinos play an important role allowing to us to check our knowledge on solar characteristics.
The main aim of this paper is to offer a practical overview of various aspects concerning the solar neutrino physics: after a short historical excursus, the different detection techniques and present experimental results and problems are analysed. Moreover, the status of art of solar modeling, possible solutions to the so called solar neutrino problem (SNP) and planned detectors are reviewed.

† e-mail:miramonti@mi.infn.it
‡ e-mail: reseghetti@santateresa.enea.it
§ now at ENEA-CRAM, Pozzuolo di Lerici

Contents

1. Introduction.

The Sun, "our own" star, has been shining for many years (last data, based on meteoritic age, are suggesting $\sim 4.6{\cdot}10^9$ y) so it is a fundamental question to find where the source of this energy is.
At the beginning of XIXth century it was supposed the gravitational energy was the true source of solar energy. In this case the Sun would have a very short life because the total amount of gravitational energy is $\sim 10^{41}$ J: if the presently measured solar luminosity ($L_\odot \sim 10^{26}$ W) has been constant during the Sun's life we obtain as a solar living time $\sim 10^7$ y, a value too short to allow any biological evolution. Different proposed models including chemical or other reactions gave very non-physical results (the Sun would shine for $\sim 10^4$ y).
To obtain right figures we must consider the relativistic energy of the star: in this case one finds for the Sun a life of $\approx 10^9 - 10^{10}$ y. The nuclear forces allow a right analysis of this problem but scientists knew their existence only starting from 1920.
Immediately before 1940 a realistic mechanism of energy production was suggested after the discovery of the quantum mechanical tunnel effect, the formulation of β-decay theory and the "creation" of a particle, the neutrino, invented to preserve the conservation laws. H.A.Bethe, [BET38a, BET38b, BET39], realised a model in which the solar energy is produced by thermonuclear reactions (specifically by the fusion of 4 atoms of H in He) *via* the so called p-p chain or the CNO cycle.
The confirmation of the robustness of this theory and of all its following developments was acquired only after 1968 by direct detection of solar neutrinos, $\nu_\odot$'s hereafter. At the same time an interesting problem remained: $\nu_\odot$ flux showed a deficit with respect to the predictions of the solar models (SMs). This is known as solar neutrino problem, SNP.
Up to now a robust and right answer seems to be out of our knowledge even if experimental results are suggesting a possible explanation based on new neutrino properties.
The number of articles and books concerning the Sun and $\nu_\odot$'s is huge therefore it is hard to list or select them: we underline [BAH88, BAH95, SCI96, GUE97, TUR98a, BRU99, FIO00, BAH01a, COU02] with respect to the Sun and helioseismological features while we remember [BAH89, BAH92, TUR93, BAH95, RIC96, CAS97, BAH98a, BAH01a, BAH02f] in $\nu_\odot$ sector. For a complete analyses see also [BET39, BUR57, PON67, CLA68, FOW84, ROL88, RAF96] while [CRE93] presents both theoretical and experimental aspects concerning $\nu_\odot$ physics at the beginning of 90s'. For a nice and detailed review concerning experimental aspects and perspectives in neutrino physics see also [BET01].
We do not include images and sketches concerning detectors: we refer the interested reader to the available WEB-pages of running and planned experiments that we have listed in Appendix.
In short, the organisation of this article is the following: sect. 2 shows a journey through

the evolution of knowledge on how the Sun works, on neutrinos and on $\nu_\odot$'s; the main features of SMs and of $\nu_\odot$'s production are shown in sect. 3; in sect. 4 methods to detect $\nu_\odot$'s are exposed; in sect. 5 present experimental results are reviewed; in sect. 6 solar neutrino problems are detailed while in sect. 7 proposed solutions are analysed; in sect. 8 the aim and the features of the next starting detectors are presented; in sect. 9 the characteristics of the proposed next generation of detectors are listed; sect. 10 sums up the perspectives in $\nu_\odot$ physics at the beginning of this century.
This paper was prepared just before the communication of the first experimental result from KAMLAND detector which seems to exclude all solutions to the SNP but the so called Large Mixing Angle (LMA) solution. We mention this conclusion only in section 2. We refer to the "Neutrino Unbound" WEB page, see. Appendix, for a complete list of published papers on the subjet.

2. Historical development.

A list of some steps of the knowledge on solar characteristics and on neutrino properties follows: its main aim is to underline how difficult was the evolution toward a model well reproducing phenomena related to the Sun, which is the nearest star.

- In the 1840's, Mayer and Waterson suggested the conversion of gravitational energy into heat as a probable source of solar radiation.
- In 1854, von Helmholtz, [HEL56], officially proposed the gravitational contraction of a mass as the origin of the energy emitted by the Sun.
- In 1859, C.Darwin ,[DAR59], made an estimation of the age of the Earth by erosion of some valley and the evolution of biological species: $3{\cdot}10^8$ y.
- Kelvin supposed that the impact of meteors on solar surface was the true mechanism of energy production; in 1862 he estimated the Sun is not older than $2{\cdot}10^7$ y and ruled out a chemical solution to this problem ($\approx 10^4$ y is the allowed age), [KEL62]. Kelvin also calculated the lifetime of an object as massive as our Sun and with the same radius which radiates the same amount of energy produced by gravitational contraction: he found $\approx 10^7$ y.
- In this period, the theoretical physicists were not able to find processes other than the previous ones so that there was a big challenge to reconcile the physically estimated value ($\approx 10^7$ y) and the biologists and geologists which proposed $\approx 10^8$ y.
- In 1899, E.Rutherford experimentally discovered the β-decay.
- In 1903, P.Curie and Laborde discovered the radium salt to be an emitter of heat constant in time without its cooling down to the surrounding medium temperature. G.Darwin and Wilson immediately proposed the radioactivity as a probable solar energy source.
- In 1904, E.Rutherford, not much time after the discovery of the emitted α particle energy, strengthened that hypothesis but no astronomical observational

data indicated an abundance of radioactive elements in the Sun as high as required to reproduce the present $L_\odot$. Furthermore the rate of radioactive emission is independent from stellar temperature but the experimental data showed the opposite behaviour.

- In 1905, A.Einstein, [EIN05], presented his theory of special relativity and the famous equation $E = mc^2$ which allows a conversion of mass in energy and *viceversa*.
- In 1911-12, O.Von Bayer, O.Hahn and L.Meitner, [BAY11a, BAY11b, BAY12], measured the spectrum of electron emitted in β radioactivity and found it to be discrete.
- In 1914, J.Chadwick, [CHA14], from experimental measurements on Radium E, deduced the electron energy spectrum to be continuous. This was an unexpected result because α and γ radioactivities showed mono-energetic particles. It was even proposed an emission of more than one electron in each decay.
- In 1919, H.N.Russell, [RUS19], supposed that the physical process which allows the Sun to shine is strictly related to T_c, the temperature of the core of the star, and it yields a substantial stability over long periods of time.
- In 1920, F.W.Aston, [AST20], measured the mass of a lot of elements; in addition he discovered that "*..an α particle (a He nucleus) is lighter than 4 protons*". Then, A.S.Eddington, [EDD20a, EDD20b], suggested that the Sun could shine by transforming protons in helium; the mass difference should be converted in energy. At this point he estimated Sun lifetime: $\approx 10^{11}$ y.
- In 1927, C.D.Ellis and W.A.Wooster, [ELL27], by a calorimetric measurement, deduced the mean value of energy liberated in β-decay of radium-E: 350 $\pm$ 40 keV; this result was confirmed in 1930 by L.Meitner: 337 $\pm$ 20 keV, [MEI30]. Moreover, no γ emission was detected. A problem arose: the maximum energy for that spectrum was 1.05 MeV and the electron showed a continuum energy spectrum. To solve this problem N.Bohr suggested that in microphysics the energy is conserved only at statistical level; he also supposed this process as a possible source of energy emitted in stars.
- In 1928, G.Gamow, [GAM28], discovered that two nuclei interact with a non-zero probability; he introduced the so called "Gamow factor" for a technical description of this process which is allowed only by quantum wave mechanics.
- In 1929, Atkinson and Houtermans, [ATK29], gave a first estimation of the nuclear reactions rate that the temperature in the stellar core allows.
- In 1930, W.Pauli, [PAU30], as a "*desperate expedient for saving the WECHSELSATZ of statistics and energy conservation*" in β-decays in which electrons are emitted, invented a neutral particles, having spin 1/2, obeying the exclusion principle, with a mass much lower than the proton mass. Then, He supposed such a particle to be always confined inside a nucleus.

- In 1932, J.Chadwick discovered the neutron, a neutral nuclear particle having a proton-like mass.
- In 1933, F.Perrin, [PER33], supposed both the momenta of the electron and the Pauli's particle to be equal and deduced a mass much lower than the electron one, the null value also included; he thought this particle as a photon with half-integer spin. In 1933-34 E.Fermi, [FER33, FER34a, FER34b], included this particle, which he re-called "neutrino", in his β-decay theory. The electron energy spectrum is strongly neutrino-mass dependent and from the radium E spectrum he suggested for ν mass a value much lower than the electron mass. The sensitivity to ν mass in the β-decay arises clearly because the larger m_ν the less available kinetic energy remains for the decay products, and hence the maximum electron energy is reduced. Pauli changed his opinion about the localisation of the neutrino.
- In 1934, H.A.Bethe and R.Peierls, [BET34], using the Fermi weak-interaction Hamiltonian and the Fermi coupling G_F, as estimated from radioactive elements, computed the cross-section for the inverse β-decay: $\sigma \sim 2.3 \cdot 10^{-44}\, cm^2\, (\frac{p_e E_e}{m_e^2})$. This result astonished both the authors which concluded "*..This meant that one obviously would never be able to see a neutrino.*"
  As a comment if one calculates the mean free path in water for a 1-2 MeV neutrino, a typical energy when a neutrino is emitted in a β-decay process, the result is $\lambda = \frac{1}{n\sigma} \sim 2.5 \cdot 10^{18}$ m, a "swimming-pool" as long as the thickness of the Galactic disc.
- In 1936, G.Gamow and E.Teller, [GAM36], modified the Fermi Hamiltonian, where only vector currents are present, to a more general operator involving scalar, vector, axial vector, pseudoscalar and tensor currents but five different coupling constants were needed to fit the experimental data. N.Bohr changed his opinion about the energy non-conservation in β-decay process. H.Bethe wrote "*..It seems therefore probable that the neutrino does not have any magnetic moment at all...The recoil of the nucleus, which can be observed in principle, will decide definitely between the hypothesis of non-conservation of energy and the neutrino hypothesis*", [BET36].
- In 1937, E.Majorana, [MAJ37], found that for neutral particles there was "*..no more any reason to presume the existence of antiparticles*" and "*..it was possible to modify the theory of β emission, both positive and negative, so that it came always associated with the emission of a neutrino*".
- In 1938, von Weizsäcker, [WEI37, WEI38], discovered the CNO cycle, in which protons are "burned", the carbon nuclei acting as a catalyst. In 1938-39 H.A.Bethe, [BET38a, BET38b, BET39], realized a set of papers reviewing the knowledge on nuclear reactions in the stars. He also derived the basic nuclear process in stars not greater than the Sun: the proton-proton reaction chain, p-p. The deduced $L_\odot$ and other parameters were in agreement with the observational data available at that time. L.Alvarez firstly detected electronic captures, [ALV38]: he showed that β-emissions and electrons are the same particles.

- In 1939, H.R.Crane made the first radiochemical experiment by measuring ^{35}Cl $\rightarrow^{35}$S: he detected no signal and deduced an upper limit on cross-section, [CRA39a]. H.R.Crane and J.Halpern, [CRA39b], found an experimental qualitative evidence of the emission of a third particle in β-decay.
- In 1942-46, S.Sakata and K.Inoue, [SAK42, SAK46], proposed the so called "two meson theory" which claims the existence of another pair of leptons.
- In 1946, B.Pontecorvo, [PON46], suggested Cl or Br as useful chemical elements to detect neutrino; he also wrote "*.. direct proof of the existence of the neutrino...must be based on experiments, the interpretation of which does not require the law of the conservation of energy, i.e. an experiment in which some characteristic process produced by free neutrinos...is observed*".
- In 1948, H.R.Crane proposed different physical processes to experimentally detect ν's, [CRA48]:
  (i) electromagnetic interaction by magnetic moment
  (ii) inverse reaction of electron capture
  (iii) (in present terms) coherent diffusion by neutral current interaction
  (iv) nuclear excitation followed by γ emission or fission
  (v) mesons production at energies as high as cosmic rays have
- In 1949, L.Alvarez, [ALV49], presented a list of background reactions, the main experimental challenge in neutrino detection.
- After the second world war, many physicists and astrophysicists developed theoretical aspects: Epstein, [EPS50], Salpeter, [SAL52, SAL54, SAL57b], Frieman and Motz, [FRI53], upgraded and completed the Bethe's work. Moreover, T.D.Lee and C.N.Yang, [LEE56], proposed the parity violation in weak interactions; as a consequence all weak interacting ν's are left-handed and $\overline{\nu}$'s are right-handed.
- In 1952-53, Langer and Moffat, [LAN52], and Hamilton *et al.*, [HAM53], gave an upper limit to ν mass by measuring the Tritium β-decay: $m_\nu \leq 250$ eV. C.L.Cowan and F.Reines, [COW53, REI53, COW56], discovered $\overline{\nu_e}$'s through the inverse β-decay using a scintillator near a nuclear reactor. In 1955 R.Davis, [DAV55], studied the feasibility of Pontecorvo's proposal by setting a tank of cleaning fluid outside a nuclear reactor.
- In 1957-58, B.Pontecorvo, [PON57, PON58], following the description given by M.Gell-Mann and A.Pais to K^0-$\overline{K^0}$ system, [GEL55], suggested that a $\overline{\nu}$ produced in a reactor could oscillate into a ν and be detected by a detector such as the Davis's one. He supposed "*..If 2-component ν theory should turn out to be incorrect, which at present seems to be rather improbable, and if conservation law of ν charge would not apply then $\nu \rightarrow \overline{\nu}$ transitions could take place in vacuo*". He also proposed to define mixed particles as $\nu = 2^{-1/2}(\nu_1 + \nu_2)$ and $\overline{\nu} = 2^{-1/2}(\nu_1 - \nu_2)$, where ν_1 and ν_2 (which are truly neutral Majorana particles) are mass eigenstates. C.S.Wu *et al.*, [WUC57], experimentally discovered the parity violation in the β-decay. L.D.Landau, T.D.Lee and C.N.Yang, A.Salam independently proposed a theory of

two-component ν, [LAN57, LEE57, SAL57a]. As a toy comment let us remember that if ν's were to look into a mirror they would be unable to see their reflected images.

- In 1958, M.Goldhaber, [GOL58], measured the ν helicity: he observed the K-electron capture in ^{152}Eu which produces ^{152}Sm* and a ν.
- In 1959 R.Davis communicated a possible detection of the reaction $\overline{\nu_e} + ^{37}Cl \rightarrow e^- + ^{37}Ar$ which is allowed only if lepton number is not conserved.
- In 1962, R.Leighton, [LEI62], analysed "solar vibrations" starting helioseismological studies. G.Danby et al., [DAN62], experimentally detected ν_μ's, the particles foreseen in the old Sakata's theory.
- In 1962-63 S.Sakata and his collaborators proposed a model including two kinds of ν's, [MAK62, NAK63a, NAK63b, OKO63]. Their main assumptions were:
  (i) ν's should be 4-component spinors in order to be the seeds of the massive baryons so that ν_1 and ν_2 should have their own masses. These are the TRUE ν's.
  (ii) ν_e and ν_μ (the WEAK ν's), which are coupled to e and μ in the weak currents, should be mixing states of ν_1 and ν_2, as many people usually think today.
- In 1963-64, a Californian astrophysicist group (Bahcall, Fowler, Iben and Sears) realised a first solar model in realistic agreement with observations, [BAH63, SEA64].
- In 1964, J.N.Bahcall and R.Davis, [BAH64, DAV64], proposed to build an underground Cl detector searching for $\nu_\odot$. The fascinating motivation they gave was "*..to see into the interior of a star and thus verify directly the hypothesis of nuclear energy generation in stars*". V.A.Kuzmin, [KUZ64, KUZ65], suggested to use the Gallium (Ga) as a target for $\nu_\odot$.
- In 1967, B.Pontecorvo, [PON67], described processes violating leptonic and muonic charge: $\nu \leftrightarrow \overline{\nu}$ and $\nu_e \leftrightarrow \overline{\nu_\mu}$.
- In 1968, the first experimental results from Homestake detector showed a deficit in $\nu_\odot$ flux: the value was at a level of 1/3 of the expected one, [DAV68]. This was the first SNP.
- In 1969, V.Gribov and B.Pontecorvo gave a good formulation of ν flavour oscillation in vacuum [GRI69].
- In the 70s', a lot of theoretical and experimental discoveries highly increased the knowledge in particle physics sector (J/ψ and B, quarks called charm and beauty, the supersymmetry and the grand unification theories... but nothing new on $\nu_\odot$ from the experimental point of view).
- In 1985-86, S.P.Mikheyev and A.Smirnov, [MIK85, MIK86], developed the Wolfenstein's proposal, [WOL78, WOL79], and presented a model of ν oscillation in matter.

- At the end of 80s', the Japanese detector KAMIOKANDE, originally a proton-decay dedicated experiment, realised the first "neutrinography" and showed that ν's come from the Sun, [HIR89]. The comparison between the results from Homestake and KAMIOKANDE implied a second SNP, [BAH90a].
- In the 90s', satellites and experiments on Earth surface strongly enhanced the knowledge on solar inner features *via* seismological measurements, [SCI96].
- In the middle of 90s', Gallium calibrated experiments detected low energy $\nu_\odot$'s and (finally) confirmed the ν production *via* p-p reactions and the solar machinery, see [GAV97, HAM99, GAV01a] and references therein. These results seemed to be not compatible with other experimental data so that a third SNP arose.
- At the end of the $2nd$ millennium, the SuperKAMIOKANDE's (SK) solar and atmospheric ν data suggested the "neutrino flavour oscillation" as a possible solution of SNP, [FUK01a, FUK01b]. If this is true, ν should have a non-zero mass and constraints in particle physics and cosmology are allowed.
- In 2001, a Canadian experiment (SNO) detected different $\nu_\odot$ flux depending on interaction process, [AHM01]: the flavour oscillation solution was enhanced. At the end of the year a terrible accident occurs at SK detector.
- In 2002, new results from SNO concerning neutral current interactions strengthen the oscillation hypothesis as "THE" right way out to solve the SNP, [AHM02a, AHM02b]. In December 2002, KAMLAND reactor experiment first result confirms LMA solution as "the" solution, see sect. 7 for details. In an exposure of about 150 days, the ratio of observed inverse β-decay events to the expected one without disappearance is $0.611 \pm 0.085(\text{stat}) \pm 0.041(\text{syst})$ for $\bar{\nu}_e$ energy greater than 3.4 MeV. This deficit is incompatible with standard predictions at the 99.95% confidence level. In the context of two-flavour neutrino oscillations with CPT invariance, all oscillation solutions to the SNP but the LMA solution are excluded, [EGU02]. The best fit is obtained with $\Delta m^2 = 6.9 \cdot 10^{-5}$ $(\text{eV})^2$ and maximal mixing, see later for details. BOREXINO detector should finish its building step.

3. How the sun shines.

We shortly review properties and characteristics of the Sun and aspects of the proposed mechanism it uses to produce energy and neutrinos. We refer for instance to [BAH89] for details and a complete description of these arguments.

3.1. Introduction.

The Sun is a G 2 type main-sequence star; it seems to be a "normal" star but X-ray and UV observations show interesting features. It has complex rotation, an unexplained magnetic activity, anomalies in surface chemical composition, an unknown mechanism acting in its corona and accelerating solar wind.
Detailed observations were carried out of the solar surface rotation by tracking

the motion of surface characteristics such as sunspots and by Doppler-velocity measurements. Sun is not rotating as a solid body: at the equator the rotation period is ~ 25 days, but it increases gradually towards the poles, where the period is estimated to be ~ 36 days. The rotational velocity at the surface of the Sun is ~ 2 km/s, dropping off rather smoothly towards higher latitudes. However, it has been found that bands of faster and slower rotation, a few metres per second higher or lower than the mean flow, are superimposed, see [KOS97, SCH99]. The origin of this behaviour is unknown.
The differential rotation seems to be linked to the dynamic nature of the solar external regions: in the outer 29 % of the Sun's radius ($\sim 2 \cdot 10^8$ m), energy is transported by convection, in rising elements of warm gas and sinking elements of colder gas, [CHR91, KOS91]. These motions also transport angular momentum, and hence provide a link between rotation in different parts of convective zone. Convection is even affected by rotation, which may introduce anisotropy in the angular momentum transport.
At the base of the convection zone, a transition occurs: the variation of rotation rate with latitude disappears, so that the inner region rotates essentially as a rigid body, at a rate corresponding to the surface rate at mid-latitudes. The region over which the transition occurs is very narrow, no more than a few per cent of the total solar radius: it is called tachocline, see [KOS96, CHA99]. It was proposed that a large-scale weak magnetic field ($B_\odot$) permeates inner regions and enforces nearly rigid rotation by dragging the gas along at a common rate, [GOU98].
Astrophysical data concerning young solar-type stars show faster rotations, by a factor up to 50: this means that the solar angular momentum probably decreased its initial value (for a complete review on rotation of solar interior see [CHR01] and references therein). The contribution due to mass loss and electromagnetic emission is hard to compute from the stellar evolution code; moreover, $B_\odot$ could have modified such processes.
The Sun has a magnetic activity probably due to a "dynamo" mechanism acting within the convective surface layers and connected with its non-uniform rotation. A strictly related effect is the sunspots appearing on the solar surface: they are modulated by a period of ~ 11 y (the first detected cycle started in 1755 A.D.) and are produced by magnetic flux tubes crossing the solar surface. Their origin could be due to a subsurface toroidal $B_\odot$ having different directions in northern and southern solar hemisphere. This small component (~ 5 % of the total intensity) sums up to a much stronger dipole field. The polarity is reversed every ~ 11 y so that the complete cycle is as long as 22 y.
The solar interior is a plasma: it is essentially neutral close to the photosphere while it is in practice fully ionised down to the centre.
The structure of the Sun is the result of an equilibrium between the energy loss at the surface and its generation in the core (with a stationary energy transport between core and surface) while, if the forces acting in the system are analysed, the hydrostatic equilibrium provides a relation between pressure gradient and gravitational acceleration (which is connected with density distribution inside the Sun). Properties of solar matter are expressed by equations of state relating pressure P, temperature T, density ρ and

chemical composition, often characterised in terms of fractional mass of hydrogen (X), helium (Y), and other elements, Z. The value of T inside the Sun is fixed by the energy balance.
In a great part of the Sun the energy transport is radiative and depends on the matter opacity, [EDD26]; a steep temperature gradient (∇) is required leading to convective instability, [SCH06]: then, it is slightly steeper than adiabatic, where P and ρ are related by:

$$P \simeq K\rho^{\Gamma_1} \tag{1}$$

where K is constant depending on convective efficiency and the exponent Γ_1 is:

$$\Gamma_1 = \left(\frac{\partial lnP}{\partial ln\rho}\right)_{ad} \tag{2}$$

Generally speaking, ∇ overcomes the adiabatic value near the solar surface where ρ is very low and conductive velocities are therefore much higher to sustain the flux of energy.
A detailed knowledge of physical phenomena inside the Sun is needed to achieve a realistic solar model. The energy production mechanism is supposed to be a series of nuclear exothermic reactions induced by thermal motion: light nuclei fuse among them to form heavier ones. The average binding energy per nucleon is a useful parameter to study the possible behaviour; it gets to a maximum in coincidence with ^{56}Fe: heavier nuclei take part to fission reactions, for light nuclei the fusion is allowed. Both these processes reach the end-point when they approach the maximum value of the binding energy per nucleon and, at the same time, this condition is the natural end-point of the nuclear burning processes inside the stars.
In any case, the difference between the masses of *in* and *out* nuclei is converted into energy, following the Einstein's relation: $\sim$ 27 MeV are produced for the basic nuclear reaction in the Sun, the conversion of 4 protons in a He nucleus.
The fusions in the core of a star supply the required radiated luminosity and the thermal pressure, due to the motion of electrons and ions that is needed to support the star against the gravity force. Moreover, the nuclear reactions imply chemical composition and temperature distribution variations inside the star.

3.2. Basic nuclear reactions.

Following the description given by solar models, the solar energy production is done by the conversion of H into He: the so called p-p chain produces the main contribution, the remaining one being due to the CNO cycle. It is hard to give a right evaluation of all solar nuclear reaction rates because of our partial knowledge of interaction cross-sections at energy as low as in the solar core but only if $T_c \geq 6 \cdot 10^6$ K the p-p reaction becomes "efficient".
Then, we detail both the cycles: in table 1 the main features of p-p chain nuclear reactions are shown while table 2 summarises the CNO cycle, which shows a "knot" due

to different reactions the ^{15}N nucleus has.
The p-p chain starts when two protons interact to form deuterium, D, (the process is dominated by weak interactions, its cross-section is very low, $\sigma \sim 10^{-47} cm^2$). Alternatively a 3-bodies process can occur: 2 protons and an electron interact producing D (p-e-p reaction), but this reaction is highly disfavoured. Some seconds later, D captures a proton forming ^{3}He; for a detailed description of D importance in p-p chain see [BAH97c]. The D production is quite a crucial point: in fact D does not accumulate in the solar interior, on the contrary only a great abundance of ^{3}He nuclei allows further nuclear reactions (even if higher T_c values are required). D and ^{3}He are burned quickly in the Sun, their lifetime being respectively $\sim 10^{-8}$y and $\sim 10^5$y: both these values are very short compared to lifetime of a proton, which is destroyed by the p-p reaction ($\sim 10^{10}$y), [BAH89]. Hence, it is assumed that both D and ^{3}He are in local kinetic equilibrium: this means that the production of D *via* p-p and p-e-p reactions is balanced by its destruction *via* p+D reaction, see for instance [GAU97] for a discussion on D/H ratio in astrophysics.

Table 1. *Reactions of the proton-proton chain: the probability of each step and the maximum kinetic energy are reported.*

REACTION	Probability (%)	Max. Kinetic Energy (MeV)
$p + p \rightarrow D + e^+ + \nu_e$	99.76	0.42341
$p + e^- + p \rightarrow D + \nu_e$	0.24	1.445
$p + D \rightarrow {}^3He + \gamma$	100	5.49
$^3He + {}^3He \rightarrow {}^4He + 2p$ P-P I	81.03	12.86
$^3He + p \rightarrow e^+ + \nu_e + {}^4He$	0.00002	18.778
$^3He + {}^4He \rightarrow {}^7Be + \gamma$	18.97	1.59
$^7Be + e^- \rightarrow {}^7Li + \nu_e$	18.95	0.8631(89.7%) 0.3855(10.3%)
$^7Li + p \rightarrow {}^4He + {}^4He$ P-P II		17.35
$^7Be + p \rightarrow {}^8B + \gamma$	0.02	0.137
$^8B \rightarrow 2\ {}^4He + e^+ + \nu_e$ P-P III		14.06

When $T_c \geq 8 \cdot 10^6$ K other fusion reactions are allowed:

- Two ^{3}He nuclei could interact originating a ^{4}He nucleus and 2 residual protons (this is the P-P I branch).
- If ^{4}He is present and $T_c \geq 1.5 \cdot 10^7$ K, ^{3}He could interact with ^{4}He producing ^{7}Be

(a radioactive isotope) which transforms into ^{7}Li by free electron capture. This reaction does not depend on nuclear Coulombian barrier. Some time later, this nucleus interacts with a free proton originating two ^{4}He nuclei (P-P II branch). Another option is possible: ^{7}Be can capture a proton originating ^{8}B which then breaks into two ^{4}He nuclei (P-P III). This reaction is dominant at $T_c \geq 2 \cdot 10^7$ K. Even ^{7}Li has a very short lifetime so that the equilibrium abundance in temperature and density range in the solar core is quickly reached.

- ^{3}He captures a proton forming ^{4}He, a positron and a neutrino, the most energetic one in $\nu_\odot$ spectrum, or produces ^{4}Li, plus a photon. Then, ^{4}Li transforms into ^{4}He, a positron and a ν. Both these processes have a very low cross-section (weak interaction). The ^{3}He abundance profile predicted by SMs shows a peak at d $\sim$ 0.28 $R_\odot$ from the centre, with a bell-like curve due to the competition between its creation and its destruction. Its abundance is expected to have an influence on the structure of the solar core at a level where helioseismology can detect it.

The second way producing energy in the Sun is the CNO (or Bethe-Von Weizsäcker) cycle occurring at T_c higher than in the p-p chain: it starts when a ^{12}C nucleus captures a proton producing ^{13}N and a photon, [WEI37, WEI38]. Its contribution to solar energy production was estimated as the main one in Bethe's seminal papers, see *e.g.* [BET39], because of incorrect T_c values. When more recent and precise T_c estimates were adopted, the CNO contribution diminished at a level of some percent; moreover, the Sun is a low-mass star, see [TUR01c] for a discussion of the influence of CNO cycle reactions on the solar structure.

Table 2. *Reactions of the CNO chain.*

REACTION	Max. Kinetic Energy (MeV)
$^{12}C + p \rightarrow \gamma + {}^{13}N$	1.94
$^{13}N \rightarrow e^+ + {}^{13}C + \nu$	1.1982
$^{13}C + p \rightarrow \gamma + {}^{14}N$	7.55
$^{14}N + p \rightarrow \gamma + {}^{15}O$	7.30
$^{15}O \rightarrow e^+ + \nu + {}^{15}N$	1.7317
$^{15}N + p \rightarrow \gamma + {}^{16}O(1\%)$ $\rightarrow \alpha + {}^{12}C(99\%)$	12.13
$^{16}O + p \rightarrow \gamma + {}^{17}F$	0.60
$^{17}F \rightarrow e^+ + \nu + {}^{17}O$	1.7364
$^{17}O + p \rightarrow \alpha + {}^{14}N$ $\rightarrow \gamma + {}^{18}F$	5.61
$^{18}F \rightarrow e^+ + \nu + {}^{18}O$	0.63

In table 3 the energy produced in solar reactions is shared following the production mechanism; the fraction carried out by $\nu_\odot$'s is also shown.

Table 3. *Thermal energy produced by different nuclear reactions and fraction of $L_\odot$ carried out by $\nu_\odot$'s.*

REACTION	Q_{eff} (MeV)	Energy ν %	$L_\odot$ %
PP I	26.19	1.95	84.87
PP II	25.65	4.00	13.52
PP III	19.12	28.46	0.01
CNO	25.03	15.66	1.60

3.3. Some technical aspects.

Let us point out the main features of physical processes inside the Sun. Charged nuclear particles interact only if they are so close each to other that strong nuclear forces become dominant with respect to Coulomb repulsive forces: typical distance is $d \approx 10^{-15}$m (the nuclear radius is $r_N \simeq 1.3\, A^{\frac{1}{3}} \cdot 10^{-15}$m, where A is the atomic mass number).
An interaction between two nuclei is usually described by a potential well with average depth of ~ 30 MeV followed by a Coulomb barrier:

$$E_{Coul} \;=\; \frac{Z_1 Z_2 e^2}{r_N} \sim Z_1 Z_2\; MeV \approx 10 MeV \tag{3}$$

where Z_1 and Z_2 are the electric charges of interacting nuclei (the thermal energy of a particle in solar plasma at $T_c \sim 1.5 \cdot 10^7$ K is $E_k \approx 10$ keV).
A Maxwell-Boltzmann distribution function describes the energy distribution of particles in solar plasma while the probability of the interaction process is:

$$P(E) \;=\; \frac{2}{\sqrt{\pi}}(kT)^{-3/2}\sqrt{E_k} exp\left(-\frac{E_{Coul}}{kT}\right) \sim exp\left(-\frac{E_{Coul}}{kT}\right) \ll 10^{-400} \tag{4}$$

This value for fusion reactions is so small that, even taking into account an extreme tail of the distribution, all solar nucleons could never interact in a "reasonable" time (nor all the baryonic matter in the Universe).
Solar nuclear fusion reactions occur *via* a strong interaction at energies ranging from $\sim$ 5 keV to 30 keV; its energy dependence in non-resonant reactions is expressed as:

$$\sigma(E) = \frac{S(E)}{E} exp\left\{-2\pi\eta(E)\right\} \tag{5}$$

$$\eta(E) = \frac{Z_1 Z_2 e^2}{\hbar v} \qquad \mu = \frac{A_1\, A_2}{A_1 + A_2} \qquad v = \sqrt{\frac{2E}{\mu}}$$

η is the Sommerfeld parameter, E is the centre-of-mass energy, μ is the reduced mass where A_1 and A_2 are the atomic mass number, v the relative velocity in the entrance

channel. The exponential Gamow penetration factor, which dominates the energy dependence, describes quantum-mechanical tunneling through the Coulomb barrier. The WKB approximation, which is usually adopted to evaluate the Gamow factor, is valid if $2\pi\eta \geq 1$ and becomes even more accurate at low energy. S(E), which is slowly varying (except for resonances), is then usually written as:

$$S(E) \simeq S(0) + S'(0)E + \frac{1}{2}S''(0)E^2. \tag{6}$$

The coefficients can often be deduced by a fitting procedure to laboratory measurements or by theoretical calculations of the cross-section made at higher energies and then extrapolated to the solar energies.
In this picture the probability P(E) depends also on the Gamow factor G:

$$P(E) \sim exp(-G) \; = \; exp\left(-\frac{4\pi}{h}\sqrt{2\mu}\int_{R_-}^{R_+}\sqrt{\frac{Z_1 Z_2 e^2}{r} \; - \; E}\, dr\right) \tag{7}$$

where E is the relative kinetic energy between two nuclei in their centre of mass. The previous relation is usually written as:

$$P(E) \sim exp\left[\left(-31.29 Z_1 Z_2\right)\sqrt{\frac{\mu}{E(keV)}}\right] \tag{8}$$

When T$\sim 10^7$ K and $Z_1Z_2 \leq 2$, as in the solar core, P(E) is $\sim 10^{-20}$; higher temperatures are required for reactions including heavier nuclei.
The rate of a non-resonant fusion reaction can be written, [BAH89]:

$$\langle \sigma v \rangle = 1.3005 \cdot 10^{-15}\left[\frac{Z_1 Z_2}{A\mu T_6^2}\right]^{1/3} f S_{eff} exp\left(-\tau\right) cm^3 s^{-1} \tag{9}$$

where T_6 is the temperature in units of 10^6K. S_{eff} (in keV b) is the effective cross-section factor for the fusion reaction and is evaluated at the most probable interaction energy (E_0); to first order in τ^{-1}:

$$S_{eff} = S(E_0)\left\{1 + \tau^{-1}\left[\frac{5}{12} + \frac{5S'E_0}{2S} + \frac{S''E_0^2}{S}\right]_{E=E_0}\right\} \tag{10}$$

where $S' = \frac{dS}{dE}$.
The quantity f, the screening factor, was first calculated by [SAL54]. The exponent τ, which is varying in the range 15 - 40, dominates the dependence of the reaction rate from T; it is given by:

$$\tau = 3\frac{E_0}{kT} = 42.487\left(\frac{Z_1^2 Z_2^2 \mu}{T_6}\right)^{1/3} \tag{11}$$

The most probable energy (the Gamow energy, E_0) at which the reaction occurs is:

$$\begin{aligned} E_0 = & \left[(\pi\alpha Z_1 Z_2 kT)^2(\frac{m\mu c^2}{2})\right]^{1/3} \\ & = 1.2204(Z_1^2 Z_2^2 A\mu T_6^2)^{1/3} \; keV \end{aligned} \tag{12}$$

For example $^3He(^3He,2p)^4He$ $E_0 \sim 21$ keV, $^{14}N(p,\gamma)^{15}O$ $E_0 \sim 26$ keV.
In most analyses the values of S and derivatives are quoted at E = 0 not at E_0: in order to relate the equations, one has to express the quantities in terms of their values at E = 0:

$$S_{eff}(E_0) \simeq S(0)\left[1+\frac{5}{12\tau}+\frac{S'(E_0+\frac{35}{36}kT)}{S}+\frac{S''E_0}{S}\left(\frac{E_0}{2}+\frac{89}{72}kT\right)\right]_{E=0} \quad (13)$$

$S_{eff}(E_0)$ is often referred to as simply "the low-energy S-factor"; in literature S is usually labelled by introducing the electric charge of reacting particles: S_{11}, S_{34} and so on.
In practice, the electrostatic repulsion between interacting nuclei is diminished by this screening: the effective energy in centre of mass is increased by a constant term $-u_0$. Consequently, the value of interaction rate is enhanced, from $\sim 4\%$ for the first reactions of p-p chain up to $\sim 40\%$ for the ^{14}N + p interaction.
The weak screening description is usually introduced, see [GRU98, BAH00b]. This approach is valid if $kTR_D \gg Z_1Z_2e^2$: in the solar case $Z_1Z_2 \leq 10$. The enhancement factor is given by:

$$f = exp\left(\frac{Z_1Z_2e^2}{kTR_D}\right), \quad (14)$$

$$R_D = \left(\frac{4\pi ne^2\zeta^2}{kT}\right)^{-1/2}$$

$$\zeta = \left\{\Sigma_i X_i\frac{Z_i^2}{A_i}+\left(\frac{f'}{f}\right)\Sigma_i X_i\frac{Z_i}{A_i}\right\}^{1/2}$$

where R_D is the Debye radius, n is the baryon number density (ρ/m_{amu}), X_i, Z_i, and A_i are, respectively, the mass fraction, the nuclear charge and the atomic weight of nucleus of type i. The quantity $\frac{f'}{f} \simeq 0.92$ describes electron degeneracy, [SAL54].
Thus, plasma screening corrections are known with uncertainties of a few percent. Corrections of the order of a few percent to the Salpeter formula come from the non-linearity of the Debye screening and from the electron degeneracy, see [JOH92, DZI95b, BRO97, GRU97] for further discussions.
Moreover, the Salpeter relation also describes screening effects on the ^{7}Be electron capture rate with an accuracy better than 1%, [GRU97].
The screening treatment is based on the mean field approximation which is the field that a particle in the plasma sees "averaged" on thermodynamically long times. Following the ergodic hypothesis, this value is equal to a mean over all particles in the system at any chosen time. In solar core $R_D \sim 0.87\ d$, where d is the mean interparticle distance, so that the mean number of particles in a Debye sphere ranges from 2 up to 5, depending on ions electric charge. The mean field approximation supposes this number is constant, then it deduces the mean field potential.
Many authors estimated this is a poor approximation and proposed different solutions trying to overcome the Salpeter's picture, see [MIT77, CAR88, SHA96, GRU98, BAH00a, SHA00, WEI01, BAH02d]. In [BRO97, GRU97, BAH00a] the validity of

"classic" treatment were confirmed. Physical interpretation of these results is currently unknown; an "antiscreening" effect, as proposed in [TSY00], is strongly disfavoured, [FIO01a]. In table 4 the influence of different screening factors on each branch of the p-p chain nuclear reactions is shown, while in fig. 1 the variations induced by screening factors on the sound speed profile inside the Sun are drawn (this is a test usually adopted to check the goodness of a SM).

Table 4. *Screening factors in solar core, for weak screening (W-S), Mitler model (MIT), no screening (NO-S) and Tsytovitch model (TSY), adapted from [FIO01a].*

	W-S	MIT	NO-S	TSY
p+p	1.049	1.045	1.0	0.949
^{3}He+^{3}He	1.213	1.176	1.0	0.814
^{3}He+^{4}He	1.213	1.176	1.0	0.810
^{7}Be+p	1.213	1.171	1.0	0.542

At present, helioseismological data restrict the variability of corrective screening factor: $0.95\, f_{Salp} \leq f \leq 1.1\, f_{Salp}$, where f_{Salp} is the value in Salpeter's description. In any case, no direct measurements of such a parameter will be possible.
If resonances are present in the reaction cross-section σ(E), equations 6 have to be substituted by Breit-Wigner relation:

$$\sigma(E) = \frac{\omega\pi}{k^2}\frac{\Gamma_\alpha\Gamma_\beta}{(E-E_{res})^2 + \frac{\Gamma^2}{4}} \qquad (15)$$
$$\omega = (1+\delta_{1,2})\frac{2I_c+1}{(2i+1)(2I+1)}$$

where k is the wave vector, I_c, i, I are, respectively, the compound nucleus, the incoming nucleus and the target nucleus spins, E_{res} is the energy at which the resonance occurs, $\Gamma_\alpha, \Gamma_\beta, \Gamma$ are the widths of the initial α channel, of the compound nucleus in the β channel and of the decay of the compound nucleus. After substitutions and taking also into account that the Maxwell-Boltzmann distribution function varies its value when the energy is near the resonance value, the interaction rate equation becomes:

$$r = \frac{n_1 n_2}{1+\delta_{1,2}}\left(\frac{2\pi}{\mu kT}\right)^{3/2} h^2\omega\frac{\Gamma_\alpha\Gamma_\beta}{\Gamma} exp\left(-\frac{E_{res}}{kT}\right) \qquad (16)$$

When T is fixed, the reactions with energy near E_{res} give the main contribution in the previous equation so that a good knowledge of their characteristics at low energy is needed.

3.4. Solar Models.(SMs)

Details about the energy production and other aspects of the solar physics are provided by SMs; among them we mention the so called "standard solar models", SSMs. Their

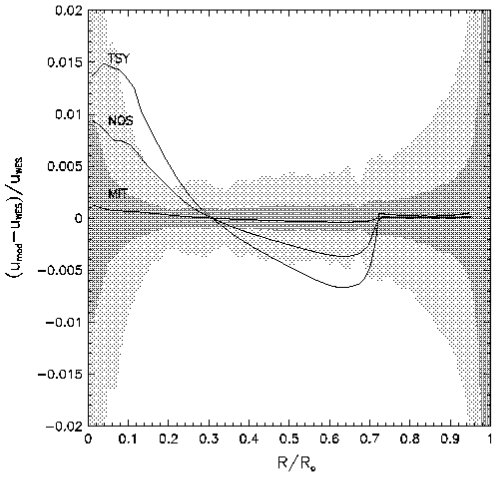

Figure 1. Fractional isothermal sound speed difference: the shaded region represents experimental and a conservative 3σ uncertainties. Three different screening factors are drawn: TSY - Tsytovich; MIT - Mitler; NOS - without screening term, from [FIO01a].

definition is often changing in time but in general they could be thought as models offering a description of the solar properties under a set of hypotheses picking out the values of physical and chemical inputs within the range of uncertainty of experimental data. SMs are required to fit the measured $L_\odot$, $R_\odot$ and Z at surface. No constraints deduced from helioseismology, see later in section 3.7, are imposed in SSMs.
Many non-standard SMs were proposed, see [BAH89, BAH97d, GUE97, CAS97, BRU99, BAH01a, BAS00, TUR01a, COU02] for detailed analyses. It was demonstrated the inconsistency of a part of these models with the deduced solar sound speed c_s in [BAH97d] or with p-mode frequencies in [GUE97]. Non-standard SMs have been used even to constrain the cross-section for the p-p interaction, to estimate the mass loss from the Sun, [GUZ95], or the anomalous energy transport by WIMPS, [CHR92].
We underline that the so called "seismic" SMs, that presently better agree with helioseismological measurements, are strictly speaking non-standard SMs.
The fundamental assumptions of SMs are:

- At the first stage of its evolution the Sun is a homogeneous spherical protostar formed by the contraction of interstellar gas. The released gravitational energy heats the solar matter. After $\sim 5 \cdot 10^7$y, the Sun goes into the "main sequence" and

the reactions of the p-p chain lead to a hydrostatic equilibrium (gravitational force is balanced by the pressure due to the thermal motion).

- The time evolution of the Sun in the "main sequence" is described by a set of differential equations where the distance from the centre of the Sun and the time from the nuclear reactions beginning are independent variables. Asymmetric distributions, angular momentum and $B_\odot$ usually are not introduced in computations. Nuclear reactions do not change the Z value but only X and Y. Moreover, a smooth variation of the remaining physical parameters is produced. The physical quantities under analysis are $m(r,t)$, the mass inside a sphere whose radius is r at time t; $P(r,t)$, $L(r,t)$, $T(r,t)$ and $X_i(r,t)$, the chemical mass fraction of i-element, at distance r from the centre at time t.

Boundary conditions are imposed: the abundance of heavy elements at the entrance in the "main sequence" is supposed to be equal to the present meteoritic one; the remaining functions at the present time are required to be coincident with data measured at solar surface.
The solar evolution is then considered in the context of "standard" particle physics model.
Three different time scales are present:

- *Hydrostatic time scale* ($t_{hyd} \approx R^{1.5} G^{-0.5} M^{-0.5}$) gives the typical time after which a star can reach a hydrostatic equilibrium after a small perturbation. For the Sun $t_{hyd} \sim 30$ minutes so that it is very near to the hydrostatic equilibrium.
- *Kelvin-Helmholtz time scale* ($t_{KH} \equiv \frac{E_G}{L} \approx 0.5\, GM^2 R^{-1} L^{-1}$) describes the evolution time of a star for which gravitational energy E_G is the only available one (the absolute value of E_G has to be inserted). For the Sun $t_{KH} \sim 1.7 \cdot 10^7$ y.
- *Nuclear time scale* ($t_N \equiv \frac{E_N}{L}$) refers to a star balancing its luminosity by release of nuclear energy E_N (in the previous relation the absolute value of this energy has to be used). In the case of the Sun, if one supposes H is the sole component, an its complete conversion in He and a constant luminosity, a $t_N \sim 10^{11}$ y is required.

Let us show some characteristics of the differential equations adopted in SMs.
The first equation imposes the conservation of a mass inside a sphere:

$$\frac{\partial m}{\partial r} = -4\pi r^2 \rho \tag{17}$$

The second equation, which states the energy conservation, is:

$$\frac{\partial L}{\partial m} = \epsilon - C_P \frac{\partial T}{\partial t} - \frac{1}{\rho} \left(\frac{\partial ln\rho}{\partial lnT} \right)_P \frac{\partial P}{\partial t} \tag{18}$$

where C_P is the specific heat at constant pressure and ϵ (the net energy produced per time and mass unity) is the dominant term: consequently the energy produced by nuclear reactions is balanced by its flux emerging from the production side. Moreover, the energy production per mass and time is correlated to all the specific nuclear reaction rates and to their specific Q-value, which is the maximum energy "injected" in the solar

matter by each reaction.
The third equation gives the relations between gravitation and pressure forces:

$$\frac{\partial^2 r}{\partial t^2} = -\frac{mG}{r^2} - 4\pi r^2 \frac{\partial P}{\partial m} \tag{19}$$

When hydrostatic equilibrium is present, the term at left side vanishes.
The energy flux is described by the following equation:

$$\Phi_c = \frac{16\sigma T^3}{3k_c\rho}\frac{dT}{dr} \tag{20}$$

where k_c is the conductive opacity.
The "transport" equation shows the outward energy flux in terms of temperature gradient (∇) which depends on typical physical processes originating those temperature variations:

$$\frac{\partial T}{\partial m} = -\frac{T}{P}\frac{Gm}{4\pi r^2}\nabla = -\frac{T}{P}\frac{Gm}{4\pi r^2}(\nabla_R + \nabla_C + \nabla_{co}) \tag{21}$$

where ∇_R, ∇_C and ∇_{co} are respectively the radiative, the conductive and the convective component of temperature gradient.
The Sun is supposed to be "stratified", depending on the dominant physical process which allows the energy propagation in matter. Energy is produced in the solar core where the transport is radiative: in this region the radiative gradient is the dominant term therefore $\nabla_R \gg \nabla_C$, the conductive component which is due to the electron plasma thermal motion. The last term (∇_{co}) is acting only in the convective region, at the distance from the centre $r \geq 0.7R_\odot$.
The energy transport is based on diffusion and ∇_R is calculated under the assumption of local thermodynamic equilibrium:

$$\nabla_R = -\frac{3}{64}\frac{kL}{\pi\sigma GmT^3} \tag{22}$$

where k is the Rosselland coefficient describing the radiative opacity. The inner solar region is opaque for photons: their mean free path has been estimated at a level lesser than 10^{-3}m, see [FIO00], the mean absorption coefficient being at a level of 0.4 cm^2g^{-1}.
When convective motions are present, the stability of the system depends on adiabatic temperature gradient (∇_A) (Schwartzschild criterion). The possible solution requires:

$$\nabla_R \leq \nabla_A = \left(\frac{\partial lnP}{\partial lnT}\right)_S \tag{23}$$

The analysis of convective motion is not trivial: in the usual description viscosity terms are neglected and the convection is assumed to be due to the motion of convective elements. At the start of the solar evolution, particles are in equilibrium with the medium, then they move adiabatically and release the thermal energy surplus into the new medium in which they are.
Up to now, only approximate descriptions of convective motions have been possible: a phenomenological approach introduces a "mixing length", see [BOE58], the distance

over which a unit of gas can be identified before it mixes. This value strictly depends on P:

$$l = \alpha \frac{d\,r}{d\,lnP} \tag{24}$$

where α is a free parameter: when it increases the convection becomes more efficient, ∇ lowers and T at surface raises. As a further effect, being fixed the $L_\odot$ value, $R_\odot$ has to decrease. In any case, this is an over-simplified approach which does not allow any knowledge on the stellar radius and on the convective region features.
The initial chemical composition of Sun, which is unknown, has a great influence on solar evolution, therefore the present values of ρ, T and chemical composition in the solar core are strictly correlated to the radiative opacity which controls ∇. Heavy elements are not completely ionised and their abundance on solar surface decreases with time due to the gravitational settling and to diffusion processes.
When compared with other time scales, motions of gas particles in convective zone are so rapid that this region may be taken chemically homogeneous. However, if macroscopic motions are absent, heavy elements tend to sink relative to lighter ones while composition gradients are smoothed by diffusion. The time scale of these processes in radiative zone is much longer.
SMs including settling and diffusion of elements were firstly detailed in [COX89] while the influence of these processes on quantities measured by helioseismological techniques was pointed out in [CHR93]. Its inclusion in SMs gave results in better agreement with helioseismological data, but it has increased the discrepancy between $\nu_\odot$ flux predictions and experimental measurements on Earth.
The mixing-length description of the convective flux is a parameterisation with weak physical basis and the dynamical effect of convective motions on solar structure is generally ignored. Inclusion of convection in more realistic solar calculations was also attempted, [CAN91].
The last "solar" equation describes the evolution of the chemical composition but it gives a good representation only in the inner radiative region, where no matter exchanges between neighbouring layers are present and nuclear reactions mainly modify the hydrogen abundance. Diffusive processes do not give significant contribution because of their slow temporal evolution; the equation is then:

$$\frac{\partial x_i}{\partial t} = \frac{m_i}{\rho}(\sum_j r_{ji} - \sum_k r_{ik}) \tag{25}$$

where r_{ik} is the rate of reaction in which nucleus "i" is transformed in nucleus "k".
In the convective zone turbulent motions change the chemical composition which is usually assumed as a constant: this approximation is allowed by the local low temperature which forbids nuclear fusion reactions. It is useful to remember that the mass of the convective region is less than 2% of the total solar mass ($M_\odot \sim 2 \cdot 10^{30}$ kg).
The introduction of the physics of the solar matter into the model is thus necessary to complete the description of the Sun. Auxiliary equations are usually equations of state and the equations for opacity and for nuclear reaction rates. The evolution in a SM is

determined by microscopic properties of solar matter, at first thermodynamics relations, such as the dependence of P on ρ, T, chemical composition and nuclear parameters.
Taking into account the thermal pressure dominance over other pressures (mainly radiative), equations of state of a fully ionised perfect gas can describe the solar matter in regions where the energy is produced within an accuracy better than 1 %,[DEG97, FIO00]:

$$kT = u\mu \qquad \mu = \frac{m_P}{1.5X + 0.25Y + 0.5} \tag{26}$$

where μ is the mean molecular weight and the isothermal sound speed squared u is given by:

$$u = \frac{P}{\rho} = \frac{c_s^2}{\Gamma_1} \tag{27}$$

where Γ_1 is the adiabatic exponent.
In general, two approaches (chemical or physical) are possible. The former introduces atoms and ions while ionisation is described as a chemical reaction, see EFF formulation [EGG73]. An evolution of this description is done in MHD description, [DAP88, HUM88, MIH88]: modifications of atomic states are "heuristic" but the probability that a state is a function of the parameters of the surrounding plasma.
The latter provides a method to include non-ideal effects. OPAL project, [IGL96], presently the most adopted in computations, is based on a general description of the basic constituents (electrons and nuclei). Configurations corresponding to bound combinations, such as ions, atoms and molecules, are considered as a clustering process while plasma effects are introduced in terms of statistical mechanics. Among non-ideal processes, the screening effect of positive charges by surrounding electrons and the interaction between bound particles (pressure ionisation) are noteworthy. In 2001 an upgrading to OPAL96 equations has been proposed where a relativistic treatment of electrons is combined with an improved activity expansion method for repulsive interactions, [ROG01].
Photons are responsible of the energy transport while convective motions, energy generation and chemical composition variations are produced only by nuclear reactions. The opacity of solar material controls the energy flow through the Sun and in practice its luminosity. Different ways to construct opacity values were followed by OPAL group, [ROG92, IGL92, IGL95, IGL96], and by Opacity Project, [SEA94], but their results agree at a level better than 10 %. In early SMs, opacities computed in [HUE77] were used.
To develop SMs calculations, experimental values have to be introduced as input parameters; usually $L_\odot$, $R_\odot$ and Z values are chosen:

- The present luminosity $L_\odot = 3.842\,(1 \pm 0.004) \cdot 10^{26} W$, [CRO96, FRO98].
- The present radius $R_\odot \simeq 6.9599\,(1 \pm 0.0007) \cdot 10^8\, m$.
- The detailed element composition for nuclei heavier than He as deduced from photospheric determinations and meteoritic analysis.

After a numerical integration of "solar" differential equations, T, ρ, P and X are then computed as a function of their distance from the solar centre.

3.5. Nuclear cross-sections.

The estimation of interaction cross-sections inside the Sun is a persistent and not easy to overcome problem: in most cases laboratory measurements are possible only at high energy and "solar" cross-sections are estimated by an extrapolation.
It was stressed the overwhelming importance of astrophysical factor S_{11}: if its value is higher than the usually adopted in SMs then T_c is lower than presently estimated, [DEG98b].
Let us consider the ^{3}He - ^{3}He and ^{3}He - ^{4}He fusion rates. If the cross-section of the first reaction were higher than the extrapolated one presently used or if the electron capture rate were lower or the ^{7}Be + p cross-section were higher, a significant and measurable modification in the $\nu_\odot$ flux would be expected, see later in section 3.10.
Experimentally speaking, the analysis of the region near the Gamow peak (the product of the Maxwell-Boltzmann distribution by the cross-section, E$\sim$ 20 keV), is a very difficult task because of the smallness of the cross-sections and the cosmic rays background.
A few years ago, a program (LUNA) of deep underground nuclear measurements has started at Laboratori Nazionali del Gran Sasso, Italy, (LNGS). A resonance at thermal solar energy was proposed to explain the first solar neutrino problem, [FET72, FOW72]: it would deplete the contribution of the reaction ^{3}He$(\alpha,\gamma)^7$Be, which starts the ^{7}Be and ^{8}B production. The latest LUNA results are based on measurements at a projectile energy of 16.5 keV, a value as low as at the solar Gamow peak, [BON99]: the obtained cross-section is 0.02 ± 0.02 pb and this means an interaction rate of 2 events per month! Resonances that could enhance the ^{3}He-^{3}He fusion rate were not found. It is impossible to lower the projectile energy because of the background reaction ^{3}He(D,p)^{4}He which has a cross-section much larger than ^{3}He(^{3}He,2p)^{4}He reactions.
In any case, further studies and measurements are needed for a better knowledge of the electron screening effect on fusion cross-sections at stellar energies: the experimental uncertainties on low-energy ^{3}He(^{4}He,γ)^{7}Be cross-section give in practice the dominant contribution to the uncertainty in ^{7}Be and ^{8}B $\nu_\odot$ flux calculation. Very recently experimental measurements concerning ^{7}Be(p,γ)^{8}B reaction have been published, [JUN02]: a higher value of astrophysical factor, even if within the previous uncertainty range, has been computed and then inserted in SMs computations, see [BAH02c]. Significant variations on physical quantities have been excluded but the ^{8}B $\nu_\odot$ flux increases, [BAH02c]. See also [HAS99, GIA00, DAV01, HAM01, STR01a] for a complete review on ^{7}Be + p cross-section measurements and relative astrophysical factor values. It has to be stressed that newest results do not agree well each other so that, as a conservative prescription, previously quoted values, as done in [ADE98, ANG99], have to be presently preferred.

3.6. Comments and problems.

As a first comment, it has to be stressed that even if SMs are an "easy" way to describe the solar evolution, neglecting rotation, $B_\odot$ ... and despite many solar quantities have no direct measurement, the agreement between experimental and predicted values is very well, maybe surprising. Differences enhance the rough knowledge of the physics acting inside the solar core.
The transport equation states both a temperature gradient, which induces an energy flux, and an energy surplus, producing a gradient, enable to slow down it. In other words if a radiative flux emerging from the solar core is present, then T must monotonically increase toward the centre as long as the energy source will rise T in the core. On the contrary, that zone must be in thermal equilibrium. When $\nabla_A \leq \nabla_R$, T decreases faster in the surrounding matter: an element adiabatically moving becomes hotter than the medium so that it receives a further contribution to its motion. If the criterion on radiative equilibrium is violated, all the regions become unstable with respect to any kind of motion of material elements. Consequently, this is a criterion to establish when a zone is convectively stable and a "mixing zone" between stable and unstable zones is present near the boundaries. This will be important in helioseismological analysis and in SMs skill to reproduce the behaviour of physical quantities inside the Sun.
Concerning the opacity, the main problem is a right estimation of the solar photon absorption cross-section: many different interactions and terms have to be considered, even if the basic contribution is due to the classic energy-independent Thompson cross-section. In radiative region the term related to heavy elements is dominant: at d = 0.6 $R_\odot$ its contribution is $\sim$ 85 % of the total value; on the contrary, in the solar core, where all the elements are fully ionized, except iron, its value decreases down to $\sim$ 45 % of the total. The opacities in the core are mainly due to electron scattering and inverse brehmsstrahlung while at d = 0.6 $R_\odot$ the bound-bound processes dominate, see fig. 2. The main sources of uncertainty for opacity are the metal content of the solar central region, which is without experimental data, and the actual calculation when one assumes a fixed chemical composition.
We list for instance processes which should contribute to the opacity value, for detailed description see [BOE87, GOU90, IGL91, BAH95, IGL95, TSY95]:

- Photon scattering on free electrons, taking also into account Doppler and collisional shifting of Raman resonance and relativistic corrections in the non-linear response due to the polarization.
- Inverse bremsstrahlung, with or without collective and relativistic effects, collective effects from ion-ion and electron-electron interactions.
- Electron degeneracy, quantum effects in scattering, stimulated scattering, frequency diffusion, plasmons contributions, refractive index corrections, variable density ...

These terms produce an uncertainty up to $\sim$ 10 - 15% on the Rosselland's coefficient value and this is a crucial point because opacity affects T_c and therefore the nuclear interaction rates: the higher the opacity the slower is the photon diffusion through the

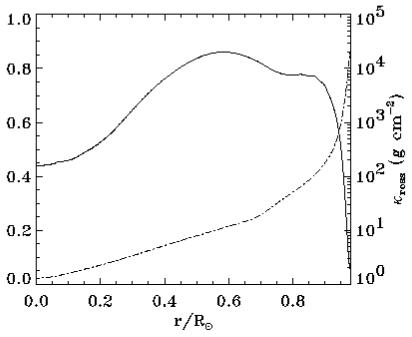

Figure 2. The contribution of the heavy elements to the opacity (full line). Superimposed is the profile of the Rosseland opacities κ_{ross} (dot-dashed line). Solar composition at 4.6 Gyr, from [COU02].

solar matter, so that T_c rises. In fact T_c depends on the radiative opacity, on Z, on the astrophysical factor S_{11} (or S_{pp}) and on the solar age. We underline that the present error on the last two quantities is at a level of 1% while the uncertainty on opacity and chemical composition is $\sim 10\%$.
Uncertainties affect even the radiative zone description: convective motions penetrates beyond the region of instability and can change ∇. Induced gravity waves might lead to a mixing over time scale of solar evolution while additional contributions to mixing could be produced by instabilities due to the solar rotations, [ZAH92, MON94, CHA95].

3.7. Helioseismology.

3.7.1. Introduction. Helioseismology has deeply increased our knolwedge of the Sun and of other sun-like stars: it analyses the mechanical seismic waves, produced by turbulences in the outer region of the convective zone, which travel through the solar matter with reflection on surfaces or refraction during the propagation toward the centre. Thanks to the movements of solar granules at the surface, the Sun forms a spherical acoustic resonator producing a broad spectrum of random acoustical noise; its period is

of about 5 minutes. This phenomenon was first analysed 40 years ago, [LEI62].
The possibility of measuring the wave travel time inside the Sun was discovered in the early 90's and was applied to probing subsurface flows, [DUV93, DUV96, KOS96]. The accurate measurements of vibrations penetrating inside the Sun down to different depths allow to deduce information on thermodynamical quantities as a function of depth.
Solar oscillations are detected by measuring Doppler shift of a spectrum line or intensity of optical radiation but their observations is a challenging task: the velocity amplitude of an acoustic p-mode is ~ 1 cm/s while the associated brightness variation is $\sim 10^{-7}$, (the expected amplitude of gravity modes is about 10 times smaller). The errors in helioseismological frequencies have been reduced at a level of $\sim 10^{-5}$ while the errors on deduced quantities are higher, $\sim 10^{-4}$.
Data concerning solar oscillations were inverted to compute c_s and ρ profiles, [DZI90, DAP91, ANT94, KOS97], and the adiabatic index Γ_1, [ANT94, ELL96, ELL98]; c_s and ρ radial profiles were also used to test opacity computations, [KOR89, TRI97], equations of state, [ULR82, ELL98, BAS98b], and elemental abundance profiles inside the Sun, [ANT98, TAK98].
Before the helioseismological measurements, three parameters were completely free in solar models: the starting Y and Z values and the mixing length. As output three observable quantities were deduced: the present $R_\odot$, $L_\odot$ and Z_{surf} . During the last fifteen years results based on inversion of helioseismological data provided strong constraints: the solar convection zone depth has been derived by c_s inversion, [CHR91, BAS97], while Y_{surf} was estimated by inversion of p-mode data, [BAS98a].
In any case, helioseismology can only check the robustness of SMs because of its impossibility to directly reconstruct the profiles of physical quantities used in SMs.

3.7.2. Technical features. The equations describing adiabatic and linear oscillations are hermitian, [CHA64], and the oscillations are thought as combination of standing waves, the eigenmodes of vibration. As usual procedure in wave mechanics, spherical harmonics $Y_l^m(\theta, \phi)$ are introduced. Scalar perturbations and displacement are written in terms of physical parameters and eigenfrequencies $\omega_{n,l,m}$, where n is the number of nodes along the radius, l is the horizontal waves number on the surface and m is the number of nodes along the equator. Solar surface oscillations have a superposition of modes with $0 \leq l \leq 1500$. If only adiabatic oscillations and small radial wavelengths, compared to $R_\odot$, are considered, a dispersion relation concerning the squared length of wave vector is valid:

$$|k|^2 = k_r^2 + k_h^2 = \frac{1}{c_s^2}\left(F_l^2\left(\frac{N^2}{\omega_{n,l,m}^2} - 1\right) + \omega_{n,l,m}^2 - \omega_c^2\right) + \frac{F_l^2}{c_s^2} \tag{28}$$

where the Lamb frequency is:

$$F_l^2 = \frac{l^2 c_s^2}{r^2} \tag{29}$$

the Brunt-Väisälä frequency is:

$$N^2 = g\left(\frac{1}{\Gamma_1}\frac{d}{dr}ln\,P - \frac{d}{dr}ln\,\rho\right) \tag{30}$$

the acoustic cut-off frequency ($\sim$ 5.8 mHz) is:

$$\omega_c^2 = c^2\left(1 - 2\frac{d}{dr}H_\rho\right) \tag{31}$$

the density scale height is:

$$H_\rho^{-1} = -\frac{d}{dr}ln\,\rho \tag{32}$$

the sound speed is:

$$c_s^2 = \Gamma_1\frac{P}{\rho} \tag{33}$$

Different oscillatory solutions are possible: the acoustic waves, when $\omega_{n,l,m} \geq N, F_l$, the gravity ones otherwise. The major restoring forces responsible for the solar oscillations are pressure and buoyancy. Pressure fluctuations are important at high frequencies *via* the production of acoustic waves; at lower frequencies, buoyancy is much stronger and produces internal gravity waves which can propagate only in convective stable regions (solar atmosphere and beneath the convective zone). Standing acoustic waves are known as p-modes; standing internal gravity waves are called g-modes. Their magnitude depends on local ρ, on P and on chemical composition.

3.7.3. Detection techniques. Ground instruments, like GONG (Global Oscillation Network Group), consisting of 6 Doppler imaging equal instruments, and satellite experiments, like SOHO (SOlar and Heliospheric Observatory), the project of an international collaboration (NASA and ESA) carrying 3 different detectors (GOLF, MDI, SOI), measure these waves (for a nice overview see [SCI96]). The seismic waves are detected by different techniques: the simplest one is the whole-disk integrated light measurement, as presently in VIRGO experiment and in future satellite detectors. A second technique uses velocity oscillations by detecting Doppler shift of spectral lines. Two kinds of observation are possible: the detection of the global Doppler velocity, measured by the displacement of specific absorption lines (Na or K), or local velocity, separating the Sun into pixels. In the former, low degree modes ($0 \leq l \leq 3$), which are the most penetrating ones, are detected (BiSON, IRIS and GOLF use this method). The global Doppler velocity shift of sodium lines is under analysis. The latter, isolating modes of higher degree, is used by MDI, which analyses Ni spectral lines.
When integrated light coming from the whole solar disk is detected, the sensitivity is limited to few modes having wavelength as large as the solar diameter.
At ground level, GONG network, which is sensitive to low l-modes, is continuously observing the solar surface. Even SOHO satellite allows continuous data taking and a reduction of detectable amplitude at small values, where influences due to the turbulence at solar surface are not present; in particular GOLF and MDI analyse the time variability

of the Doppler velocity.
The observations have to be made over a long time without any interruptions; solar oscillation frequencies are deduced from time series of the intensity or from radial velocity data (more frequently used). In this case modes with very small amplitudes and velocity not greater than some mm/s can be identified.

3.7.4. Data analysis and results. Presently about thousand of p-modes could be used in inversion relations (they are a fraction of the total number of measured frequencies) but only modes with l$\leq$ 150 are useful to study solar interior because higher frequencies propagate exclusively on the shallow outermost layers. P-mode frequencies are measured with an accuracy better than 0.01% but no more than 5% of their total amount is produced in the solar core; on the contrary the most part of gravity waves should come from the solar core.
Two ways are possible to extract information from experimental data:

- The direct method, when detected and expected acoustic frequencies are compared.
- The indirect method, when inversion relations are used to reconstruct the radial profile of variables as c_s^2, ρ or Γ_1 which are then compared to theoretical ones.

As example in fig. 3 the c_s profile is shown: values vary from $\sim$ 510 km/s in solar core down to $\sim$ 80 km/s at 0.95 $R_\odot$, [BAH01a].

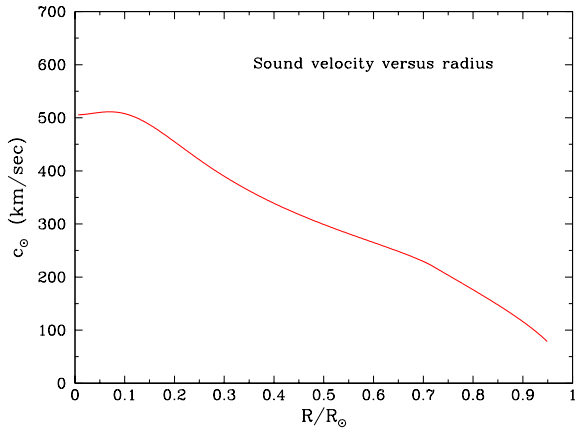

Figure 3. Calculated solar sound speed versus radius for the reference SM, [BAH01a]. The difference between computed and observed values is overall lesser than 0.5 km/s, from [BAH01a].

The sensitivity of c_s to different "ingredients" of a SM is strong: a 2% variation in the p-p reaction rate implies a 0.2% variation on c_s, as much as a similar change of the opacity coefficient. Moreover, a 10% variation of this parameter along the solar radius has a negligible effect on c_s but T_c is modified at a level of 1% and significant variations in $\nu_\odot$ flux are foreseen, see section 3.10.
The measured oscillation frequencies give information on solar interior *via* "inversion"

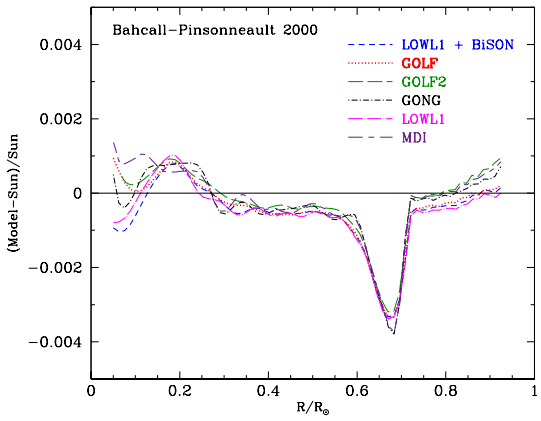

Figure 4. Fractional difference between the sound speed calculated in [BAH01a] and the values measured in six helioseismological experiments. Systematic uncertainties due to the assumed reference SM and the width of the inversion kernel are each ~ 0.0003, from [BAH01a].

procedure. If $f(r)$ is a function describing a solar inner property, $\nu_{l,n}^{exp}$ is an observed frequency and $\nu_{l,n}^{the}$ the corresponding frequency as computed in a SM then:

$$\frac{\delta\,\nu_{l,n}}{\nu_{l,n}} \;=\; \int_0^R K^n(r)\frac{\delta\,f(r)}{f(r)}dr \tag{34}$$

where $K^n(r)$ is a function of SM relating variation in frequency $\delta\nu_{l,n}$ with $\delta f(r)$. Inversion technique tries to form linear combinations of terms, as expressed in previous equation, by varying l and n with a weight $c_{l,n}(r_0)$ chosen to obtain a value $\frac{\delta f}{f}$ localised in r_0. The "averaging kernel" $H(r_0,r)$ indicates the localisation of the measure of $\frac{\delta f}{f}$:

$$\begin{aligned}\int_0^R H(r_0,r)\frac{\delta\,f_1(r)}{f_1(r)}dr \;&=\; \sum_{l,n} a_{l,n}(r_0)\frac{\delta\,\nu_{l,n}(r)}{\nu_{l,n}(r)} \\ H(r_0,r) \;&=\; \sum_{l,n} a_{l,n}(r_0)K^n(r)\end{aligned} \tag{35}$$

Hence, it is possible to calculate the difference between $\frac{\delta f}{f}$ as computed by using a SM and the observed values. It has to be stressed that this procedure becomes difficult going toward the solar core.

Usually, the rms difference between the measured (as deduced from helioseismological inversion formula) and the SMs estimated one is plotted. Uncertainties from measured frequencies are smaller than those allowed by present inversion relations; in any case they are at a level lower than 0.5% in the total analysed region. A constant uncertainty of $\sim 3\cdot 10^{-4}$ comes from each source of the c_s profile: the adopted SM, the width of the kernel of the inversion procedure and the experimental errors. The finite resolution of the inversion kernel leads to those rms systematic uncertainties although errors are much larger in the solar core and at the base of the convective zone. On the other hand, the uncertainties in ρ profile are an order of magnitude larger than the previous, see for instance figures 4 and 5. Among a lot of interesting results, a sharp transition between

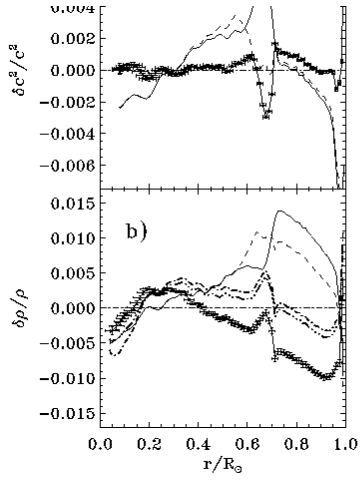

Figure 5. In a) the difference in the square of the sound speed between the Sun and the model [COU02](full line with errors) while in b) is shown the difference in the density. The plain lines with no error bar are for the Saclay standard SM, [BRU98], while the dashed lines are for the Btz model, [BRU99]. Two other SMs based on [COU02] are considered on the density figure: a model with the $^3He(^4He,\gamma)^7Be$ reaction rate reduced by 10% (dot-dot-dot-dashed line) and a model with the CNO poly-cycle reaction rates reduced by 70% (dot-dashed line), from [COU02].

differential rotation in the external convective zone and a practically rigid rotation in the radiative zone has been found. This transition appears as a peak in c_s difference profile and allows an accurate evaluation of the base of the convective zone where a change between temperature gradient is "physically" present. Up to now the origin of this behaviour is not clear. The bump close to the transition zone between convective and radiative regions can be reduced by a local enhancement of the opacity coefficient introduced in SMs, but this is a trick, and the true physical motivation is unknown.
The depth of the convective zone was analysed starting from 90s', [DEM91], firstly without element diffusion, [BAH90b, PRO91, BAH92].
The measurements of the g-modes is needed to further progress in the solar core analysis: these frequencies, which are proportional to Brunt-Väisälä value and mainly produced in the region below 0.2 $R_\odot$, are about 10 times more sensitive to core perturbations. The main experimental difficulties come from the estimated amplitude of their speed,

less than 1 mm/s, and from broad fluctuation of the solar noise in that frequency range. A long time of data taking (several years) is needed to improve the signal to noise ratio. The sensitivity of g-modes to physical parameter variations is low: a slight opacity enhancement and modified nuclear reaction rates change the g-modes frequencies at a level below the experimental resolution. In any case, g-modes must be identified at a lower order to be able to give useful information. The dependence of the g-modes on physical processes is not easy to anticipate therefore the identification of such modes is difficult. Up to now measurements of c_s are possible at distance from the solar core greater than $0.07 \pm 3.6\%$ $R_\odot$, [TUR01c], (only g-modes may improve this situation). Presently few "candidate" frequencies seem to be present in SOHO's data.

Temporal variations of rotation rate in solar interior and possible correlation between solar activity, namely the sunspots number, and variation on $R_\odot$ value have been recently analysed. In the first case, a slightly different rotation rate was detected into the outer part of the convective zone, from the solar surface down to 0.9 $R_\odot$ from the solar centre; nothing significant seems to be present at greater depth. Moreover, no statistically important variation in solar rotation rate near the base of the convective zone was found, [ANT00].

Sometines, SMs are directly compared with the p-mode oscillation frequencies, see [GUE97], while in the most part of the SMs the c_s profile is used: in fact the inversion procedure allows to remove uncertainties arising from external solar region where turbulence and non adiabatic effects are present.

The possibility of estimating the solar age *via* helioseismological data was shown in [DZI99] by using Small Frequencies Separation Analysis (SFSA). The analysed quantities have a strong sensitivity to the c_s gradient near the solar centre and a weak correlation with the description of outer layers. The so computed value is $t_\odot = 4.66 \pm 0.11 \cdot 10^9$ y (the lifetime on the pre-main sequence has to be added), see also [MOR00]. This value, which is $\approx 2.9\%$ greater than the standard one, produces a rather important change in c_s profile and reduces the differences with respect to the "real" Sun.

A good agreement between computed SMs and solar properties as deduced from helioseismology has been obtained by including relativistic corrections in equations of state: in fact the adiabatic exponent and c_s are better reproduced, see [ELL98, BON01]. In [BON02a] new results have been computed by using updated equations of states, including relativistic contributions in OPAL and MHD equations: the so obtained solar age is $t_\odot = 4.57 \pm 0.11\ 10^9$y, in excellent agreement with the meteoritic age $t_\odot = 4.57 \pm 0.02 \cdot 10^9$ y, [BAH95]. As a further result, the most favoured value for the zero-energy astrophysical factor has been deduced $S_{11} = 4.00 \cdot 10^{-25}$ Mev b.

Many SMs reproduce p-mode frequencies within an uncertainty of 0.1% without any special adjustment of the input parameters. Over the entire region of the Sun for which the helioseismological values are determined ($0.05 \leq x \leq 0.95\, R_\odot$) the computed profiles of P and ρ agree very well with helioseismological data, the difference being lesser than 1%. In these regions T varies by a factor of 20 while the molecular weight changes at

a level of few percent. The agreement is worse in the deepest solar core and in the most external layer. A direct reconstruction from helioseismology either of T_c and of $\nu_\odot$ flux is impossible: data only constrain the range of the allowed values, checking the agreement of different SMs with measurements (*e.g.* the ^{8}B and ^{7}Be ν fluxes are differently constrained, at a level not greater than 25% for the latter, [RIC99]).

3.8. Reference solar model.

For many years Bahcall's SMs have been seen as "reference" model or "the" SSM, [BAH88, BAH92, BAH95, BAH98a]. The last one updates and refines the analyses within a "classic" treatment, [BAH01a, BAH02c].
As input parameters the model takes cross-sections from [ADE98, ANG99], the OPAL96 opacities from [ROG96a], the low temperature opacities from [ALE94], equations of state from [IGL96], the solar composition from [GRE98] (even if the OPAL96 equations of state are not available with these values), the electron and ion weak screening treatment from [GRU98]; the He and heavy metal diffusion from [THO94, BAH95]. Furthermore, a new electron density profile and time evolution are done and the mixing length treatment has been applied. The pre-main sequence evolution is not included because its effect on the internal solar structure is estimated negligible on $\nu_\odot$ production, [BAH94a, MOR00].
The physical variables under analysis (M, R, T, ρ, P, L, source densities of 8 different ν fluxes, H-^{3}He-^{4}He-^{7}Be-^{12}C-^{14}N-^{16}O mass fraction, electron density) are given in 875 separate radial shells in the Sun. $L_\odot = 3.844 \cdot 10^{26}\, W$, (3.842 in $\nu_\odot$ flux calculations), $R_\odot = 6.9598 \cdot 10^8\, m$, $t = 4.57 \cdot 10^9\, y$ are the input values.
The structure of the Sun is estimated to be affected only very slightly by the solar radius: in fact the available values differ as much as less than 1 part in 10^3, [BAH97b].
The time evolution of many parameters, including the depth of the convective zone, has been calculated from the Sun entrance into the main sequence up to an age of $8{\cdot}10^9$ y. The derived c_s well agrees with helioseismological data: the fractional difference is less than 10^{-3} over the interval 0.05 - 0.95 $R_\odot$ while in the region $x \leq 0.25\, R_\odot$, where $\nu_\odot$'s are produced, this discrepancy is lesser than $7 \cdot 10^{-4}$, see fig. 4.
We resume the most important conclusions:

- $R_\odot$ increases monotonically with a rise of 13% up to now; it will further increase by a factor of 1.17, see fig. 6.
- $L_\odot$ rises its value from the $\sim$ 67% up to $\sim$ 136% of the present one.
- The ^{3}He-^{3}He termination reactions produce 87.8% of the present $L_\odot$, the ^{3}He-^{4}He and CNO cycle contributing respectively at a level of the 10.7% and 1.5%: at an age of $8{\cdot}10^9$ y these values will become 57.6%, 20.4% and 22.0%. The energy loss due to solar expansion varies from 0.03 up to 0.07%, see fig. 7.
- T_c increases from $\sim 1.4{\cdot}10^7$K up to $\sim 1.9{\cdot}10^7$K, see fig. 8; $R_\odot$ shows the same behaviour, in fact the ratio $R_\odot/T_c$ is almost constant, within $\sim$ 1.5%.
- The hydrogen mass fraction in the solar core decreases from the starting value of $\sim$ 0.7 to the present one (0.34) to the final value of $\sim$ 0.15 of the total solar mass.

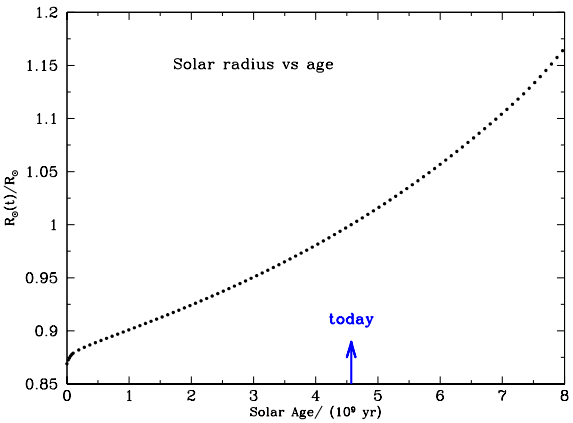

Figure 6. $R_\odot(t)$ as a function of the solar age with respect to the present value, from [BAH01a].

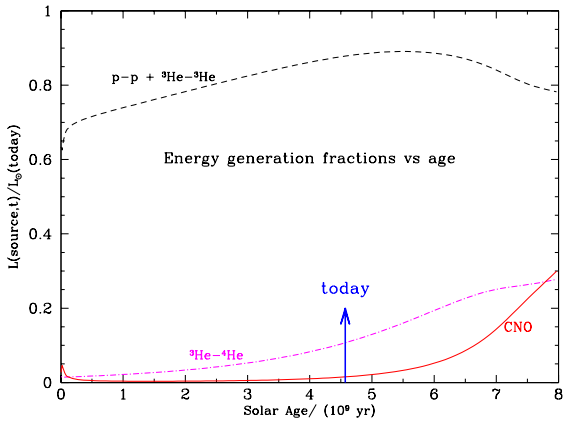

Figure 7. The fraction of $L_\odot$ with respect to the present value produced by nuclear fusion reactions versus solar age, from [BAH01a]: the $p-p$ branch, terminated by the ^{3}He-^{3}He reaction, (dashed curve); the ^{3}He-^{4}He branch (dot-dashed curve); the CNO cycle (solid line), from [BAH01a].

- $\nu_\odot$ flux values are given in table 8; some uncertainties are increased with respect to the previous Bahcall's SSM, [BAH98a].

Different astrophysical factors have been used in [BAH02c] and a new ^{8}B $\nu_\odot$ flux has been computed (without significant variations in the remaining solar quantities); in following papers, see [BAH02f], this upgrading has been not confirmed, due to a more conservative analysis of the presently available experimental measurements of related fusion cross-sections.

3.9. Other solar models.

Many SMs were presented and it is impossible to list them or their features; we mention [PRO94, CHR96, CAS97, GUE97, DAR98, BRU99, DAR99, SCH99, TUR01c, WAT01,

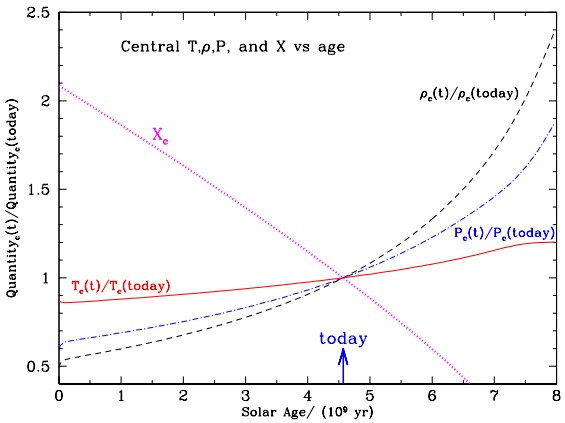

Figure 8. The temporal evolution of T_c (solid line), ρ_c (dash line), P_c (dot-dash line) and X_c (dotted line), from [BAH01a].

COU02] among models proposed in the last decade. We refer to [BOO02]for a detailed analysis of the individual influence of parameters like radius, time evolution, luminosity, heavy element abundance, equations of state ... on SM calculations.
Even non-standard SMs were suggested searching for the explication of the experimental $\nu_\odot$ deficit compared with the theoretical expectation based on the standard evolutionary SMs, see sections 3.10 and 7.1. We mention models having a core with low Z, [JOS74, LEV94, JEF97]: in this case low opacity and lower T_c have to be expected.
Presently, many researchers are working on the so called "seismic" SMs, a dynamical evolution of standard SMs in which strong constraints on solar parameters and on evolution are deduced from helioseismology. In general, "seismic" SMs are directly derived from seismic measurements and use primary inversion of data producing c_s and ρ profiles. After the addition of "normal" physical conditions, P and T profiles and the Y value are computable, [KOS91, DZI95a, BAS96a, BAS96b, SHI96, ANT98].
In SMs the chemical abundance distribution is obtained by following the time evolution, where the nuclear reactions and the diffusion processes are taken into account. The chemical composition is assumed to be uniform at zero-age; in many non-standard SMs other time evolution processes are introduced and/or the initial conditions at t = 0 are different. Seismic SMs do not follow the time evolution: the helioseismologically determined c_s profile is imposed as a constraint.
If only the X, Y and Z value are introduced, c_s is a function of P, T, X and Z

$$c(P,T,X,Z) = c_{obs}(r) \tag{36}$$

This inversely relates X with P, T, Z and c_s,

$$X = X(P,T,Z,c_{obs}) \tag{37}$$

If Z is given, the basic equations can be solved with the proper boundary conditions. The helioseismically reconstructed $\rho_{obs}(r)$ profile can be used as further constraint in computing a seismic SM and in addition to c_s it determines the Z profile as a part of

the solution. Both the weak dependence of the equations of state upon Z and the error of $\rho_{obs}(r)$, which is much larger than that of $c_{obs}(r)$, even by a factor of 10, have to be pointed out.
Very recently, the contributions of solar rotations and $B_\odot$ have been added in solar codes to better estimate the evolution, [COU02]; in any case the way the convection acts is not clear.
In [BRU98, BRU99] a new term is introduced in the "standard solar equations" describing physical processes which better reproduce properties in the layer between convective and radiative zone. The aim is a change in rotation rate which is supposed to contribute to a turbulent mixing in a thin layer where $B_\odot$ could maximally act. A macroscopic diffusion, describing the mixing in a shear layer between the convective zone (where a differential rotation is present) and the radiative zone (which is rotating as a "solid") is added *via* a diffusivity term in equation describing chemical evolution:

$$\frac{\partial X_i}{\partial t} = -\frac{\partial(4\pi\rho r^2 X_i V_i)}{\partial m} + nuclear\,terms \tag{38}$$

where the velocity V_i of species i with respect to the centre of mass depends both on microscopic and macroscopic diffusion and on concentration gradient. It is possible to imagine an anisotropic turbulence with viscous transport much stronger in the horizontal than in vertical direction.
In order to solve the solar equations, simplifying assumptions concerning the strength of velocities, ρ variation and tachocline dimension are introduced. The mixing in the tachocline depends on rotation and differential rotation rate; moreover, it is related to horizontal diffusivity and Brunt-Väisälä frequency. The tachocline width evolution in time and the efficiency of the mixing are also analysed.
Opacities from [IGL96], the equations of state from [ROG96a], the solar chemical composition from [GRE96], the reaction rates from [ADE98, ANG99] (with the exception of proton capture on Li from [ENG92]), the nuclear screening from [MIT77, DZI95b], the microscopic diffusion from [MIC93]; an estimated solar age of $4.55{\cdot}10^9$ y after a $5{\cdot}10^7$ y of pre-main sequence phase have been used as input parameters. In fig. 9 the solar sound speed difference profile computed for either Z calibrated or Z free SMs are shown. Among many interesting results, a good ^{7}Li depletion has been obtained without a corresponding ^{9}Be deficit, according with newest photospheric observation, [BAL98]. These results seem to be dependent on the adopted Brunt-Väisälä frequency. This SM presents a mixing at the base of the convective zone, an increased value both for Z at the surface and for the opacity; the discrepancy between the seismic c_s profile and the reconstructed one is lower. In any case, Z at surface is within the experimental uncertainties, [TUR00, TUR01a].
A "seismic" SM has been proposed in [TUR01c]. Thanks to the long duration of SOHO data taking, low order modes ($n \leq 9$) of lowest degree ($l = 0, 1, 2$), which are more insensitive to the turbulence of upper solar layers, have allowed an upgrade of the inversion method used to compute the c_s profile. The new c_s fractional error is $\sim 2{\cdot}10^{-4}$, with a small increase up to $\sim 5{\cdot}10^{-4}$ in the more external region. The spatial uncertainty

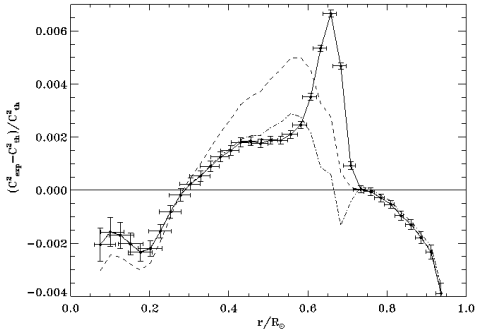

Figure 9. The effect of calibration on the sound square speed difference between the SM [BRU98] and two SMs including a macroscopic diffusion term: B_t calibrated in Z/X (- - -) and B_{tz} with a non calibrated Z_0 =Z_0^{std} = 0.01959 (dash dot line), from [BRU99].

remains at a level ranging from 1 up to 3.5 %. These constraints are imposed to the [BRU99] model; moreover, the p-p reaction rate has been enhanced at a level of 1% while Z_0 is 3.5% greater than in [BRU99]. A smaller radius ($R_\odot = 6.95865 \cdot 10^8$ m) and a 10^7 y pre-main sequence time have been introduced in computations. A good agreement with helioseismological c_s profile is obtained, even if a large difference is present in very external solar layers, $x \geq 0.95\, R_\odot$. The computed $\nu_\odot$ flux does not show significant deviations from the previous estimated one in [BRU99].

An upgraded "seismic" SM has been proposed in [COU02]: it is computed with a 1D quasi-static stellar evolution code which includes pre-main sequence and solves the stellar structure equations by a spline coefficient method as in [BRU99, TUR01c]. The main characteristics are: the nuclear reaction rates from [ADE98], the screening treatment from [MIT77], the astrophysical factor from [ENG92, HAM98a]; the time step and the rotation law were modified to take into account the Li burning in pre-main sequence, [PIA02]; the opacities from [IGL96] for T$\geq$ 5600 K, for lower T values from [ALE94]; the equation of state from [ROG96b] while the microscopic diffusion is from [MIC93] and the turbulent mixing at the base of the convection zone is from [BRU99]. Large screening and mixing in the central region are excluded following [TUR01b].

The inversion procedure for c_s and ρ profiles is based on the Optimally Localised Averaging method, [KOS99]. Hydrodynamic prescriptions are introduced to define tachocline: they reduce the influence of the diffusion of heavy elements toward the solar centre and allow to burn ^{7}Li on the main sequence. A correct ^{7}Li abundance at the solar surface is computed, the value according to [GRE93].

The p-p cross-section, which has a strong influence on c_s, is increased by 1% so that T_c slows down; Z_0 is higher (3.9%) therefore the Rosselland opacities and the mean molecular weight are different. In fig. 2 the profiles of heavy metal contribution and Rosselland opacities are plotted as a function of the distance from the solar core. In

such a model, c_s decreases in the core because the raise of μ dominates the T raise due to a greater opacity value. On the contrary, at d$\geq$ 0.3 $R_\odot$ the raise in T overcomes the increase of μ so that c_s goes up. The higher Z initial does not modify the c_s profile.
In order to reduce the differences at the base of the convective zone, the parameters defining the tachocline have been modified by introducing a lower width, a slightly greater rotation rate and a higher Brunt-Väisälä frequency.
However, a better agreement with solar parameters has been searched for by calibrating this SM at a radius value different from the standard photometric one. Recent analyses based on f-mode frequencies have given respectively $R_\odot = 6.9578 \cdot 10^8$m, [SCH97], and $R_\odot = 6.9568 \cdot 10^8$m, [ANT98], while optical determination indicates $R_\odot = 6.9551 \cdot 10^8$m, [BRO98]. Presently there is neither an answer explaining these discrepancies, nor the effect of the solar cycle on the radius. The value used in computation is $R_\odot = 6.95936 \cdot 10^8$m.
The impact of solar age has been checked: if $t_\odot$ increases, the discrepancy on c_s below 0.2 $R_\odot$ diminishes while the differences in ρ are greater. $t_\odot = 4.6$ Gyr seems to be a satisfactory value (the value needed to best reduce the discrepancy on ρ below 0.6 $R_\odot$ is 4.55 Gyr). A higher $t_\odot$ value is strongly disfavoured by ρ while c_s does not rule it out (but does not strongly support it too).
In fig. 5 the solar sound speed difference profile is shown for the basic model; for comparison also ρ difference profiles concerning different SMs are drawn.
Different $B_\odot$ profiles have been introduced in the calculations but none of the so computed models greatly modify the $\nu_\odot$ flux predictions: it seems that $B_\odot$ has a quite slight impact.
Italian contributions to solar modeling and their critical evolutions were done by V.Castellani, G.Fiorentini, O.Straniero and coll., [STR89, CAS97]. In [CAS97] a "helioseismological" constrained SM was proposed, FRANEC being the code for computation. Opacity from [ROG95], equations of state from [ROG96b], Z value from [GRE93], molecular opacity at T$\leq 10^4$K from [ALE94], He and heavy metal diffusion from [THO94], a time evolution step of $\sim 3 \cdot 10^7$y, updated nuclear cross-sections are the main input parameters.
Papers concerning refinements and constraints both in solar and $\nu_\odot$ physics were published, [RIC97, DEG97, DEG98a, FIO99a, FIO99b, CAS99, DZI99, RIC99, FIO00, RIC00, FIO01a, FIO01b, FIO01c, FIO02]: the influence of screening factor, plasma collective effects, solar age, solar radius and opacity on $\nu_\odot$ flux, characteristics of ^{7}Be $\nu_\odot$ and ^{8}B $\nu_\odot$ component and relations between them, uncertainties in solar parameters have been analysed in detail.
The model done by A.Dar and G.Shaviv, [DAR96, DAR98, DAR99], uses quite different values for nuclear reaction rates, modified screening and diffusion description. Each element is separately diffused inside the Sun and diffusion coefficients are calculated for the local ionisation state; both these values are in agreement with [RIC96]. Moreover, Z value from [GRE96] was introduced, Y value being an adjustable parameter.
Watanabe and Shibahashi have realized "seismic" SMs both with homogeneous Z and

with low-Z core, see [WAT01] and references therein. In this case, the low-Z solar core is larger than in SSMs, therefore the opacity is decreased as well as T_c, μ is smaller to balance the lower T_c; the X value is increased, the core density is higher to compensate the lower nuclear reaction rate due to the lower T_c; P is higher. All the other parameters and equations are "standard". The effect of various uncertainties in microphysics upon the seismic SM with homogeneous Z and the theoretically expected $\nu_\odot$ fluxes (which were investigated by a Monte Carlo simulation) are summarised in table 11.
In [WIN01] SMs which upgrade models previously computed in [GUE97] are analysed. Routines and equations are "standard" but an enhanced contribution due to heavy elements, slightly different values of $L_\odot$ and shells have been introduced: 16 non-standard SMs and 4 SSMs have been computed. Among non-standard SMs, only two models are marginally compatible with observations: in any case an upper limit to Z contribute to the accretion of the Sun during its early main sequence phase is provided. A "good" SSM, having predictions in agreement with experimental results within the errors, is present but Z_{surf} is high and ^{8}B $\nu_\odot$ flux is large.
Table 5 and table 6 summarize characteristics of different SMs.

BAH01a is the reference Bahcall's SSM; values up to Rad_{508} are concerning SSMs which use only different input parameters with respect to [BAH01a]. Model NACRE uses the charged particle fusion cross-sections from [ANG99]; model ASP00 uses a lower abundance $Z/X = 0.0226$ [ASP00]. Models from GRE93 up to Rad_{508} use the value of Z quoted in [GRE93]. Model Pre-MS is evolved from the pre-main sequence stage; model Rot incorporates mixing induced by rotation and is a "reasonable" upper bound to the degree of rotational mixing consistent with the observed Li solar depletion. Rad_{78} is a model using a solar radius of $6.9578 \cdot 10^8$ m, [ANT98], while in Rad_{508} the adopted value is $6.95508 \cdot 10^8$ m, [BRO98]. These models are consistent with the helioseismological data; their rms sound speed differences with respect to [BAH01a] are: 0.03% (Pre-MS), 0.08% (Rot), 0.15% (Rad_{78}), and 0.03% (Rad_{508}).
No-Diff model does not use diffusion of elements; Old model uses older equations of state and opacities; $S_{34} = 0$ model introduces a null ^{7}Be production, so that no $\nu_\odot$'s from ^{7}Be or ^{8}B are present; Mixed model modifies the solar core composition following [CUM96]. The remaining SMs are quoted in references.

3.10. Solar neutrinos.

Following the SMs, even ν's are produced in p-p and CNO reaction chains, see table 1 and table 2. Energy conservation law constrains the total $\nu_\odot$ flux to be fixed by $L_\odot$. If the Sun is supposed to be in steady state with nuclear energy production equal to $L_\odot$, the basic reaction $4\,p^+ + 2\,e^- \rightarrow {}^4_2 He + 2\,\nu_e$ produces 26.732 MeV, the Q value of the reaction.

Table 5. *Characteristics of solar models. The quantities T_c (in units of 10^6 K), ρ_c (10^2 gm cm^{-3}), and P_c (10^{17} erg cm^{-3}) are the present central temperature, density, and pressure; Y and Z are the He and heavy element mass fractions, the subscript "$_0$" shows the zero-age main sequence value while "$_c$" indicates the values in the solar core. The symbol "-" means not indicated.*

Model	T_c	ρ_c	P_c	Y_0	Z_0	Y_c	Z_c
BAH01a	15.696	152.7	2.342	0.2735	0.0188	0.6405	0.0198
NACRE	15.665	151.9	2.325	0.2739	0.0188	0.6341	0.0197
ASP00	15.619	152.2	2.340	0.2679	0.0187	0.6341	0.0197
GRE93	15.729	152.9	2.342	0.2748	0.02004	0.6425	0.02110
Pre-MS	15.725	152.7	2.339	0.2752	0.02003	0.6420	0.02109
Rot	15.652	148.1	2.313	0.2723	0.01934	0.6199	0.02032
Rad_{78}	15.729	152.9	2.342	0.2748	0.02004	0.6425	0.02110
Rad_{508}	15.728	152.9	2.341	0.2748	0.02004	0.6425	0.02110
No-Diff.	15.448	148.6	2.304	0.2656	0.01757	0.6172	0.01757
Old	15.787	154.8	2.378	0.2779	0.01996	0.6439	0.02102
$S_{34} = 0$	15.621	153.5	2.417	0.2722	0.02012	0.6097	0.02116
Mixed	15.189	90.68	1.728	0.2898	0.02012	0.3687	0.02047
PRO94	15.66	154.7	–	0.2707	0.01907	0.6370	0.02013
RIC96	15.67	154.53	2.350	0.2793	–	0.6465	–
CAS97	15.69	151.8	–	0.2690	0.0198	0.630	0.0198
GUE97	15.74	153.11	2.355	–	0.0200	–	0.0211
BRU99	15.71	153.1	–	0.2722	0.01959	0.6405	0.02094
DAR99	15.61	155.4	–	0.2509	0.01833	0.6380	0.01940
MOR99	15.73	153.8	–	0.2723	0.0197	0.6418	0.0210
SCH99	15.7	152.0	–	0.275	0.020	–	0.018
WAT01	15.61	156.0	2.378	–	–	0.6437	0.0180
WIN01	15.885	154.17	2.3605	–	0.0220	–	0.0232
COU02	15.739	153.02	2.3375	0.2759	0.02035	0.6445	0.02168

A roughly estimated $\nu_\odot$ flux on the Earth is thus:

$$\Phi \simeq \frac{2\,S_\odot}{Q\,-\,2\,E_\nu} \sim 6.5 \cdot 10^{10}\,\nu_e\,cm^{-2}\,s^{-1} \tag{39}$$

$$S_\odot = \frac{L_\odot}{4\,\pi\,d^2} \sim 1.367\,kW m^{-2} = 8.533 \cdot 10^{11}\,MeV\,cm^{-2} s^{-1}$$

where d is the Earth-Sun distance and $S_\odot$, the present "solar constant" is affected by an uncertainty of $\sim 0.4\%$.

The $\nu_\odot$ energy spectrum can be thought as a "superposition" of β-decay spectra with an addition due to the electron capture processes, see fig. 10; it is computed in the

Table 6. *Characteristics of the convective zone and surface: Y_{surf} and Z_{surf} are the He and heavy element abundances at surface, α is the mixing length parameter, R_{CZ} and T_{CZ} are the radius and temperature at the base of the convective zone, and M_{CZ} is the mass included within the convective zone. The symbol "–" means not indicated.*

Model	Y_{surf}	Z_{surf}	α	R_{CZ} ($R_\odot$)	M_{CZ} ($M_\odot$)	T_{CZ} (10^6 K)
BAH01a	0.2437	0.01694	2.04	0.7140	0.02415	2.18
NACRE	0.2443	0.01696	2.04	0.7133	0.02451	2.19
ASP00	0.2386	0.01684	2.05	0.7141	0.02394	2.18
GRE93	0.2450	0.01805	2.06	0.7124	0.02457	2.20
Pre-MS	0.2455	0.01805	2.05	0.7127	0.02443	2.20
Rot	0.2483	0.01797	2.03	0.7144	0.02388	2.15
Rad_{78}	0.2450	0.01806	2.06	0.7123	0.02461	2.20
Rad_{508}	0.2450	0.01806	2.06	0.7122	0.02467	2.20
No-Diff.	0.2655	0.01757	1.90	0.7261	0.02037	2.09
Old	0.2476	0.01796	2.04	0.7115	0.02455	2.21
$S_{34} = 0$	0.2422	0.01811	2.03	0.7151	0.02309	2.17
Mixed	0.2535	0.01782	1.85	0.7315	0.01757	2.02
PRO94	0.2422	0.01758	1.677	0.715	0.02340	–
RIC96	0.2584	–	1.768	0.716	–	2.175
CAS97	0.238	0.0182	1.90	0.716	–	2.17
GUE97	–	0.018	–	0.716	0.0234	–
BRU99	0.2508	0.01858	1.755	0.7141	–	2.194
DAR99	0.2308	0.0170	–	0.7130	–	2.105
MOR99	0.2436	0.0181	1.924	0.7138	–	–
SCH99	0.245	0.18	–	0.713	0.0264	2.19
WAT01	0.2455	0.018	–	–	–	–
WIN01	0.2519	0.0198	–	0.7128	0.02449	–
COU02	0.2508	0.01918	1.934	0.7115	0.025	2.22

standard way:

$$\frac{dN}{dp_e} \propto (E - E_{kin,e})^2 \; p_e^2 F(Z, E_{kin,e}) \tag{40}$$

where p_e is the momentum of the electron.

Eight ν sources are available within the p-p and CNO reaction chains: six of them give rise to continuous energy spectra while the remaining two, p-e-p and ^{7}Be, produce monochromatic lines. The global energy fractions carried out by $\nu_\odot$'s are different for the various reaction chains, see table 3, but the most part of the energy released to solar matter is produced in the p-p I branch: since only one ν source is present, its amount is strictly related to $L_\odot$ and therefore less dependent on adopted SM.

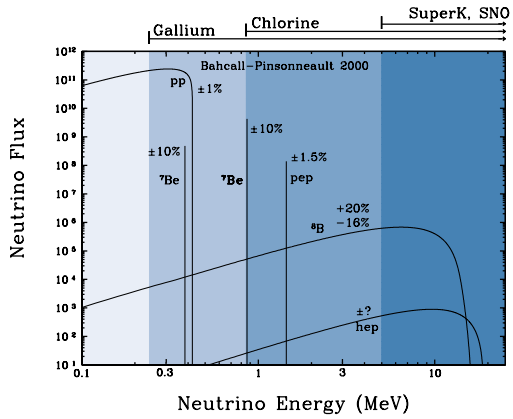

Figure 10. The p-p neutrino energy spectrum with related uncertainties as computed in reference solar model, [BAH01a]; the detection energy range allowed for different experiments is also shown, from [BAH01a].

The relative contribution of various $\nu_\odot$ sources is depending on inner solar conditions, mainly T_c, ρ and chemical composition.
In [BAH96a] a power law between nuclear fusion reactions, $\nu_\odot$ flux and T_c was found: $\Phi(pp) \propto T_c^{-1.1\pm0.1}$, $\Phi(pep) \propto T_c^{-2.4\pm0.9}$, $\Phi(Be) \propto T_c^{10\pm2}$, $\Phi(B) \propto T_c^{24\pm5}$, $\Phi(N) \propto T_c^{24.4\pm0.2}$, $\Phi(O) \propto T_c^{27.1\pm0.1}$ and $\Phi(F) \propto T_c^{27.8\pm0.1}$. Hence, T_c indicates the dominant process in p-p chain: the p-p I when $T_c \leq 1.6\cdot10^7$K; p-p II if $1.6\cdot10^7K \leq T_c \leq 2.3\cdot10^7K$ and p-p III at higher temperature. All $\nu_\odot$ flux components, with the exclusion of p-p term, are strongly T_c dependent, so that $\nu_\odot$ flux and solar features are strictly related. Produced $\nu_\odot$'s are of electronic type: they escape from the Sun without any interaction with the solar matter and reach the Earth. Following the hypotheses done in SMs, this flux is not reduced and without changes in energy spectrum. Their experimental detection and the determination of their energy spectrum enable us to check the solar interior and T_c; moreover, a test for solar and stellar astrophysics is allowed. In practice $\nu_\odot$'s are the most efficient instruments to evaluate the nuclear aspects into the central solar regions.
Fig. 11 presents the $\nu_\odot$ production as a function of the distance from the solar centre and of the mass fraction inside this sphere. The right location of these maxima is weakly SM dependent: it is possible to estimate more than 90% of the total p-p $\nu_\odot$ production at distance x$\leq$ 0.2 $R_\odot$; ^{7}Be $\nu_\odot$'s are produced at x$\leq$ 0.06 $R_\odot$, ^{8}B $\nu_\odot$'s at x$\leq$ 0.05 $R_\odot$.
The number of produced $\nu_\odot$'s depends on their reaction rate r which is related to the value of all physical parameters in each inner solar point; therefore it is the selected SM that changes their flux.
If N_i is the number of $\nu_\odot$'s produced in a specific nuclear reaction i, then:

$$N_i = 4\pi \int_0^{R_\odot} x^2 r_i(x, P, T, ..)dx \tag{41}$$

where the distance from the solar centre is x while $r_i(x, P, T, ..)$ is the rate of the i-reaction. The integral has to be computed at each distance the reaction occurs: the

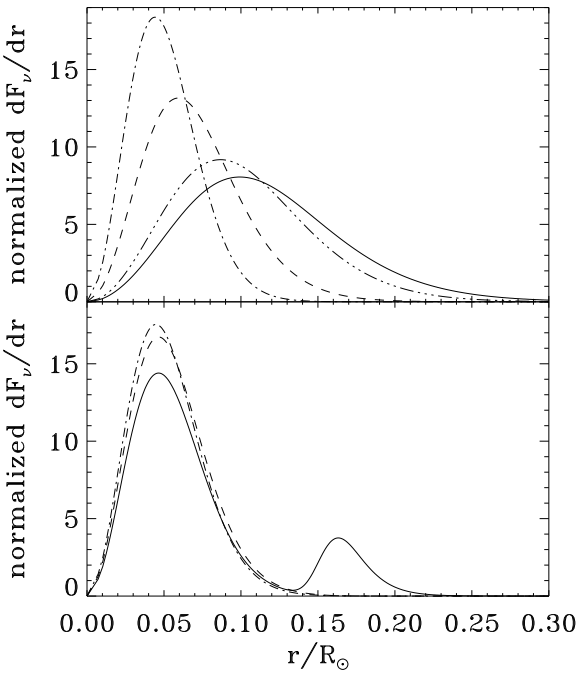

Figure 11. Neutrino production as a function of the distance from the solar centre. In the upper figure: p-p (plain curve), ^{8}B (dot-dashed curve), ^{7}Be (dashed curve), pep (dot-dot-dot-dashed curve) neutrinos are shown. In the lower figure: ^{13}N (plain curve), ^{15}O (dashed curve), ^{17}F (dot-dashed curve) neutrinos are reported. $(1/F_t)\,(dF/dr)$ is drawn for each component where F is the flux in s^{-1}, r the fractional radius, F_t the total flux for the selected component, from [COU02].

maximum distance from the solar centre depends on the selected nuclear process but it is in any case lesser than $R_\odot$ because of the threshold temperature, see fig. 11.
The p-p $\nu_\odot$'s are the most abundant: they are produced in the first step of the fusion reaction chain and have a continuous energy spectrum up to 420 keV. Their flux is practically SM independent, being related to $L_\odot$. A small fraction is due to the 3-bodies reaction, p-e-p, with the emission of a monoenergetic ν at E = 1.44 MeV.
^{7}Be $\nu_\odot$'s are monoenergetic; the prediction of their flux is quite stable; they are produced in a secondary branch of the cycle; $\sim 90\%$ of them are emitted in a line at 863 keV, the remaining at E = 386 keV.
^8B $\nu_\odot$ flux is affected by a large uncertainty. The suppression of this component would have no impact on $L_\odot$; they are produced in a very small branch of the p-p chain, but their energy extends up to 14 MeV and therefore they are more easily detected than the previous ones.
CNO $\nu_\odot$'s give a small contribution in the ongoing experiments because their flux and energy are low; ^{13}N and ^{15}O β-decays correspond to the thermal energy derived from the reactions having ^{12}C and ^{13}C as starting nuclei. On the other hand, the $\nu_\odot$ flux from ^{17}F β-decay is a potential measure of the primordial ^{16}O abundance but it gives a very small contribution to $L_\odot$, [BAH82].

The so called Hep component of the $\nu_\odot$ flux is the most energetic and mysterious. Its value is affect by a great uncertainty ($\sim 100\%$); it is the less abundant in $\nu_\odot$ flux by many orders of magnitude, [BAH98b].
In table 7 the $\nu_\odot$ production in the Sun is quoted,[COU02].

The reference model, [BAH01a], also proposes a time evolution of the $\nu_\odot$ flux up to

Table 7. *The $\nu_\odot$ production in the Sun, adapted from [COU02].*

Reaction source	SUN $10^{33}\nu\, s^{-1}$
p-p	167300
p-e-p	393.6
^{7}Be	13720
^{8}B	14.08
^{13}N	1631
^{15}O	1406
^{17}F	8.72

an age of $8{\cdot}10^9$ y, see fig. 12. The p-p $\nu_\odot$ flux remains almost constant in time: at the beginning of the main sequence its value was the 75% of the present one and its variation is $\sim 4\%$ per 10^9 y. It will reach its maximum (4% higher than the present value) at the age of $6.0{\cdot}10^9$ y and then it will decline very slowly. The ^{7}Be $\nu_\odot$ flux started at a low level (14% of the present one) and it will increase monotonically by a factor of 2.6 . At the beginning of main sequence, the ^{8}B $\nu_\odot$ flux was very small ($\sim 3\%$ of the present one); it will increase up to a value greater by a factor of 8.1 with a fast rise of 120% per 10^9 y. The ^{13}N $\nu_\odot$ flux was 11 times larger than the present one during the first 10^8 y on the main sequence; then it decreased down to 1/3 to the present one at an age of $1.8{\cdot}10^9$ y and it started to go up steadily as T_c increases. Its final value will be larger by a factor of 18 with respect to the present value.

3.11. Solar neutrino flux on Earth.

Usually all SMs assume standard model for electroweak interactions without mass and magnetic moment for ν's; moreover, the energy emission from the Sun is supposed to be isotropic. The solar matter is in practice totally transparent for ν's (the mean free path for $\nu_\odot$'s is $\approx 10^{18}$ m, a value much greater than $R_\odot \approx 10^9$ m).
The flux which should be measured on Earth surface is then:

$$\Phi_i = \frac{N_i}{4\pi d^2} \tag{42}$$

The distance d between Earth and Sun is variable from $1.471{\cdot}10^{11}$ m in January (perihelion) up to $1.521{\cdot}10^{11}$ m in July (aphelion) because of the ellipticity of the

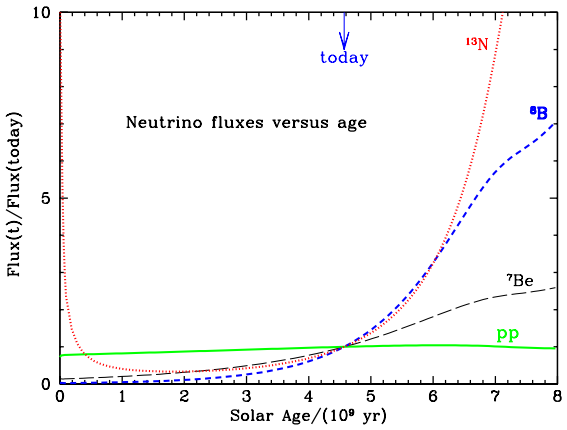

Figure 12. P-p (solid line), ^{7}Be (long dashes), ^{8}B (short dashes), and ^{13}N (dotted line) neutrino fluxes as a function of solar age with respect to the present value are shown, from [BAH01a].

terrestrial orbit, therefore:

$$d = d_0(1 + \epsilon \cos \pi t) \tag{43}$$

where ϵ =0.0165 is the eccentricity. Consequently, the $\nu_\odot$ flux varies at a level of some percent between January and July.
The total interaction rate of $\nu_\odot$'s inside a detector having a mass M is:

$$I = MN_{Av}\frac{X}{A}\sum_i \Phi_i \int_{E_{thr}}^{E_{max}} \frac{d\lambda_i}{dE}\sigma(E)dE \tag{44}$$

σ(E) is the ν capture cross-section, Φ_i is the integral flux on Earth of i-type $\nu_\odot$'s, X is the isotopic abundance of nucleus with mass number A, N_{Av} is the Avogadro's number and $\frac{d\lambda_i}{dE}$ is the differential normalized energy spectrum of $\nu_\odot$'s produced by i reaction.
The interaction rate per target atom is:

$$R = \sum_i \Phi_i \int_{E_{thr}}^{E_{max}} \frac{d\lambda_i}{dE}\sigma(E)dE = \sum_i \Phi_i \overline{\sigma_i} \tag{45}$$

where $\overline{\sigma_i}$ is the capture cross-section averaged on the energy spectrum.
R is usually measured in SNU, the Solar Neutrino Unit, which means 1 capture per second per 10^{36} target nuclei: this is the not a flux unit but an interaction rate unit.
In table 8 the values of $\nu_\odot$ flux on Earth from different SMs are listed. There is a general good agreement among results computed under different working hypotheses: if models with unusual assumptions are excluded, p-p $\nu_\odot$ values agree within 1% while the differences on ^{7}Be and ^{8}B components are respectively at a level not greater than 10% and 35%.

3.11.1. Time variations. It is usually assumed that the Sun is in a steady state therefore SMs do not predict $\nu_\odot$ flux variation on short time-scale. In any case, different effects are suspected to produce modulations:

Table 8. *Solar neutrino fluxes on Earth from different solar models, the unit is $\nu\, cm^{-2}s^{-1}$; the multiplying factor is also reported. Interaction rates on Cl and Ga are shown in the last two columns. The symbol "-" means not computed or not indicated.*

Model	p-p 10^{10}	p-e-p 10^8	Hep 10^3	^{7}Be 10^9	^{8}B 10^6	^{13}N 10^8	^{15}O 10^8	^{17}F 10^6	Cl SNU	Ga SNU
BAH01a	5.95	1.40	9.3	4.77	5.05	5.48	4.80	5.63	7.6	128
NACRE	5.97	1.39	9.4	4.85	5.54	4.93	4.24	5.39	8.0	128
ASP00	5.99	1.41	9.4	4.62	4.70	5.25	4.56	5.33	7.1	126
GRE93	5.94	1.39	9.2	4.88	5.31	6.18	5.45	6.50	8.0	130
Pre-MS	5.95	1.39	9.2	4.87	5.29	6.16	5.43	6.47	7.9	130
Rot.	5.98	1.40	9.2	4.68	4.91	5.57	4.87	5.79	7.4	127
Rad_{78}	5.94	1.39	9.2	4.88	5.31	6.18	5.45	6.50	8.0	130
Rad_{508}	5.94	1.39	9.2	4.88	5.31	6.18	5.45	6.50	8.0	130
No-Diff	6.05	1.43	9.6	4.21	3.87	4.09	3.46	4.05	6.0	120
Old	5.95	1.41	9.2	4.91	5.15	5.77	5.03	5.92	7.8	130
$S_{34} = 0$	6.40	1.55	10.1	0.00	0.00	6.47	5.64	6.70	0.8	89
Mixed	6.13	1.27	6.2	3.57	4.13	3.04	3.05	3.61	6.1	115
PRO94	5.98	1.42	1.23	4.79	5.46	5.02	4.27	5.16	7.71	130.1
RIC96	5.94	1.38	–	4.80	6.33	5.59	4.81	6.18	8.49	132.8
CAS97	5.99	1.40	–	4.49	5.16	5.30	4.50	–	7.4	128
GUE97	5.95	1.40	1.22	4.94	5.96	5.64	4.89	5.92	8.35	133
BRU99	5.98	1.41	–	4.70	5.99	4.66	3.97	–	7.04	127.1
DAR99	6.10	1.43	–	3.71	2.49	3.82	3.74	4.53	4.10	115.6
MOR99	5.91	1.40	–	4.90	5.68	5.73	4.96	6.41	8.31	130.1
SCH99	–	–	–	–	5.18	–	–	–	7.79	128.7
WAT01	5.98	1.44	2.11	4.72	4.77	4.43	4.15	5.22	7.17	126
WIN01	5.90	1.38	2.03	5.07	5.63	7.30	6.48	7.50	8.16	136
BAH02c	5.95	1.40	9.3	4.77	5.93	5.48	4.80	5.63	8.6	129.9
COU02	5.92	1.39	–	4.85	4.98	5.77	4.97	3.08	7.48	128.1

- **Day-Night effect** = The line of sight between a detector and the Sun intersects different part of Earth so that a little variation in $\nu_\odot$ flux could be present due to different density the $\nu_\odot$'s cross.
- **Winter-Summer effect** = The distance between Sun and Earth is not constant because of eccentricity of terrestrial orbit; a difference at a level of some % is expected but it is below the present detectors sensitivity, with the exception of SuperKAMIOKANDE.
- **Other solar features** = Many authors have looked for a correlation between the $\nu_\odot$ flux and solar features: sunspots number, [BAH87, BIE90, DOR91], $B_\odot$ strength at

surface, [MAS93, OAK94], green-line corona intensity, [MAS95b, MAS95c, MAS96], solar wind flux, [MCN95].
If $\nu_\odot$'s have a non-standard interaction with $B_\odot$ a further effect is possible. In fact solar equatorial plane forms an angle of 7°.25 with the Earth's orbital plane: therefore the solar core, where $\nu_\odot$'s are produced, is viewed from the Earth by different position. The line of sight crosses the solar equator where $B_\odot$ weaker than at higher latitude should be present.

3.12. Uncertainties in the neutrino flux.

The procedure for estimating the uncertainties in $\nu_\odot$ flux calculation was described in detail in [BAH89] and then upgraded in [BAH92, BAH95, BAH98a, HAX99, BAH01a]. The equations describing the solar evolution depend on many quantities which are not exactly known. The $\nu_\odot$ flux is affected by many uncertainties; among them we underline:

- Fusion cross-sections give a dominant contribution because of the competition between different solar nuclear reactions. Typical solar energy per nucleus, from 5 to 30 keV, are well below the laboratory limits so that extrapolations *via* nuclear calculations are needed. Only the interaction cross-section between two ^{3}He nuclei has been measured down to $\sim$ 15 keV (these values indicate centre of mass energy). Uncertainties are present due to the extrapolation procedure, to the atomic electron screening and to the plasma effects. Terms concerning ^{3}He and ^{7}Be interactions are fundamental because they establish the relative importance among the different terms in p-p chain; on the other hand the proton capture by ^{14}N constrains the CNO cycle. Nuclear matrix treatment also presents uncertainties mainly when transitions involving excited states have to be included in computations, see [GOO80, FUJ96, AKI97].
- $L_\odot$ changes its value at a level of $\sim 0.1\%$ during the solar cycle and affects T_c; the $\nu_\odot$ flux, which depends on T_c, is modified. The pre-main sequence solar phase ($\sim 5 \cdot 10^7$ y) is an estimated value; the contribution of $R_\odot$ and $B_\odot$ and their variability are presently under analyses.
- Solar chemical composition at the beginning is an important term because of the influence of heavy elements on opacity and on ∇. Different results have been obtained within an uncertainty of about 6%. In table 9 the dependence of each branch of p-p chain from different screening factors and the related variations in $\nu_\odot$ flux are reported.

- Radiative opacity depends on the inverse of the photon diffusion length in the solar plasma: it constrains T_c and the ν flux. Difficulties related to the opacity calculations been detailed in section 3.6.

It has to be stressed that Hep $\nu_\odot$ flux is presently quoted without uncertainties due to the difficulty in nuclear cross-section calculations; a conservative estimated error is at a

Table 9. *The fractional differences, (model - W-S)/W-S, in %, of several solar quantities computed in SMs with different screening factors: Helium abundance at surface(Y_{surf}), depth of the convective zone (R_{CZ}), central temperature (T_c), isothermal sound speed squared at the solar core (u_c), $\nu_\odot$ fluxes (Φ_i). Labels W-S, MIT, NO-S and TSY describe respectively weak screening, Mitler, no screening and Tsytovich treatment of screening processes, adapted from [FIO01a].*

	MIT	NO-S	TSY
Y_{surf}	- 0.076	- 0.86	- 1.4
R_{CZ}	+ 0.037	+ 0.34	+ 0.59
T_c	+ 0.45	+ 0.54	+ 1.4
u_c	+ 0.10	+ 1.0	+ 1.4
Φ(pp)	+ 0.033	+ 0.45	- 0.35
$\Phi(^7Be)$	- 0.19	- 2.4	- 5.9
$\Phi(^8B)$	- 2.7	-12.0	+11.0

level of $\sim 100\%$, [BAH01a].
Frequently the computed errors are asymmetric because of the asymmetry in the uncertainties of the input parameters.
In table 10 and table 11 contributions to the $\nu_\odot$ flux uncertainty are reported from two different SMs, [WAT01, BAH02c].

Table 10. *Average uncertainties in $\nu_\odot$ flux as computed in the reference solar model. The ^7Be electron capture rate increases by 2 % the uncertainty in ^7Be $\nu_\odot$ flux, adapted from [BAH01a, BAH02c].*

Frac.	p-p	$^3He^3He$	$^3He^4He$	^7Be+p	Z/X	Opac.	$L_\odot$	Age	Diffus.
Uncert.(%)	1.7	6.0	9.4	4.0	6.1	-	0.4	0.4	15.0
Φ(p-p)%	0.2	0.2	0.5	0.0	0.4	0.3	0.3	0.0	0.3
$\Phi(^7Be)$%	1.6	2.3	8.0	0.0	3.4	2.8	1.4	0.3	1.8
$\Phi(^8B)$%	4.0	2.1	7.5	4.0	7.9	5.2	2.8	0.6	4.0
Cl (SNU)	0.3	0.2	0.6	0.3	0.6	0.4	0.2	0.4	0.3
Ga (SNU)	1.3	1.0	3.3	0.6	3.1	1.8	1.3	0.2	1.5

3.13. Conclusions.

Solar models assume the Sun at thermal equilibrium: they relate the present $\nu_\odot$ flux to the present $L_\odot$ and to nuclear energy production rate; in any case they have to predict a $\nu_\odot$ flux as great as measured by a Gallium detector if it is supposed that all $\nu_\odot$'s are

Table 11. *Sensitivity of neutrino fluxes, central density and the surface helium abundance to the uncertainties in the input physics in a seismic SM. The first ten entries are due to the nuclear cross-section factors, adapted from [WAT01].*

	Cl 7.17 SNU	Ga 126 SNU	^{8}B $4.77{\cdot}10^6$ cm^{-2}s^{-1}	ρ_c 156 g cm^{-3}	Y_{conv} 0.246
p-p: $4.00(1^{+0.021}_{-0.013}){\cdot}10^{-22}$ keV b	$^{+0.372}$	$^{-3.1}_{+1.8}$	$^{-0.477}_{+0.282}$	$^{-3.0}_{+1.6}$	$^{+0.0008}_{-0.0003}$
p-e-p: $\pm1\%$	±0.002	0.0	0.000	0.0	0.0000
^{3}He^{3}He: 5.4$\pm$0.32 MeV b	∓0.131	∓0.8	∓0.094	±0.3	∓0.0001
^{3}He^{4}He: 0.53$\pm$0.05 keV b	±0.408	±2.6	±0.293	∓1.0	±0.0003
^{7}Be+e: $\pm2\%$ (1σ)	∓0.106	∓0.2	∓0.093	0.0	0.0000
^{7}Be+p: $19^{+4}_{-2}(1\sigma)^{+8}_{-4}(3\sigma)$ eV b	$^{+1.057}_{-0.456}$	$^{+2.2}_{-1.0}$	$^{+0.927}_{-0.400}$	0.0	0.0000
^{12}C+p: 1.34$\pm$0.21 keV b	0.000	0.0	0.000	0.0	0.0000
^{13}C+p: 7.6$\pm$1 keV b	0.000	0.0	0.000	0.0	0.0000
^{14}N+p: $3.5^{+1.0}_{-2.0}(3\sigma)$keV b	$^{+0.023}_{-0.069}$	$^{+0.5}_{-1.6}$	$^{-0.007}_{+0.021}$	$^{-0.2}_{+0.6}$	$^{+0.0001}_{-0.0002}$
^{16}O+p: 9.4$\pm$1.7 keV b	±0.001	0.0	0.000	0.0	0.0000
$(Z/X)_s$: 0.0245$\pm$0.0006	±0.120	±0.5	±0.094	∓0.2	±0.0026
$L_\odot$: $3.844(1\pm0.004){\cdot}10^{26}$ W	±0.203	±1.3	±0.153	±0.5	±0.0005
Sound-speed profile	±0.030	±0.1	±0.022	±0.3	±0.0001
$r_{CZ}/R_\odot$: 0.713$\pm$0.001	∓0.031	∓0.2	∓0.023	0.0	±0.0031
ν cross-section	±0.173	$^{+5.1}_{-2.4}$	–	–	–
Opacity: $\pm5\%$	±0.083	±0.4	±0.062	±0.2	±0.0075
EOS: ideal ($\Gamma_1=\frac{5}{3}$)	-0.007	-0.3	$+0.006$	-0.6	$+0.012$
Total: $\sqrt{\sigma^2+\sigma^2+\cdots}$	$^{+1.24}_{-0.95}$	$^{+6.6}_{-5.3}$	$^{+1.04}_{-0.72}$	$^{+2.0}_{-3.2}$	±0.004

produced by p-p interaction. In fact such an experiment can measure low energy $\nu_\odot$'s produced in the first step of p-p chain.

Temperature values computed by different SMs agree within 1% and helioseismological data provide a strong support to this finding. There is a general good agreement between experimental c_s and the values computed in SMs. Z_{surf} agrees very well with the meteoritic composition but the present accuracy does not exclude a small effect of diffusion between the initial composition and the photospheric observations.

A microscopic diffusion was introduced in SMs: the so obtained $\nu_\odot$ flux predictions at higher energy are increased of $\sim 20\%$. Consequently, "turbulent" terms, which partially reduce the flux, were added. Even if different treatments of diffusion processes are possible, results are very similar, [THO94, BAH95, TUR98b]. SMs without element diffusion are not consistent with helioseismology. Despite these improvements, the observed surface abundance of elements such as ^{7}Li and ^{9}Be shows in general a depletion even strong.

The density ρ is a little bit more sensitive than c_s to the p-p reaction rate and depends

on many physical parameters whose uncertainties can be quite large: S_{11}, opacities, microscopic diffusion processes, Z, $t_\odot$ and $R_\odot$.
The structure of radiative zone is very sensitive to these quantities: they are closely related since a change in Z modifies the opacity and the microscopic diffusion, which in turn re-modifies Z, as a consequence of an iterative calibration process.
Along the solar evolution Z_c varies mainly because of the CNO cycle and the microscopic diffusion therefore the opacity has to be modified. There are SMs using higher Z_0 value: this could indicate that some forgotten hydrodynamic phenomenon could act: the use of ρ, rotation profiles in the core and gravity modes may be helpful to clarify this point.
A crucial progress has been achieved in the He abundance evaluation: $Y_{surf} = 0.249 \pm 0.003$; this value is not far from the cosmological value but it is smaller than Y_0 as computed by SMs. Other physical processes have to be introduced to enable us to good reproduce all the observed elemental abundances.
The small differences in solar radial profiles of physical quantities seem to be constrained by *ad hoc* opacity modifications, always in the present uncertainty range.
If one uses non-standard SMs other possibilities are open. It could be possible a mild mixing in nuclear region, for example close to the ^{3}He peak, in order to improve the solar structure but helioseismological results reject this solution: a strong disagreement (at a level of some %) is present in c_s profile.
In the low-Z core models, the p-mode frequencies require a central core with mass $M < 0.06\, M_\odot$. All mixed core models with $M > 0.02\, M_\odot$ are excluded by p-mode frequencies; if $M < 0.02\, M_\odot$ the calculated $\nu_\odot$ flux is much higher, see [GUE97].
The influence of p-mode frequencies on mixed-shell SMs depends on mixing features but the $\nu_\odot$ flux is at a level well above than in SSMs. Helioseismology does not completely rule out SMs in which ^{3}He and other trace elements are slowly mixed in a region where the ^{4}He abundance is practically uniform. In this case the ratio ^{7}Be/^{8}B might be changed without substantial modifications of c_s in that region, [GUE97].
There is a good agreement between solar c_s and estimated profiles below 0.6 $R_\odot$, but tachocline and upper layers are poorly described: in the first zone the turbulent pressure is as important as the gas pressure; moreover, tachocline and external solar region are shear layers in which rotation rates change rapidly.
At present, only a static description of the radiative region is possible, contrary to the convective one, and the history of the angular momentum is not introduced in the stellar equations. A 1-D stellar evolution code cannot provide an efficient treatment of these dynamic regions. Neither the rotation of the Sun nor $B_\odot$ are taken into account, whereas it is widely thought that the tachocline is the base of the magnetic dynamo process. Of course, the $\nu_\odot$ emission and the solar core physics are rather insensitive to the tachocline and beyond, but the $\nu_\odot$ behaviour may depend on these layers (*e.g.* if ν's have a magnetic moment).
If $B_\odot$ acts, a magnetic pressure term P_{mag} is added in the stellar structure equations

($P_{mag} = \frac{B^2}{8\pi}$, in cgs units) and the basic hydrostatic equilibrium equation is modified:

$$\frac{dP_{gas}}{dm} = -\frac{GM}{4\pi r^4} - \frac{dP_{mag}}{dm} \tag{46}$$

therefore the wave velocity changes in two ways, [COU02]. In fact the gas pressure is modified because of the hydrostatic equilibrium and a part of the Alfvén speed $v_a = \frac{B^2}{4\pi\rho}$ (in cgs units) is added. $B_\odot$ has a 3-D structure and the angle between the field lines and the seismic waves determines the way these latter are accelerated: the wave velocity is no more an isotropic quantity but a 1-D stellar code cannot reproduce these events. The main problem is to select a reliable $B_\odot$(r) for the solar interior: in fact large scale field should be important either in radiative and tachocline regions and below the solar surface. Despite the present accuracy, c_s is not suited to the determination of the large scale magnetic features of the Sun. In any case, the magnetic contribution is small when compared to large uncertainties the remaining parameters have.
As a final remark, the global consistency of the solar description has to be stressed as well as the stability of the values of $\nu_\odot$ flux done by different SMs along the last 30 years, mainly concerning the p-p contribution. In fact, even if "seismic" constraints are imposed on the "classical" treatment for the solar properties, numerical results do not vary at large level. Hence, SMs enable us to reproduce the measured physical solar parameters within a small uncertainty range even if simplified assumptions are done.

4. Solar neutrino detection.

Before the analysis of the experimental aspects concerning $\nu_\odot$'s physics, let us remember the conclusion given by H.Bethe on the detectability of $\nu_\odot$'s, [BET34]:
"..This meant that one obviously would never be able to see a neutrino."
Experiments aiming the detection of $\nu_\odot$'s were, and still are, a real challenge for many reasons:

- The reaction rate is very low, much less than one event per day and per ton of target material; the mean energy is low ($\sim$ MeV) and in an energy region where many sources of background are presents (natural radioactivity, secondary cosmic rays...).
- It is impossible to have "beam-off" measurements.
- There are no artificial ν sources with an energy spectrum as $\nu_\odot$'s have.

No viable suggestions concerning the ν detection were available until the end of the second world war: in 1946 B.Pontecorvo suggested a radiochemical method to capture ν's emitted by a nuclear reactor using Cl or Br as a target, [PON46]. Three years later L.Alvarez wrote a paper detailing technical procedures to realize a Cl detector near a pile and he stressed out the background problem, [ALV49]. Both these works supposed ν's and $\overline{\nu}$'s to be equivalent.
Because of the big amount of technical difficulties, $\nu_\odot$'s were experimentally detected only in the 70s', by Homestake Cl experiment, the sole $\nu_\odot$ experiment up to 1985,

[DAV68, DAV70, DAV71].
In the middle of 80s', KAMIOKANDE, in Japan, started to operate and revealed that ... $\nu_\odot$'s come from the Sun, [HIR89, KAJ94]: it realized a "neutrinography" of the Sun by using an exposure time of some years. In the 90s', the Ga experiments, SAGE and GALLEX, which detected low-energy $\nu_\odot$'s coming from the p-p chain, [ANS92, ANS95], showed that the Sun produces energy through the conversion of H into ^{4}He and confirmed the main hypothesis on the stellar energy production and the deficit in $\nu_\odot$ flux. The latest SK and SNO measurements, [FUK01a, FUK01b, AHM01, AHM02a, AHM02b], strongly suggest ν properties beyond the particle standard model.

4.1. Interaction processes.

We will now summarize the main features of the $\nu_\odot$'s detection. The basic physical processes are the ν capture on nucleus and the ν - electron scattering; it is possible a more refined classification:

(i) $\nu_e + (A,Z) \rightarrow e^- + (A,Z+1)$
(ii) $\nu_x + (A,Z) \rightarrow \nu_x + (A,Z)$
(iii) $\nu_e + e^- \rightarrow \nu_e + e^-$
(iv) $\nu_x + e^- \rightarrow \nu_x + e^-$

The odd cases are charged current (CC) interactions, the even ones describe neutral current (NC) processes. Concerning NC and CC interaction on nucleus, we detail reactions on D, a target material which presently a canadian experiment (SNO) uses.
We resume some characteristics of different interactions:

(i) Electron elastic scattering (ES): $\nu_x + e^- \rightarrow \nu_x + e^-$; this reaction is predominantly sensitive to ν_e's and strongly directional: the electron is emitted preferentially in the forward direction respect to the propagation of incoming $\nu_\odot$. The angle between the directions of incoming $\nu_\odot$ and the electron depends on energy of $\nu_\odot$ and on detector threshold (if the $E_{thr} = 5$ MeV, the angle fast increases from 0 up to $\sim 20°$ when the energy of $\nu_\odot$ goes up to ~ 20 MeV then it gets to its asymptotic value of ~ 24 °).
(ii) Charged current interaction (CC): $\nu_e + d \rightarrow p + p + e^- \ (Q = 1.44\, MeV)$; this reaction has a relatively large cross-section.
(iii) Neutral current interaction (NC): $\nu_x + d \rightarrow p + n + \nu_x \ (Q = 2.2\, MeV)$; this reaction is sensitive to all ν flavours. The signature of the reaction is given by the detection of a neutron but it is still a difficult process to be revealed and depends on the final radiopurity of the whole apparatus.

The ratios between interaction rates are:

$$\frac{CC}{ES} = \frac{\nu_e}{\nu_e + 0.154(\nu_\mu + \nu_\tau)} \tag{47}$$

$$\frac{CC}{NC} = \frac{\nu_e}{\nu_e + \nu_\mu + \nu_\tau} \tag{48}$$

If the incoming particle is a ν_e, both NC and CC interactions are allowed while only NC interactions are possible when ν flavour is other than electronic one. It is impossible to distinguish between ν_μ and ν_τ interaction. Under standard assumptions both these ratios are equal to the unity.
The ratio between NC and CC is presently used as a test for $\nu_\odot$ flavour oscillations, see later in section 7.2; its value depends on energy.
Table 12 and table 13 show the composition of the $\nu_\odot$ flux and the expected interaction rate as measurable on terrestrial detectors for interaction on nuclei.

Table 12. *Neutrino fluxes and interation rates on Cl and Ga computed with different nuclear reaction cross-sections: [ADE98] (left side), [ANG99] (right side). The cross-sections for neutrino absorption on Cl are from [BAH96c], the cross-sections for Ga are from [BAH97a]. Errors on flux are quoted in first column; the Hep component is without errors due to uncertainties in calculations, adapted from [BAH01a].*

Source & error(%)	Flux $\nu\, cm^{-2}s^{-1}$	Cl (SNU)	Ga (SNU)	Flux $\nu\, cm^{-2}s^{-1}$	Cl (SNU)	Ga (SNU)
p-p($\pm$ 1.0)	$5.95{\cdot}10^{10}$	–	69.73	$5.96{\cdot}10^{10}$	–	69.85
p-e-p($\pm$ 1.5)	$1.40\cdot10^{8}$	0.22	2.86	$1.39\cdot10^{8}$	0.22	2.84
Hep	$9.3\cdot10^{3}$	0.04	0.07	$9.4\cdot10^{3}$	0.04	0.07
^{7}Be($\pm$ 10)	$4.77\cdot10^{9}$	1.15	34.20	$4.81\cdot10^{9}$	1.15	34.49
^{8}B($^{+20}_{-16}$)	$5.05\cdot10^{6}$	5.76	12.12	$5.44\cdot10^{6}$	6.20	13.06
^{13}N($^{+21}_{-17}$)	$5.48\cdot10^{8}$	0.09	3.31	$4.87\cdot10^{8}$	0.08	2.94
^{15}O($^{+25}_{-19}$)	$4.80\cdot10^{8}$	0.33	5.46	$4.18\cdot10^{8}$	0.28	4.75
^{17}F($\pm$ 25)	$5.63\cdot10^{6}$	0.0	0.06	$5.30\cdot10^{6}$	0.0	0.06
Total	$6.545{\cdot}10^{10}$	$7.6^{+1.3}_{-1.1}$	127.8^{+9}_{-7}	$6.546{\cdot}10^{10}$	$8.0^{+1.4}_{-1.1}$	128^{+9}_{-7}

4.2. Detection techniques.

Different techniques were tried to detect $\nu_\odot$'s by interaction with target mass, see [CRE93] for a detailed analysis. In $\nu_\odot$ - nucleus interaction the energy threshold at which reaction occurs is defined by the Q-value of the detection reaction itself. If the detector is not able to record the time of each event and "integrates" each $\nu_\odot$ with $E \geq E_{thr}$, it is also impossible to distinguish the origin of different contribution.

Geochemical experiments = People should study a very long meanlife isotope produced in a deep underground ore. In this case, it could even be possible to estimate the constancy of the $\nu_\odot$ flux over long time. ^{98}Mo or ^{205}Tl should be good candidates but many problems in the evaluation of background forbid the feasibility of experiments using such a technique.

Table 13. *Expected neutrino capture rates on nucleus (in SNU). The null value means not calculated or negligible, "-" means not measurable by the detector, "*" means not shared, adapted from [BAH01a, EJI00b].*

Type	^{37}Cl	^{71}Ga	^{100}Mo	^{127}I	^{2}H	^{40}Ar	^{7}Li	^{115}In
p-p	–	69.73	639	–	–	–	–	468
p-e-p	0.22	2.86	13	0.0	–	–	9.2	8.1
Hep	0.04	0.07	0.0	0.0	0.02	0.02	0.1	0.05
^{7}Be	1.15	34.20	206	9.4	–	–	9.1	116
^{8}B	5.76	12.12	27	13.0	6.0	7.2	19.7	14.4
^{13}N	0.09	3.31	22	0.0	–	–	2.3	32.1*
^{15}O	0.33	5.46	32	0.0	–	–	11.8	32.1*
^{17}F	0.0	0.06	0.0	0.0	–	–	0.1	0.2
Total	7.59	127.81	939	22.4	6.02	7.22	52.3	638.85

Radiochemical experiments = The isotopes produced by $\nu_\odot$'s are extracted using the different chemical behaviour of these atoms compared to the target ones. Presently, only experiments having Ga as target mass use this technique. Due to the low interaction rate, the amount of analysed isotopes is very small so that a target mass of $\sim$ 100 tons is needed to have a production of 1 atom per day. The detectors are sensitive only to ν_e's by inverse β-decay. Radiochemical experiment indicates only the total rate at which $\nu_\odot$'s with $E \geq E_{thr}$ are captured; the energy spectrum cannot be measured. The nuclei produced by $\nu_\odot$'s interactions are usually unstable for electron capture and their amount can be established by looking for their decay or by resonance ionisation spectroscopy. In any case, a chemical separation from target nuclei is needed. Several isotopes enable us to build a detector: ^{37}Cl, ^{71}Ga, ^{127}I, ^{7}Li, ^{81}Br; up to now ^{37}Cl and ^{71}Ga have been used. Ga experiments are sensitive to the low-energy component of the $\nu_\odot$ flux but cannot do any $\nu_\odot$ spectroscopy. A problem for this technique is the very small number of interesting nuclei produced during each data taking session and the extremely efficient extraction yield needed for the separation.

Direct counting experiments = The main aim is to detect in real-time particles emitted after $\nu_\odot$ interaction, measuring the $\nu_\odot$ energy spectrum and temporal variation on $\nu_\odot$ flux, if present. Usually, scintillation or Čerenkov light after the ν interaction are detected; among possible solutions (not presently operating) time projection chambers, low-temperature detectors and scintillators are in R&D. The most intriguing aspects that these options allow are the $\nu_\odot$ spectroscopy and the different flavour recognition.

An interesting idea to measure low energy $\nu_\odot$'s in real time is the coincidence technique for ν capture on nuclei. The target material should be either a large amount of $\beta\beta$ isotopes (^{176}Yb, ^{100}Mo, ^{160}Gd) or highly forbidden β-decay

emitters like ^{115}In (4-fold forbidden). The possibility to apply the same technique for CdTe(CdZnTe) semiconductor detectors, which have already a wide field of application in γ-ray astronomy and medical physics, has been recently suggested. CdTe semiconductor detectors. Ge and GaAs semiconductor detectors for $\nu_\odot$ experiments were also considered relying on the detection of electrons from ν-electron scattering.

The detection principle for $\nu_\odot$'s using coincidences relies on the reactions:

$$\nu_e + (A, Z) \rightarrow (A, Z+1)_{g.s.} + e^- \rightarrow (A, Z+2) + e^- + \overline{\nu}_e \quad (49)$$

$$\nu_e + (A, Z) \rightarrow (A, Z+1)^* + e^- \rightarrow (A, Z+1)_{g.s.} + \gamma \quad (50)$$

Therefore, either coincidence between two electrons for the ground state transitions or the coincidence of an electron with the corresponding de-excitation photon(s) is required. The energy of electrons produced in the first part of the coincidence is:

$$E_e = E_\nu - (E_f - E_i) \quad (51)$$

with E_ν as ν energy, E_f and E_i as the energy of the final and initial nuclear state involved in the transition.

D, ^{40}Ar, ^{81}Br, ^{115}In ... are good candidate isotopes: up to now only SNO, a Canadian detector which is using D, is running.

The structure of the interaction cross-section is the following:

$$\sigma \propto G_F^2 |M|^2 p_e E_e F \approx 10^{-46} \left(\frac{E}{m_e}\right)^2 cm^2 \quad (52)$$

where G_F is the Fermi constant, M is the nuclear matrix element, p_e and E_e are respectively the momentum and the energy of the electron, F includes Coulomb corrections.

In order to calculate the interaction rate R per target atom the uncertainties due to the selected SM, to the absorption cross-sections and to transitions toward excited nuclear levels (because of the great complexity in nuclear matrix sector) have to be taken into account, see tables 10, 11 and 16.

On the other hand, if the experiment detects $\nu_\odot$ elastic scattering off electron, at present only Čerenkov effect in water is used. A track or a flash produced by a charged particle gives evidence of $\nu_\odot$ interaction. The emitted light is collected by an array of PMT's and a fiducial volume is defined. This technique allows the reconstruction of the direction of incoming $\nu_\odot$'s and the estimation of the energy spectrum and its shape. The energy threshold is fixed by electronic setup.

A big challenge in these detector is the analysis of the low-energy spectrum because background raises exponentially at lower energy: up to now $E_{thr} \geq 5.0$ MeV so that only high energy components of $\nu_\odot$ flux are detectable (^{8}B and Hep $\nu_\odot$'s).

KAMIOKANDE, SK and SNO, which use this technique, have confirmed that ν's come from the Sun; moreover, the energies of detected $\nu_\odot$'s are fully compatible with predictions given by SMs.

4.3. Background.

The background is probably the main problem in $\nu_\odot$ experiments: it can either hide the true signal or produce a false one. To avoid this serious trouble it is needed to determine the features of all possible known sources of noise and to emphasize the expected signal as much as possible. The most important contributions to the background come from cosmic radiation and from radioactivity in structures, materials and environment.
The charged component of cosmic radiation and high energy atmospheric ν's can be identified with sufficient confidence but they can interact either in detector or in its structure and/or in surrounding medium originating "side reactions" which produce fake signals. Hence, detectors are homed deep underground, in mines or tunnels under the mountains, independently of the detecting technique: in this way, the cosmic ray flux ($\sim$ 180 events m^{-2} s^{-1} at sea level) reduces to a value less problematic in comparison with $\nu_\odot$ interaction rate.
Further problems come from long-lived cosmogenic isotopes, produced *en plein air* and from the decay of isotopes in the detector structure: in most cases critical isotopes are ^{222}Rn, ^{40}K and all intermediate products of ^{232}Th and ^{238}U chains.
A contamination level not greater than $\sim 10^{-16}$ g/g is often required, [BOR98]: this is an example of the difficulties that the researchers have to overcome.
In order to summarize the energy dependence of background, the main term up to 3 MeV is coming from structure, wall and ore radioactivity, α and β contributions being complementary. At higher energy neutron capture processes are dominant, due to reactions where α's from U and Th are involved. As a standard procedure, low activity concrete, "clean" materials, water and lead are searched for.

5. Experimental Results.

We now shortly expose the main features and results of experiments which have measured $\nu_\odot$ flux. Up to 2002 seven detectors claimed evidence of $\nu_\odot$'s: Homestake, KAMIOKANDE, GALLEX, SuperKAMIOKANDE, SAGE, GNO and SNO; the last three experiments are on run in spring 2002.

5.1. The Chlorine experiment.

The first experiment searching for the $\nu_\odot$'s detection was proposed in 1964, [DAV64], immediately after the publication of the first SM. The building operations for Cl detector began in 1965 at Homestake gold mine (USA), at a depth of 4200 mwe.
The detected reaction is a ν absorption on nucleus, $^{37}Cl\,(\,\nu_e\,,\,e^-\,)\,^{37}Ar$ at E$\geq$ 814 keV, [DAV94], and can be induced by ^{7}Be, CNO and p-e-p $\nu_\odot$'s but the dominant contribution is from ^{8}B component.
Among technical and economical motivations, the ^{37}Cl isotope has a good abundance in nature and it is cheap; moreover, ^{37}Ar can be separated without problems from target mass and the inverse reaction has a right period for radiochemical detection.

The target was a tank filled with 615 tons of perchloroethylene (C_2Cl_4). Helium stream was used to "extract" ^{37}Ar and carrier Ar: after an exposure time ranging up to 3 months, the produced ^{37}Ar nuclei, which are unstable and transform back into ^{37}Cl *via* electron capture (half-life = 35 days), were analysed in proportional counters searching for Auger electrons emitted when ^{37}Ar decays. Tritium, Kr and Ar isotopes different from ^{37}Ar were searched for to be removed, in fact they constitute the most serious background in the counting procedure. The event selections were based on the pulse amplitude and the rise time: only fast rising pulses were estimated as good signature of an event because they are electronic captures. Periodical calibration were done both on preamplifiers and on counters. In 1970 an electronic system to analyse the pulse rise time enhanced the experimental sensitivity. Usually, only results after 1970 were quoted.

The detector took data continuously from 1967 to 1994 with the exception of a period from May 1985 to October 1986.

^{37}Ar atoms produced by cosmic rays ($\sim$ 0.28$\pm$ 0.08 SNU) and neutron contribution (0.13 $\pm$ 0.13 SNU) were the main components of background; smaller terms were due to α particles produced from U and Th and to cosmic ray ν's. When the counting rate in a single run was found to be formally negative, a zero value was adopted. The average value was computed with a maximum likelihood analysis. The total systematic error (1.5% for extraction, 5% for neutron, 3% for cosmic ray background) was at a level of 6 %.

In the middle of 50s', $\nu_\odot$ flux was estimated at a level of $\sim 10^{14} \nu\, cm^{-2}\, s^{-1}$; this value was based on CNO dominant contribution (it is equivalent to $\sim$ 40000 SNU). A more complete theoretical knowledge on solar parameters lowered the value down to 3900 SNU, [CAM58a, CAM58b, FOW58], but only the formulation of a first SM in 1963-64, [BAH63, SEA64] gave a more realistic estimated interaction rate: 40 $\pm$ 20 SNU.

In 1968 the $\nu_\odot$ flux in the Cl experiment was estimated in the range 8 - 49 SNU, [BAH68], but first experimental results gave an upper limit of 3 SNU, [DAV68]. This disagreement was the origin of the solar neutrino problem or the SNP of first kind.

The final interaction rate, based on 1970-1994 runs, was 2.56 $\pm$ 0.16 $\pm$ 0.15 SNU, [CLE98, LAN98], the 1 σ statistical error was $\sim$ 6 % of the measured rate. Let us stress the value predicted in [BAH01a]: $7.59^{+1.3}_{-1.1}$ SNU.

It was suggested a possible anticorrelation of $\nu_\odot$ flux with the activity of the Sun, namely its sunspots number, [DAV96] and reference therein, see also [MAS95a, MAS95b, MAS95c]. It was pointed out that this conclusion was extrapolated from the data detected in 1979-80 without further confirmations in the following years. For a review on this problem see [BOG00]: the main conclusion is that the claim of anticorrelation with sunspots number seems to be due to technical procedures in analyses.

Let us remark the importance of this experiment, even historically speaking, because it firstly detected $\nu_\odot$'s and confirmed the main features of energy production mechanism in stars. Moreover, it showed the feasibility of radiochemical technique, it overcame a lot of troubles in background evaluation and suppression, it was continuously running

over about 3 decades and the only experiment until 1987. We underline that anyone has never used this technique and no calibration was made.

5.2. The KAMIOKANDE experiment.

KAMIOKANDE (Kamioka Nucleon Decay Experiment), originally designed to search for proton decay, showed that the interacting ν are coming from the Sun and that their energies are compatible with the predictions of SSMs.
This experiment, homed in a mine in Japan, was a real-time water detector measuring the Čerenkov light emitted by electron recoil produced in ES interactions from electrons at $E \geq 9.0$ MeV (some time later the threshold was lowered down to 7.0 MeV), therefore only ^{8}B and Hep $\nu_\odot$'s were detectable, [FUK96].
This detector first showed the main challenge for the Čerenkov technique: a good cut criterion for track recognition and timing. In fact the total trigger rate for all the detector was ~ 150000 events per day while the expected signal was less than 1! The angular resolution in track reconstruction was $\sim 27^\circ$ and a global systematic error ($\sim 10\%$) came from uncertainties in the angular resolution, in the energy scale and in the fiducial volume cut.
¿From 1987 to 1995, with 2079 days of running time 597^{+41}_{-40} events were achieved (the expected number was ~ 1200).
The final measured flux was $\Phi = 2.80 \pm 0.19 \pm 0.33 \cdot 10^6\, \nu\, cm^{-2}\, s^{-1}$, [FUK96].
Searching for a possible explanation of SNP in term of particle solution, see later in section 7.2, the $\nu_\odot$ flux as measured when $\nu_\odot$'s do not cross the Earth before the detection (Day time) and otherwise (Night-time) were computed. More precisely the D flux requires $\cos\theta_z < 0$ while for N flux $\cos\theta_z > 0$, θ_z being the angle between the detector vertical axis and the vector from the Sun to the Earth.
No significant differences were found: $\Phi_D = 2.70 \pm 0.27 \cdot 10^6\, \nu\, cm^{-2}\, s^{-1}$, $\Phi_N = 2.87^{+0.27}_{-0.26} \cdot 10^6\, \nu\, cm^{-2}\, s^{-1}$.
In order to study the time variations correlated with solar activity, as Homestake experiment suggested, the events were divided into short time periods, 200 days, but this further analysis did not indicate any anticorrelation with sunspots number, [HIR89, KAJ94].
We underline the quality of the detector and the technical skill of the people operating on that detector; they were also able to observe the burst of ν's emitted in SN1987a explosion.

5.3. The SuperKAMIOKANDE experiment.

SuperKAMIOKANDE, an enlarged version of KAMIOKANDE, began its data taking in spring 1996. Many physical items are under investigation with this real-time cylindrical detector: proton-decay, atmospheric and supernova ν's and, of course, $\nu_\odot$'s [SUZ95, SUZ97]. Owing to the huge mass (~ 50000 tons even if the fiducial mass for $\nu_\odot$'s is ~ 22500 tons) and the low energy threshold, more accurate analyses are possible.

The inner part of the cylinder ($\sim$ 32000 tons) is viewed by 11146 inward-facing 20"-PMT's while the external one has 1885 outward-facing 8"-PMT's which are employed as anti-counter. The total coverage given by PMT's is at a level of $\sim$ 40 %.
In any case, SK is sensitive only to ^{8}B and Hep $\nu_\odot$'s but it enables us to search for possible time modulations (D-N effect, seasonal variations and so on) and to study the energy spectrum of recoil electrons and Hep $\nu_\odot$ flux, [FUK98a, FUK98c, FUK99, SMY00, FUK01a, FUK01b].
The analyses concern a sample of 1496 day of running-time, from May 1996 to July 2001, with different energy threshold: in first step E_{thr}= 6.5 MeV, in latest analysis E_{thr}= 5.0 MeV. This value is due to the background and to the trigger.
Each event has been classified depending on arrival direction and energy. The sample includes 22400± 800 events, corresponding to $\sim$ 15 events per day, [FUK02, SMY02a, SMY02b, SMY02c, SMY02d]; the calculated flux is $\Phi = 2.35 \pm 0.02 \pm 0.08 \cdot 10^6\, \nu\, cm^{-2}\, s^{-1}$ while the ratio with respect to the flux estimated in [BAH01a] is $R = 0.465 \pm 0.005\, ^{+0.016}_{-0.015}$, see also table 14 where the energy spectrum is shown. The total systematic error is $^{+3.5\%}_{-3.0\%}$: the main contribution comes from reduction cut efficiency, energy scale and resolution, systematic shifts in event vertex and angular resolution of the recoil electron momentum. The available SK zenith angle-recoil energy spectrum consists of six night + one day bins for six energy bins between 5.5 and 16 MeV electron recoil energy, plus two daily averaged points for the lowest ($5.0 < E < 5.5$ MeV) and the highest ($E > 16$ MeV) energy bins. On the other hand, the D-N energy spectra are based on 19 energy bins each for D and N periods; even the running time has been shared in D and N time, see fig. 13 and table 15. The fractional difference is -0.021± 0.020 $^{+0.013}_{-0.012}$, [FUK02, SMY02b, SMY02c, SMY02d]. It seems that this difference assumes larger value at higher energy.
The data have been also divided either in 10 days of measurements or in 45 days of data taking. The seasonal variation of $\nu_\odot$ flux due to the Earth orbit eccentricity is in good agreement with the hypothesis of d^{-2} dependence, where d is the Sun-Earth distance: the flux averaged over 45 days of data taking has been computed and analysed: χ^2-test yields 4.7 to be compared with 10.7 under the assumption of constant flux. Even a 10 day binning has been checked but no statistically significant deviations from expected distribution have been found. Other long-term variations, like anticorrelation with number of sunspots, seem to be not present. Let us remember that the sunspots number increased from 1998 to 2000 in coincidence with a solar activity maximum.
The high energy component of $\nu_\odot$ flux has been searched for: 4.9 ± 2.7 events with $E \geq$ 14.0 MeV were detected (1 event was expected) and an upper limit to this flux has been established ($\Phi_{Hep} \leq 7.9 \Phi_{BAH01a}$). As a further result an upper limit to the solar $\overline{\nu}_e$ flux has been deduced ($\phi < 2\%$ of the total flux).
It has to be stressed that a severe accident occurred at the end of 2001 during technical operations: $\sim$ 6800 inner PMT's and $\sim$ 1100 outer PMT's were destroyed. The data taking will restart probably late 2002 after a partial replacement of PMT's but with a higher energy threshold and a lower light coverage (SUPERKAMIOKANDE II).

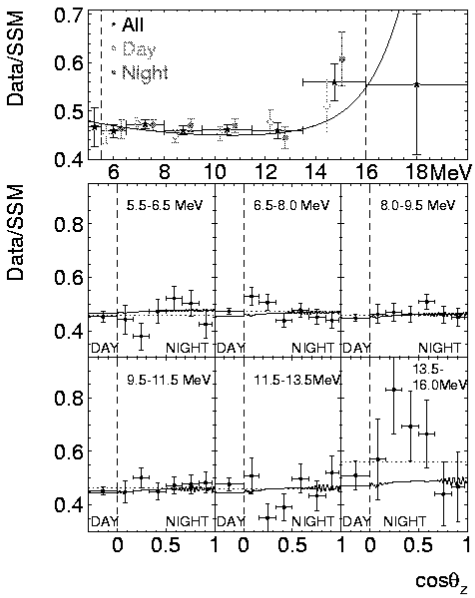

Figure 13. Upper panel: SK energy spectrum; day and night values are also drawn. Lower panel: SK zenith-angle energy spectrum between 5.5 and 16 MeV. The dotted line is the combined rate in that bin. Error bars reflect the statistical uncertainty only. Superimposed is an oscillation prediction ($\tan^2\theta$=0.34 and Δm^2=6.0·10^{-5}eV^2) near the best-fit point, from [SMY02a].

The results SK has obtained can be summarized in this way:

- Confirmation of a reduced $\nu_\odot$ flux but with the larger presently available statistics.
- No distortion in the energy spectrum.
- No relevant D-N asymmetry.
- Time variation of the flux related to the terrestrial orbit.

5.4. The Gallium experiments.

Three experiments, SAGE, GALLEX and GNO, have detected $\nu_\odot$'s interactions on Ga target, through a reaction suggested by Kuzmin, [KUZ64, KUZ65], which is only sensitive to CC interactions:

$$^{71}Ga\,(\,\nu_e\,,\,e^-\,)\,^{71}Ge \qquad E \geq 232.69 \pm 0.15\,keV \tag{53}$$

The target mass of these experiments should require about one year world-production of Ga (the cost of Ga is $\sim 10^3$ US \$; let us remember that the isotopic abundance of

Table 14. *SK rates and uncertainties for eight energy bins. The quoted rates, statistical and systematic uncertainties (of the spectrum shape) in the third column are in units of flux predicted by [BAH01a] . These systematic uncertainties are assumed to be uncorrelated in energy while uncertainties of the ^8B $\nu_\odot$ spectrum, of the energy scale and of the energy resolution are fully correlated in energy (but uncorrelated with each other), adapted from [SMY02a].*

Bin	Range [MeV]	Rate±stat±syst [BAH01a]
1	5.0-5.5	$0.4671\pm0.0404^{+0.0165}_{-0.0138}$
2	5.5-6.5	$0.4580\pm0.0141^{+0.0066}_{-0.0065}$
3	6.5-8.0	0.4729±0.0084±0.0065
4	8.0-9.5	0.4599±0.0093±0.0063
5	9.5-11.5	0.4627±0.0103±0.0063
6	11.5-13.5	0.4621±0.0168±0.0063
7	13.5-16.0	0.5666±0.0390±0.0078
8	16.0-20.0	0.5554±0.1458±0.0076
Total	5.0-20.0	$0.4653\pm0.0047^{+0.0138}_{-0.0122}$

Table 15. *Subdivision of bins 2–7 flux ratio with respect to the [BAH01a] model value, according to the solar zenith angle θ_z. The range of $\cos\theta_z$ is given for each bin: $\cos\theta_z < 0$ is 'Day' and $\cos\theta_z > 0$ is 'Night'. The rates are given in units of 0.001*[BAH01a] SM. Only statistical uncertainties are quoted. All systematic uncertainties are assumed to be fully correlated in zenith angle, adapted from [SMY02a].*

Bin	Day	Mantle					Core
	-0.97–0.0	0.0–0.16	0.16–0.33	0.33–0.50	0.50–0.67	0.67–0.84	0.84–0.97
2	453±20	442±53	379±49	472±45	522±45	503±49	426±52
3	474±12	530±34	506±30	438±26	478±26	451±28	439±31
4	448±13	463±36	470±33	462±29	509±29	461±32	451±35
5	453±15	449±40	502±38	451±32	473±32	477±35	483±40
6	477±25	509±67	351±55	391±49	498±53	434±56	521±64
7	511±54	570±150	831±167	694±131	665±127	441±118	469±131
1-8	459.9±6.7	483±18	476±17	451±15	496±15	467±16	456±17

^{71}Ga is 40 %, the remaining 60 % is due to ^{69}Ga. The produced ^{71}Ge atoms, which turn back into ^{71}Ga *via* electron capture with a half-life of 11.4 days, are extracted from Ga every 3 or 4 weeks and its electron capture is detected by the observation of Auger electrons and X-rays within shielded proportional counters having a volume of about 1 cm^3.

The known background sources are side reactions, ^{69}Ge, Tritium (which is present in germane gas) and ^{222}Rn.

The number of Ge atoms extracted in a single run is very small, less than 10 atoms. Thanks to the low-energy threshold, interactions are mainly produced by p-p $\nu_\odot$'s, see table 12 and table 16, and are from ground to ground nuclear state, so that the nuclear part of computations is "easier" to be done.
The measurement of the p-p $\nu_\odot$ flux is an important goal for these detectors due to the independence of such a component from SMs: therefore it is possible to check the consistency of the theories on nuclear reactions.

Table 16. *Characteristics of $\nu_\odot$ flux and interaction rates on Ga target, from [BAH97a, BAH01a, COU02]. Flux 1 and Flux 2 are in$\nu\, cm^{-2}s^{-1}$ while rate 1 and rate 2 are expressed in SNU. Flux 1 and rates 1 are from [BAH01a], flux 2 and rates 2 are from [COU02].*

Reac. source	Uncer. σ (%)	σ_{Ga} $10^{-45}cm^{-2}$	Flux 1	Flux 2	Rate 1	Rate 2
p-p	± 2.3	1.172	$5.95{\cdot}10^{10}$	$5.916\cdot 10^{10}$	69.73	69.34
p-e-p	$^{+17}_{-7}$	20.4	$1.4{\cdot}10^{8}$	$1.392{\cdot}10^{8}$	2.86	2.84
Hep	$^{+32}_{-16}$	7140	$9.3{\cdot}10^{3}$	-	0.07	-
^{7}Be	$^{+7}_{-3}$	7.17	$4.77{\cdot}10^{9}$	$4.853{\cdot}10^{9}$	34.20	34.79
^{8}B	$^{+32}_{-15}$	2400	$5.05{\cdot}10^{6}$	$4.979{\cdot}10^{6}$	12.12	11.95
^{13}N	$^{+6}_{-3}$	6.04	$5.48{\cdot}10^{8}$	$5.767{\cdot}10^{8}$	3.31	3.483
^{15}O	$^{+12}_{-5}$	11.37	$4.80{\cdot}10^{8}$	$4.967\cdot 10^{8}$	5.46	5.648
^{17}F	$^{+12}_{-5}$	11.39	$5.63{\cdot}10^{6}$	$3.083{\cdot}10^{6}$	0.06	0.0351

5.5. SAGE.

Soviet American Gallium Experiment (SAGE) started its operations in 1990: its detector, consisting in 7 so called "reactors", is homed at Baksan (Russia), at a depth of $\sim$ 4700 mwe, [ABD94, GAV97, ABD99b, SAG99]. It uses Ga in metallic form as a target (Ga is liquid at T$\geq$ 300 K). Ge is extracted *via* immersion in HCl and H_2O_2 solutions in teflon-lined reaction vessels (this procedure is very difficult). The metallic form allows a compact detector with a reduced background and an easier calibration. The Ga target mass has been variable, up to 57 tons; the present value is 49 tons.
The extraction procedure is based on the separation of Ge into an aqueous phase when metallic Ga is mixed with an acid solution and an oxidizing agent. The mixture is stirred, then Ga comes back into emulsion while Ge goes to the surface of the emulsion droplets. When H_2O_2 is finished, the emulsion breaks down and the phases separate: then, Ge is concentrated by distillation and HCl is added; at this point the Ar purification starts. After a three times repeated Ge extraction in CCl_4, the obtained germane is inserted in proportional counters and the counting procedure begins. For each extraction the best

estimate of the ^{71}Ge production rate is done by measuring likelihood function.
It is interesting to point out that the first published interaction rate was very close to zero, but with a very large uncertainty; on the contrary the latest result, based on January 1990 - December 2001 runs, is $70.8\,^{+5.3}_{-5.2}\,^{+3.7}_{-3.2}$ SNU, [ABD02].
It has to be stressed that problems in data acquisition were present during 1996-1999 so that SAGE coll. has applied an *a posteriori* correction to the detection efficiency. In any case an analysis on systematic effects and uncertainties has been done: the total systematic effects has been computed at a level of $^{+3.7}_{-3.2}$ SNU, see also table 17.

Table 17. *Systematic effects in SAGE and their uncertainties (in SNU). The values for extraction and counting efficiencies are based on a rate of 70.8 SNU, adapted from [ABD02].*

Extraction efficiency	Ge carrier mass	±1.5
	Extracted Ge mass	±1.8
	Residual carrier Ge	±0.6
	Ga mass	±0.2
Counting efficiency	Counter effects	±1.3
	Gain shifts	+2.2
	Resolution	-0.4,+0.5
	Rise time limits	±0.7
	Lead and exposure times	±0.6
Backgrounds	Neutrons	<-0.02
	U and Th	<-0.7
	muons	<-0.7
	Internal radon	<-0.2
	External radon	0.0
	Other Ge isotopes	<-0.7
Total		-3.2,+3.7

A calibration of the apparatus with a ^{51}Cr source of 19.1 ± 0.2 PBq strengthened the detection of $\nu_\odot$'s and the efficiency of the analysis (the ratio observed/expected ^{71}Ge production rate is $R = 0.97 \pm 0.12$, [ABD96, ABD99a] .
Looking for time correlation, all the data have been analysed yearly, monthly and bimonthly, the same distance from the Sun being the selecting parameter, but no statistically significant effect has been found, [ABD02]; in table 18 yearly and monthly average interaction rates are shown. The difference between winter and summer interaction rate has been computed; its value is - $6.7^{+10.7}_{-10.3}$ SNU.
This experiment should continue up to 2006, [GAV01b].

Table 18. *Combined analysis of all runs during yearly and monthly intervals. The quoted value in SNU is the best fit result of the likelihood procedure, adapted from [ABD02].*

Year	Nr. of data	SNU	Month	Nr. of data	SNU
1990	5	43	January	11	58
1991	6	112	February	12	60
1992	13	76	March	9	102
1993	15	84	April	9	54
1994	10	73	May	12	75
1995	13	102	June	11	79
1996	10	55	July	15	52
1997	16	62	August	15	78
1998	12	56	September	20	68
1999	14	87	October	17	73
2000	22	67	November	15	59
2001	22	65	December	12	105

5.6. GALLEX.

The GALLEX (GALLium EXperiment) detector was operating from 1991 to 1997 at LNGS, Italy. The target was a 101 tons solution of $GaCl_3$ in water and HCl containing 30.3 tons of natural Ga corresponding to $\sim 10^{29}$ nuclei of ^{71}Ga.
The tank containing 8-molar Ga chloride solution was equipped with provisions for a N_2 purge and with a central tube for inserption of either a man-made ν source or of a neutron monitor. The surrounding rock gave a 3600 mwe shield to cosmic rays.
In short the experimental procedure was the following [ANS92]:

- The solution was exposed to $\nu_\odot$'s for 3 or 4 weeks; at the end $\sim$ 16 nuclei of ^{71}Ge should be present as a volatile $GeCl_4$ (if SMs are correct and all ν's produced in the Sun reach the Earth without flavour change).
- The ^{71}Ge was chemically extracted and converted into GeH_4 (Germane gas) and introduced into miniaturized proportional counters, [WIN93], mixed with Xe as counting gas. At the end $95 - 98\%$ of the ^{71}Ge present in the solution at the time of the extraction was in the counter.
- The ^{71}Ge electron capture (meanlife 16.5 days) $^{71}Ge\,(\,e^-, \nu_e\,)^{71}Ga$ was observed for a period of 6 months. A good determination of the time constant counter background was also permitted.
- Data taken during the counting time were analysed with a maximum likelihood technique to obtain the most probable number of ^{71}Ge detected. The mean background was less than 0.1 counts per day.
- A correction was made to account for contributions to the observed signal from

sources other than $\nu_\odot$'s (mainly interactions generated by high energy muons from cosmic rays and by natural radioactivity). 7 SNU have to be subtracted from the measured ^{71}Ge production rate.

GALLEX solution was also exposed to an artificial ν source ^{51}Cr, a nucleus having a lifetime of 40.0 days and decaying by electron capture: $^{51}Cr\,(e^-, \nu_e)\,^{51}V$. ν_e's are produced with a discrete energy spectrum having values similar to the solar spectrum. Two expositions were done, 63.4 $\pm$ 0.5 PBq and 69.1 $\pm$ 0.6 PBq being the activities of the used sources: the first published ratio observed/expected interaction rate was $R = 0.93 \pm 0.08$ but a new analysis of the counter efficiency and of source intensity has lowered the previous result. The latest upgraded value is $R = 0.89 \pm 0.07$, [CAT02]. This means that in GALLEX unknown systematic errors were of about 10%.
A further test was the calibration with ^{71}As to check the correctness of "chemistry" in the detector. It was found a complete agreement with the expected value: the experimental result was 99.9$\pm$ 0.8% of the estimated one, [HAM98b].
The final result of GALLEX experiment was 77.5 $\pm$ $6.2^{+4.3}_{-4.7}$ SNU, [HAM99], see also [ANS95, HAM96] for intermediate results. The statistical error was at a level of $\sim$ 8% of the measured rate; the systematic term adds a contribution of $\sim$ 6%.

5.7. GNO.

Gallium Neutrino Observatory (GNO) experiment [GN096] is homed at LNGS and started in 1998; it upgrades of GALLEX experiment, in fact it uses the same 30 tons target, [ALT00, BEL01, CAT02], but with a new data acquisition system and largely improved electronics. The Ge extraction from the Chloride solution procedure is not changed with respect to GALLEX.
An improvement on the global error is expected to come from GNO: a new Rn cut procedure is still operative, then a reduction of systematic errors at a level of 3-5 % by a direct measurement of the volume efficiency of all the counters and a neural network analysis technique are foreseen.
At present, the contributions to the systematic errors due to energy cuts, pulse shape cuts, event selection, Rn cut inefficiency and ^{68}Ge are reduced with respect to GALLEX experiment so that the total systematic error in GNO is lowered from 4.5 SNU down to 3.0 SNU.
The GNO interaction rate, based on data performed from May 1998 to January 2002 (43 runs), is $65.2 \pm 6.4(stat.) \pm 3.0(syst.)$ SNU, [KIR02]; this value differs at a level of 1.7 σ from GALLEX result and could suggest a constant $\nu_\odot$ flux over 10 years.
The combined GALLEX+GNO (1991-2002) results is $70.8 \pm 4.5(stat.) \pm 3.8(syst.)$ SNU. The difference between winter and summer interaction rate over the whole period is -11 $\pm$ 9 SNU, [KIR02]. In fig. 14 single extraction values with error bars are shown.
To further reduce the counting errors other aspects are under analysis: machined counters made by a plastic material, more uniform in shape, and a low temperature calorimeter to "read" the energy thermally deposited from a decay with a

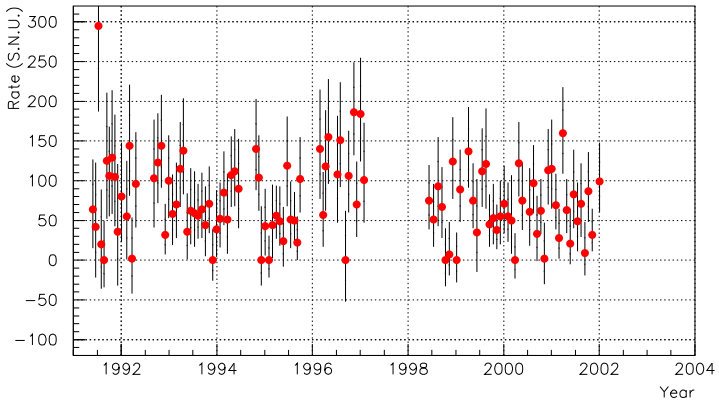

Figure 14. Single extraction interaction rate of GALLEX+GNO experiments from 1991 up to May 2001, from [KIR02].

superconductor phase transition thermometer. The use of a new cryogenic detector which should allow an efficiency at a level of $\sim$ 100 % (the present value is $\sim$ 70 %), an energy resolution better by a factor of 7, no X-ray escape effects and no pulse-height degraded events is under evaluation, [FER01, CAT02].
In 2003, a new calibration by inserting a ^{51}Cr source will be carried out: a precise determination of absolute ν cross-section on Ga, within an uncertainty at a level of 5 %, is expected. In the original GNO proposal an increase of the target mass up to 100 tons with an intermediate step at a level of 60 tons, was foreseen by adding Ga in liquid form but these steps up to now are not funded. A joint experiment with SAGE collaboration has been even suggested but difficulties seem to rule out at present any development in this direction.

5.8. SNO.

The Sudbury Neutrino Observatory (SNO) experiment was proposed in the 80s', [SNO87]: it measures at the same time and in the same detector CC and NC interaction events using Čerenkov technique. It is worth to underlining that physicists looked for results coming from this experiment from many years, [YIN92, BAH96c, MAR00, BAH00a, BAH00b, BAH01d, BAR01a].
The detector is homed at a depth of 6010 mwe in the "INCO Creighton Mine", near Sudbury (Canada): the inner part is an acrylic transparent spherical shell 12 m in diameter filled with 1000 tons of heavy water (D_2O) surrounded by 1700 tons of ultrapure H_2O. A further outer volume of 5300 tons of ultrapure H_2O is used as a shield from neutrons and γ's from the rock. The background due to U and Th contamination is respectively at a level lesser than $4.5{\cdot}10^{-14}$ g/g and $3.5{\cdot}10^{--15}$ g/g.
The emitted Čerenkov light is collected by 9456 PMT's, 20 cm in diameter. The time resolution of 1.7 ns allows an event reconstruction within 30 cm of precision. About half of the light produced within 7 m of the detector centre strikes a PMT. The total coverage is at a level of $\sim$ 31 %. A fiducial volume was defined to accept events with

vertices within 5.50 m from the detector centre.
The energy threshold of 5.0 MeV allows contributions from CC interaction events in D_2O, ES events both in D_2O and H_2O, capture of neutrons from NC interactions and backgrounds and low energy Čerenkov events. After a calibration with ^{252}Cf source the neutron detection efficiency was estimated at a level of 14.4%. Only ^{8}B and Hep $\nu_\odot$'s can produce detectable interactions; the expected count rate is $\sim$ 20 events per day, [EWA92, MCD99, VIR00, SNO00, AHM01, SNO01].
It is worthwhile to note that SNO experiment represents a milestone in the $\nu_\odot$ physics thanks to many different parameters it could measure, [BAH00a]:

- CC and NC interactions.
- First and second moment of the recoil energy spectrum.
- D-N rates for both NC and CC interactions.
- Winter/summer CC interactions.
- NC to CC and ES to CC double ratio.

The value of ^{8}B $\nu_\odot$ flux or its flavour content, if any, can be extracted from CC and ES reaction, independently from SM calculations. The comparison of CC and ES interactions, as measured in SNO itself and in SK, allows an estimate of the flux of ν_x (x$\neq$ e) and $\overline{\nu}$.
Moreover, it is possible to measure the spectral shape of ^{8}B $\nu_\odot$'s with good statistics and the energy of the recoil electrons for CC and ES interactions.
SNO provides a "*verification*" of the SK data on ES interactions with a detector installed at a deeper depth and crossed by a much lower flux of atmospheric muons.
During 1999 there was an intense program of electronics, optical and energy calibration and it was possible to lower the trigger threshold and the Rn below the target levels. Phase 1 has provided an accurate measurement of ν_e flux *via* CC interaction, [MCD01]. The flashes recorded from November 1999 to May 2001 (306.4 days of running time) have been analysed: $1967.7^{+61.9}_{-60.9}$ CC events, $263.6^{+26.4}_{-25.6}$ ES events and $576.5^{+49.5}_{-48.9}$ NC events were detected (only statistical errors are given), [AHM02a]. The estimated systematic uncertainties are: for CC events $\pm$ 5.2% (exp.) and $\pm$ 1.8 % (theor.); for NC events $^{+9.1}_{-8.9}$% (exp.) and $\pm$ 1.3 % (theor.); for ES events $^{+5.0}_{-4.8}$% (exp.).
Recent improvements in theoretical calculation of the ν_e-D cross-section for CC interactions, [ORT00, BEA01, BUT01, KUR02, NAK01, NAK02], have been introduced in computations.
The deduced ^{8}B $\nu_\odot$ fluxes are, [AHM02a], see also fig. 15:

$$\begin{aligned}
\Phi_{CC} &= 1.76^{+0.06}_{-0.05}(stat.) \pm 0.09(sys.) \cdot 10^6\, cm^{-2}s^{-1} \\
\Phi_{ES} &= 2.39^{+0.24}_{-0.23}(stat.) \pm 0.12(sys.) \cdot 10^6\, cm^{-2}s^{-1} \\
\Phi_{NC} &= 5.09^{+0.44}_{-0.43}(stat.)^{+0.46}_{-0.43}(sys.) \cdot 10^6\, cm^{-2}s^{-1}
\end{aligned} \tag{54}$$

The ES flux is fully compatible with SK result. The excess of the NC events with respect to CC and ES interactions has been explained as a strong signal of ν flavour

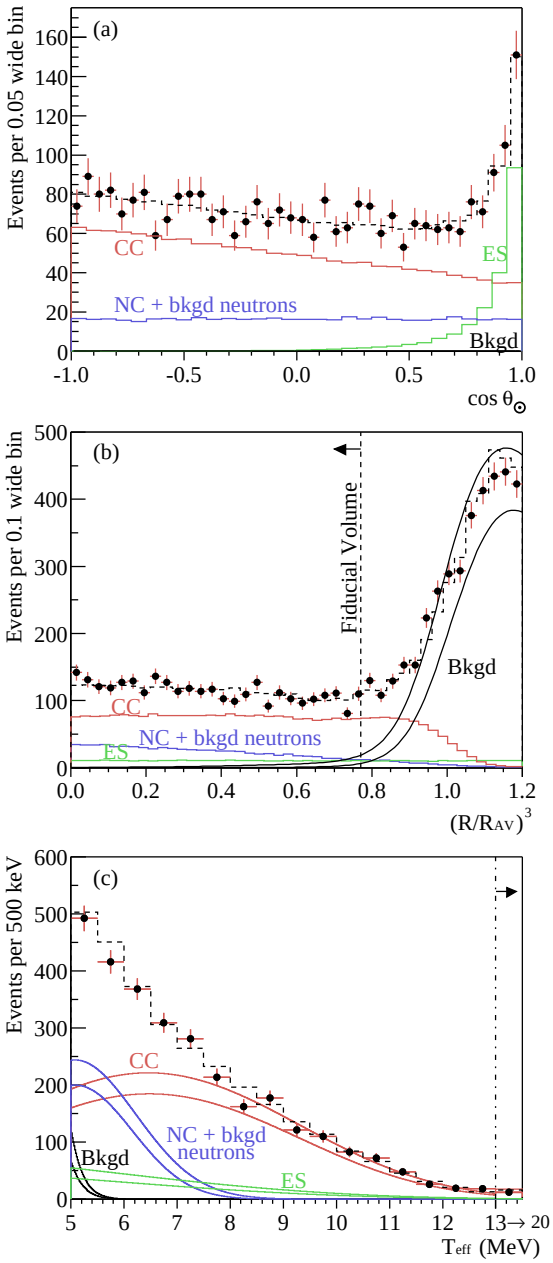

Figure 15. SNO data:(a) Zenithal distribution of events at a distance R $\leq$ 5.50 m. (b) Distribution of the volume weighted radial variable $(R/R_{AV})^3$. (c) Kinetic energy spectrum for R $\leq$ 5.50 m. Also shown are the Monte Carlo predictions for CC, ES and NC + bkgd neutron events scaled to the fit results, and the calculated spectrum of Čerenkov background (Bkgd) events. The dashed lines represent the summed components, and the bands show $\pm 1\sigma$ uncertainties. All distributions are for events with $T_{\rm eff} \geq 5$ MeV, from [AHM02b].

transformation, see later in section 7.2. Under the assumption of undistorted ^{8}B spectrum the non-electronic $\nu_\odot$ flux has been computed:

$$\Phi_{\mu+\tau} \;=\; 3.41^{+0.45}_{-0.43}(stat.)^{+0.48}_{-0.45}(sys.) \cdot 10^6\, cm^{-2} s^{-1} \qquad (55)$$

If errors are added in quadrature this flux is 5.3 σ above the null value; if the previous constraint on energy spectrum is removed, the $\nu_\odot$ flux, as deduced from the NC interaction data, is in agreement with [BAH01a] but its value is higher. Moreover, a much larger statistical error is present:

$$\Phi_{NC} \; = \; 6.42 \pm 1.57(stat.)^{+0.55}_{-0.58}(syst.) \cdot 10^6 \, cm^{-2} s^{-1} \tag{56}$$

Even D and N spectra and rates have been analysed, [AHM02b]: the total livetimes were 128.5 days for D-time and 177.9 days for N-time. If a solution to SNP is given in terms of oscillations among known ν flavours, any asymmetry is expected for NC events unless a "sterile" component is present. In the same description CC interactions should have non-zero asymmetry. A calibration with ^{16}N source puts in evidence a 1.3% per year drift in the energy scale, which has been removed in calculations. The results are reported in table 19, see also fig. 16.

In CC events a D-N asymmetry at a level of + 2.2σ is present (- 0.9σ for ES events

Table 19. *D-time and N-time fluxes in SNO data and A_{D-N} asymmetry under the hypothesis of undisturbed ^8B $\nu_\odot$ energy spectra are shown, adapted from [AHM02b].*

signal	Φ_D $10^6 \, cm^{-2} s^{-1}$	Φ_N $10^6 \, cm^{-2} s^{-1}$	A(%)
CC	$1.62 \pm 0.08 \pm 0.08$	$1.87 \pm 0.07 \pm 0.10$	$+14.0 \pm \; 6.3^{+1.5}_{-1.4}$
ES	$2.64 \pm 0.37 \pm 0.12$	$2.22 \pm 0.30 \pm 0.12$	$-17.4 \pm 19.5^{+2.4}_{-2.2}$
NC	$5.69 \pm 0.66 \pm 0.44$	$4.63 \pm 0.57 \pm 0.44$	$-20.4 \pm 16.9^{+2.4}_{-2.5}$

and - 1.2 σ for NC interactions). The signal extracted from ν_e component is A_e = 12.8 $\pm$ $6.2^{+1.5}_{-1.4}$ % while A_{TOT} = -24.2 $\pm$ $16.1^{+2.4}_{-2.5}$ %. If the assumption of no-asymmetry is added, then A_e = 7.0 $\pm$ $4.9^{+1.3}_{-1.2}$ %; this value has to be compared with the SK result $A_e^{SK} = 5.3 \pm 3.7^{+2.0}_{-1.7}$ %.

The deployment of NaCl to increase the NC detection capability started in May 2001. After 8 months of data taking, SNO will reduce its statistical error and should be able to give a more precise answer concerning the ν flavour oscillation solution.

6. The solar neutrino problem. (SNP)

¿From the first experimental result published in early 1968 it was possible to confirm the existence of solar neutrinos: all the experiments gave and currently confirm a positive signal but there was evidence of an interaction rate lower than the theoretical predictions; moreover, different data appeared even inconsistent. A puzzling situation was present until 2002. SNO experiment, which is able to distinguish among ES, CC and NC interactions, has detected three different $\nu_\odot$ fluxes: this result strongly supports an explanation of SNP in terms of new particle physics, as early recommended in [BAH90a]. Table 20 summarizes the presently available experimental results and theorethical fluxes

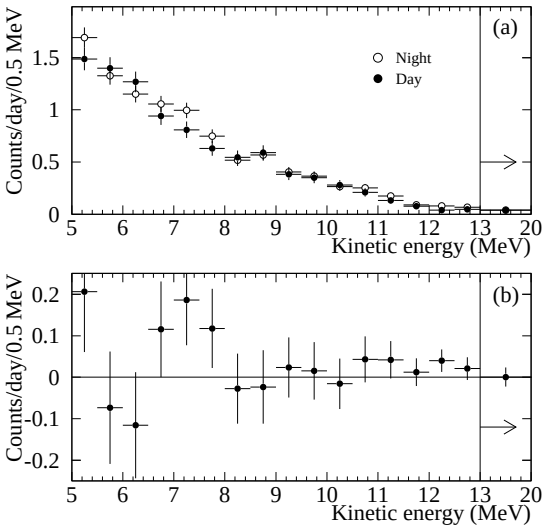

Figure 16. SNO data: (a) Energy spectra for D and N events including signals and backgrounds. The final bin extends from 13.0 to 20.0 MeV. (b) N - D difference between the spectra. D rate = 9.23 ± 0.27 ev/day; N rate = 9.79 ± 0.24 ev/day, from [AHM02a].

or interaction rates.

6.1. Present experimental situation.

Homestake experiment first detected $\nu_\odot$'s and showed the first SNP: the flux was lower of the predicted one by a factor of 3. Many years later KAMIOKANDE and SK measured a ^{8}B $\nu_\odot$ reduced by a factor of 2 with respect to the predictions of SMs. In Ga experiments the interaction rate was $\sim$ 60 % of the expected one. SNO, which has confirmed SK result concerning ES interactions, has identified CC and NC interaction events: it has measured three different values giving a robust indication that a component other than electronic one is present in $\nu_\odot$ flux reaching terrestrial detectors.
The presently available experimental results can be summarized in this way:

(i) The measured rates vary from $\sim$ 30% up to 100% of the values predicted by SMs but a more intriguing situation comes from the analysis of different contribution to the $\nu_\odot$ flux.
Highest experimental errors are at level $\sim$ 15% (SNO) while the theoretical uncertainties on $\nu_\odot$ flux vary from $\sim$ 10% up to $\sim$ 25%. Hence, it is difficult to eliminate the measured discrepancy in terms of errors in experimental and theoretical procedures.

(ii) SK "confirms" KAMIOKANDE; GALLEX, GNO and SAGE are each other compatible while SNO ES interaction rate strengthens SK by a different technique; Cl experiment is lonely and not reproduced.

Table 20. *Solar neutrino experiments: energy threshold, experimental results and predictions from [BAH01a].*

Experiment	E_{th}	Measurements	Predictions	Data
HOMESTAKE	0.814	2.56 ± 0.23	$7.6^{+1.3}_{-1.1}$	1970
615 t C_2Cl_4	MeV	SNU	SNU	1994
KAMIOKA	7	2.80 ± 0.38	$5.05^{+1.01}_{-0.81}$	1987
3000 t H_2O	MeV	$10^6 \nu\, cm^{-2} s^{-1}$	$10^6 \nu\, cm^{-2} s^{-1}$	1995
GALLEX	0.233	77.5 ± 7.7	127.8^{+9}_{-7}	1991
101 t $GaCl_3$	MeV	SNU	SNU	1997
SAGE	0.233	70.8 ± 6.5	127.8^{+9}_{-7}	1990
50 t Ga Metal	MeV	SNU	SNU	2001
GNO	0.233	65.4 ± 7.1	127.8^{+9}_{-7}	1998
101 t $GaCl_3$	MeV	SNU	SNU	2002
GALLEX+GNO	0.233	70.8 ± 5.9	127.8^{+9}_{-7}	1991
101 t $GaCl_3$	MeV	SNU	SNU	2002
SK	5.0	2.35 ± 0.08	$5.05^{+1.01}_{-0.81}$	1996
22500 t H_2O	MeV	$10^6 \nu\, cm^{-2} s^{-1}$	$10^6 \nu\, cm^{-2} s^{-1}$	2001
SNO	5.0	ES 2.39±0.268	$5.05^{+1.01}_{-0.81}$	1999
		CC 1.76±0.11		
		NC 5.09±0.64		
1000 t D_2O	MeV	$10^6 \nu\, cm^{-2} s^{-1}$	$10^6 \nu\, cm^{-2} s^{-1}$	2001

(iii) It seems unlikely that different experimental procedures and systematics could have unknown inefficiencies: the Ga experiments verified their total efficiency with strong man-made ^{51}Cr sources, yielding the expected results and reducing the probability of any inefficiency at a level of $\sim 10\%$. Moreover, they are based on different operational techniques and their results, which are each other compatible, confirm the foundations of stellar structure and evolution theory through the experimental observation of p-p fusion in the solar interior. As a further remark, in the limit of their modest statistics, Ga data do not yet exhibit any statistically significant $\nu_\odot$ flux variation in time which should imply a production rate constant in time.

(iv) Using the computed ν interaction cross-sections on Cl and the ^{8}B ν_e flux, as observed in SK and SNO ES events, a rate of ~ 3.7 SNU would be foreseen in Cl detector, a value well above the observed rate of 2.56 ± 0.23 SNU with a difference as great as 6 σ. The net flux coming from p-e-p, ^{7}Be and CNO $\nu_\odot$'s should be completely disappeared: in fact its rate is negative (- 1.1 ± 0.5 SNU). It should be possible to conclude that something peculiar occurs to $\nu_\odot$'s having intermediate energy.

(v) $L_\odot$ (or the energy conservation law) fixes the $\nu_\odot$ production rate: under the hypothesis that nothing happens to p-p and p-e-p $\nu_\odot$'s produced inside the Sun,

the minimum interaction rate that Ga detectors should measure is 79.5 ± 2.0 SNU, [BAH90a]. It is indeed necessary to add to the previous value a ^{8}B $\nu_\odot$ contribution as great as measured by SK and SNO ES flux: 5.6 ± 1.5 SNU, where the main component of the error is due to capture cross-section uncertainty. ^{7}Be $\nu_\odot$'s, which are thought to be needed in reaction chain producing ^{8}B $\nu_\odot$, should add 5.9 ± 1.4 SNU therefore a minimum signal of 91.0 ± 3.0 SNU is foreseen for Ga detectors, [RIC99]. Moreover, if one supposes that SNO NC interaction result confirms SMs, or that part concerning ^{8}B $\nu_\odot$ flux predictions, then it seems to be allowed to estrapolate the same conclusion to the ^{7}Be $\nu_\odot$ flux, which is the "parent" of ^{8}B component. Consequently, the terms to be added in previous analysis are 12.1 ± 2.5 SNU (^{8}B $\nu_\odot$'s) and 34.2 ± 3.4 SNU (^{7}Be $\nu_\odot$'s) so that the deficit in Ga experiments becomes dramatic: the measured interaction rate by combining SAGE and GALLEX+GNO data is 70.8± 4.5 SNU.

(vi) Ga experiments should suggest an interaction rate essentially coincident with the predictions concerning p-p and p-e-p components as given by SMs, therefore either the remaining nuclear reactions do not contribute to the $\nu_\odot$ production or a deficit in p-p and p-e-p $\nu_\odot$ flux is present. This is hard to accept, due to the strong correlation between p-p component and the present $L_\odot$.

(vii) The NC interactions in SNO indicate a ^{8}B $\nu_\odot$ flux in a good agreement with values estimated in many SMs; on the other hand, ES and CC interaction results, which are depending on flavour of interacting $\nu_\odot$'s, show a strong deficit. As a (natural) conclusion, a component other than electronic one seems to be present in the $\nu_\odot$ flux interacting in detectors on Earth.

(viii) The presently available results concerning temporal variations of $\nu_\odot$ flux are:

- **Day-Night effect** = Radiochemical detectors, which integrate the $\nu_\odot$ flux over long exposure times, cannot detect D-N difference; only real-time detectors enable us to analyse this effect. SK results do not show any significant difference between D and N fluxes while SNO data concerning CC interactions put in evidence an asymmetry at a level of + 2.2σ.
- **Winter-Summer effect** = There are no experimental indications of this effect.
- **Other solar features** = Recently, data from GALLEX and GNO experiments have been analysed searching for correlation with solar modulations, [STU99, STU01, STU02]. A bimodal distribution of measured rates per run has been obtained: its significance is not clear and this result is under further analysis. It has been suggested that the number of Ge atoms extracted in a single run has to be introduced in such statistical analysis not the interaction rate. A time-power spectrum analysis has enhanced periodicities either in Cl either in GALLEX+GNO data: they range from 24.5 up to 28.4 days, 28.4 and 26.9 days being the most significant values (very similar to solar X-ray modulations). No indications about non-standard interactions with $B_\odot$.

7. SNP: Proposed solutions.

Many different ideas were suggested to explain the SNP: we review some features of the most important solutions.

7.1. Astrophysical solution.

The first proposed way-out to the SNP was a change in SMs *via* the modifications both in solar physical parameters needed to lower the $\nu_\odot$ flux and in technical description (velocity distribution, screening treatment, initial solar conditions, solar elemental abundances, solar age, cross-sections for stellar reactions, opacities ...). Let us remember that many quantities are theoretically estimated (usually by an extrapolation from experimental available results) therefore uncertainties are propagated in calculations.
Immediately after the publication of Homestake results, Ezer and Cameron proposed that a mixing process in the solar core could have reduced the $\nu_\odot$ flux, [EZE68]; in 1981 a similar approach was suggested by [SCH81a]. In 90s' helioseismological data put in evidence that SNP cannot be ascribed to the parameters entering SMs, see *e.g.* [BAH90a, BAH02a], in fact T and ρ theoretical profiles are in good agreement with measured data. In order to lower the predicted $\nu_\odot$ flux, T_c should differ from the SMs expected values by more than 5% but theoretical profiles agree with helioseismological data at a level better than 0.1%.
Other proposals were presented: a reduction of ^{7}Be abundance in the central solar region; changes in nuclear reaction rates at the extreme boundaries of the uncertainty range done by [BAH01a]; deviation from the Maxwell-Boltzmann distribution by introducing a corrective term $\sim exp\left[-\frac{E}{kT} - \delta(\frac{E}{kT})^2\right]$; quantum treatments, different screening factors and opacities.
We underline that the effects of the surrounding plasma on nuclear reaction rates, namely reactions concerning ^{7}Be, are not known with accuracy, not only in solar plasma but even in laboratory experiments. Many studies have suggested to modify the "weak screening" approach. As a matter of fact interacting nuclei do have a kinetic energy much larger than mean value and the interaction rate is very sensitive to the high energy tail of velocity distribution inside the Sun. Different factors could modify the Maxwell-Boltzmann distribution, which is assumed to be true: diffusion, radiative flows, internal fluctuating electric and magnetic fields. SMs using these parameters were realized and their predictions seem to be compatible with the helioseismological constraints: a consistent depletion on $\nu_\odot$ flux except for Ga experiments is produced.
We mention the works done by Quarati and coll. which developed a totally different approach, [KAN97, KAN98, COR99], by using both a non extensive statistics in solar core and quantum uncertainty effects in the solar plasma analysis, [LAV01]. In their opinion Tsallis statistics, [TSA88], should give a better description of particles behaviour in solar plasma, where strong interactions at small distances among many particles could occur and the reaction collision time is comparable with the inverse plasma frequency. Further effects are produced by random electric microfields: a slow

varying component due to the plasma oscillations, a fast random component due to the diffusive cross-section and a further component due to the two-body Coulomb interaction. Equations relating these effects with parameters entering the Tsallis distribution were deduced; electron screening contribution is neglected because of its smallness. Even quantum corrections were introduced, following [GAL67, STA00], and the equilibrium distribution function uses momentum rather energy: the computed c_s profiles well agree with predictions given by usual SMs while the estimated $\nu_\odot$ flux is compatible with experimental data.
In [TUR00, TUR01a] the influence of these parameters on physical solar measurable quantities and on $\nu_\odot$ flux was analysed. The obtained interaction rates range from 2.8 to 6.7 SNU for Cl detector and from 102 to 125 SNU for Ga experiment; the ^{8}B ν flux varies from 1.7 to 4.7 $10^6 \nu\, cm^{-2} s^{-1}$.

7.2. Particle solution.

A "popular" solution to SNP is within particle properties sector; among other possibilities the most favoured one proposes ν flavour oscillations.
We mention a seminal Pontecorvo's paper on the subjet, [PON67]:
"*From an observational point of view the ideal object is the Sun. If the oscillation length is smaller than the radius of the Sun region effectively producing neutrinos...direct observations will be smeared out and unobservable. The only effect on Earth's surface would be that the flux of observable sun neutrinos must be two times smaller than the total (active and sterile) neutrino flux.*"
Neutrino flavour oscillations are quantum processes requiring both mass and mixing of the ν flavours or, otherwise, a step beyond the standard particle model (we remember that in non-standard particle theories the flavour mixing can be defined even without massive ν's). If the weak interaction states are not the mass eigenstates, the first ones are superposition of definite mass states which can be either Dirac or Majorana particles, either active or sterile ν's.
The mathematical description of the oscillation process is given as in quark sector by introducing a mixing matrix (similar to the CKM matrix); a CP violating phase term is also possible but usually it is not included because of its smallness. For a good and exhaustive presentation see [KUO89].
When solar data are under analysis, the simplest and "easier" explanation of SNP requires 2 flavour oscillation; in this picture 2 parameters, a mixing angle θ and a difference mass term Δm^2, are needed and sufficient to describe this solution. Following [FOG96, GOU00], it is better to analyse the experimental data in term of $\tan^2\theta$ rather than $\sin^2 2\theta$ in order to study solutions with $\theta \geq \pi/4$, the so called "dark side"; these analyses are given in "exclusion" plots.
The mixing matrix is real and orthogonal (a rotation by an angle θ is present).
The $\nu_\odot$ motion from the Sun to the Earth is "in vacuum" and is described by a

"Klein-Gordon" equation, see [RAF96, HAX00] for a complete review of the technical treatment. In the more general case:

$$|\nu(t=0)\rangle = a_e(t=0)|\nu_e\rangle + a_\mu(t=0)|\nu_\mu\rangle \tag{57}$$

from which one calculates:

$$i\frac{d}{dx}\begin{pmatrix} a_e \\ a_\mu \end{pmatrix} = \frac{1}{4E}\begin{pmatrix} -\Delta m^2\cos 2\theta_V & \Delta m^2 \sin 2\theta_V \\ \Delta m^2 \sin 2\theta_V & \Delta m^2 \cos 2\theta_V \end{pmatrix}\begin{pmatrix} a_e \\ a_\mu \end{pmatrix} \tag{58}$$

where θ_V is the mixing angle in vacuum and x = t, that is, set c = 1.
Under usual approximations, a "Schrödinger-like" time-dependent solution can be found, the Hamiltonian of the system being the kinetic term.
The probability to detect a different flavour is computable: the transition depends on distance, on momentum and on the square mass differences of the physical neutrinos. The appearance probability at a distance L is:

$$P(\nu_{1,2}) = \sin^2 2\theta_V \sin^2\left(1.27\Delta m^2(eV)^2\frac{L(m)}{E(MeV)}\right) \tag{59}$$

where $\Delta m^2 = |m_2^2 - m_1^2| > 0$. The survival probability is complementary to the unity value.
The first oscillation maximum occurs when L/E $\sim \Delta m^{-2}$ while the term $\sin^2 2\theta$ (the oscillation probability amplitude) has a maximum when $\theta_V = \pi/4$. The time a ν has to transform its flavour (state) is proportional to L/E, where L is the distance between the ν source and the observer. The ratio E/L varies from $\sim 10^{-11}$ for $\nu_\odot$'s up to $\sim$ 1 for high energy ν's from accelerators. The Sun-Earth distance (d=1.496 $\cdot 10^{11}$ m = $7.58 \cdot 10^{23}$ MeV) gives a lower bound on mass difference.
The evolution equation changes in the presence of matter to:

$$i\frac{d}{dx}\begin{pmatrix} a_e \\ a_\mu \end{pmatrix} = \frac{1}{4E}\begin{pmatrix} 2E\sqrt{2}G_F n_e(x) - \Delta m^2\cos 2\theta_V & \Delta m^2 \sin 2\theta_V \\ \Delta m^2 \sin 2\theta_V & -2E\sqrt{2}G_F n_e(x) + \Delta m^2 \cos 2\theta_V \end{pmatrix}\begin{pmatrix} a_e \\ a_\mu \end{pmatrix} \tag{60}$$

where G_F is the weak coupling constant and n_e(x) the electron density (either solar or terrestrial). The term $2E\sqrt{2}G_F n_e(x)$ represents the effective contribution to M_ν^2 that arises from neutrino-electron scattering. The indices of refraction of electron and muon neutrinos differ because the former scatter by CC and NC interactions, while the latter have only NC interactions. The difference in the forward scattering amplitudes determines the density-dependent splitting of the diagonal elements of the new matter equation.
The new Hamiltonian is not diagonal in the mass basis: a complexe treatment to diagonalize the operator and to compute the survival probability and the time evolution has to be applied, [BAR80, OHL00, BAR01a], but matter steady eigenstates do not coincide with the vacuum ones. Sometimes, analytical solutions are possible; as example when n_e is constant, the mixing angle is:

$$\tan 2\theta_M = \tan 2\theta_V \left(1 - \frac{L_V}{L_e}\frac{1}{\cos 2\theta_V}\right)^{-1} \tag{61}$$

where the oscillation length in vacuum L_V is:

$$L_V \;=\; \frac{4\pi E}{\Delta\, m^2} \tag{62}$$

and the ν_e interaction leght is:

$$L_e \;=\; \frac{\sqrt{2}\,\pi}{G_F\, n_e} \tag{63}$$

Independently of the smallness of θ_V, θ_M gives a maximal mixing when a resonance condition is present:

$$\cos 2\theta_V \;=\; \frac{L_V}{L_e} \tag{64}$$

The mass difference has to be positive; moreover, either ν's or $\overline{\nu}$'s can show this resonance, but not at the same time. Maximum mixing corresponds to the maximum mixing angle only in vacuum within a two flavour oscillation description: this conclusion is not valid when matter is present or within a more than two flavour analysis.
The appearance probability in matter becomes:

$$P(\nu_1 \;\rightarrow \nu_2) \;=\; \sin^2\, 2\theta_M\, \sin^2 \frac{\pi\, L_V}{L_{M(E)}} \tag{65}$$

where the energy dependent matter oscillation length $L_{M(E)}$ is:

$$L_{M(E)} \;=\; L_V \cdot \left(1 \;-\; 2\frac{L_V}{L_e}\, \cos 2\theta_V \;+\; \left(\frac{L_V}{L_e}\right)^2\right)^{-1/2} \tag{66}$$

The probability of flavour mixing shows a typical resonance behaviour and assumes the maximum value at the resonance energy.
If the density of the medium is variable, as in solar case, the evolution equation cannot be solved analitically with the exception of few peculiar cases. An adiabatic low varying density is an interesting situation: when an outgoing ν_e crosses regions with slow decreasing density θ_M can decrease and reach the resonance condition. A further propagation toward lower density regions leads to the "transition" to a vacuum value θ_V: if this value is small, then ν_e is near its lowest energy state and even the flavour mixing is small.
The probability of converting a ν_e to a different flavour in the Sun is therefore strictly related to the electron density profile, in fact $\nu_\odot$ can resonantly oscillate only when peculiar values of electron density occur.
The computations become much more complex in three flavour oscillation approach: two oscillations can occur with different flight times (or frequencies). The probability to observe a a different neutrino flavour has a structure similar to eq. 59 but the amplitude depends on two mixing angles. In this case, the interval [0,π/2] has to be considered and the description in terms of $\tan^2\theta$ is needed. The unitary mixing matrix is written as a product of three rotation: θ_{12} is connected to the solar data, θ_{23} is due to the atmospheric sector, θ_{13} is presently constrained by measurements at reactors. A further

term is related to CP sector. In this description the matrix is:

$$\begin{pmatrix} c_{12}c_{13} & s_{12}c_{13} & s_{13}e^{-i\delta} \\ -s_{12}c_{23} - c_{12}s_{23}s_{13}e^{i\delta} & c_{12}c_{23} - s_{12}s_{23}s_{13}e^{i\delta} & s_{23}c_{13} \\ s_{12}s_{23} - c_{12}c_{23}s_{13}e^{i\delta} & -c_{12}s_{23} - s_{12}c_{23}s_{13}e^{i\delta} & c_{23}c_{13} \end{pmatrix} \quad (67)$$

where c_{ij} or s_{ij} are the periodic functions of angles θ_{ij} (i,j=1,2,3) while δ is a phase related to CP.
In this case the survival probability is:

$$P^{(3)}(\nu_e \to \nu_e) = cos^4\theta_{13}P^{(2)}(\nu_e \to \nu_e) + sin^4\theta_{13} \quad (68)$$

where $P^{(2)}(\nu_e \to \nu_e)$ is the survival probability within a two flavour mixing description. A realistic flavour oscillation picture foresees that ν_e's are produced in the solar core, then they can oscillate into active ν and/or sterile ν's. If this process happens before ν_e's reach the Earth, these ν's are undetectable in experiments based on captures on nuclei (Cl and Ga). Only SNO can presently identify $\nu_\odot$ component other than electronic one. In 1990, the use of the luminosity constraint as a test independent of SMs of the hypothesis of $\nu_\odot$ flavour oscillations was proposed, [SPI90],(many papers described the $\nu_\odot$ spectrum as sum of 3 terms, low-intermediate-high energy $\nu_\odot$'s, [DAR91, HAT94a, CAS94, BER94, FOG95, PAR95, BAH96b, HEE96]).
Different patterns were considered in ν oscillation analysis.

- **Vacuum oscillations (VAC)**. As suggested by Pontecorvo, [PON67], the ν oscillation length is the Sun-Earth distance and the ν survival probability is energy dependent. The $\nu_\odot$ flux is differently suppressed due to the possibility of a fine-tuning. A distortion of the energy spectrum is expected. A strong seasonal modulation should be present because of the variation of the distance between the Sun and Earth, [BER95]. Concerning the D-N asymmetry, VAC solution at E$\geq$ 2 MeV has rapid oscillations but the detectability of fluctuations both at high and low energy is very difficult due to the rough resolution in energy the detectors presently have.
  In the case of the ^{7}Be flux a variation of 10-30 % is foreseen while a reduction lesser than 10 % should occur in Ga and Cl experiments. The suggested mass difference values are in the region $\Delta m^2 \approx 10^{-10}(\mathrm{eV})^2$.
- **MSW solution**. Flavour oscillations can be resonantly enhanced by "matter effect", or Mikheyev-Smirnov-Wolfenstein (MSW) effect, [WOL78, WOL79, MIK85, MIK86]. The (even complete) flavour conversion can occur through coherent $\nu - e^-$ scattering at the very high electron density prevailing in the solar interior and the resonance condition is:

  $$\frac{n_{e,res}}{N_{Av}} \approx 66 \cos 2\theta_V \left(\frac{\Delta m^2}{10^{-4}\, eV}\right)\left(\frac{10\, MeV}{E}\right) \quad (69)$$

  where $n_{e,res}$ is the electron density at resonance in cm^{-3}, N_{Av} is the Avogadro number, $\Delta\, m^2$ is absolute value of the difference between the masses of two different flavours, E is the neutrino energy. In fig. 17 the electron density profiles as

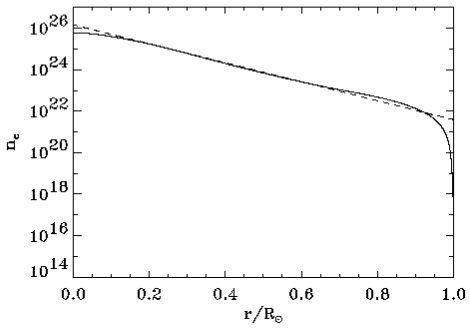

Figure 17. The electron number density computed in [COU02] as a function of distance from the solar centre. The approximation proposed in [BAH01a] (dashed line) is also drawn, from [COU02].

computed in [COU02] is shown.
If right handed ν's are taken into account, another density has to be considered:

$$n_{ster} \;=\; n_e - 0.5 n_n \;=\; n_e \left(\frac{1+3X}{2(1+X)} \right) \tag{70}$$

where n_n is the neutron density and X is the H fraction. In fig. 18 the ratio between electron and neutron density as a function of the distance from the solar center is shown.
For a detailed analysis of survival probability computation in different solutions see *e.g.* [BAH01d].
Experimental results suggested different sets of MSW parameters which can account for the $\nu_\odot$ fluxes, energy spectra and D-N asymmetry: *large mixing angle* (LMA), *small mixing angle* (SMA), *low mass* (LOW). The area above $\Delta m^2 \approx 10^{-5}\mathrm{eV}^2$ near the maximal mixing is called LMA solution; the SMA solution is located between $\Delta m^2 \approx 10^{-5} - 10^{-6}\mathrm{eV}^2$ and $\tan^2\theta \approx 10^{-3}$. The LOW solution ranges in the mass region $\Delta m^2 \approx 10^{-7} - 10^{-9}\mathrm{eV}^2$ while the lower part is called quasi-Vacuum (Q-VAC) solution.
Depending on Δm^2, $\nu_\odot$ oscillations can be driven by the oscillation phase or by

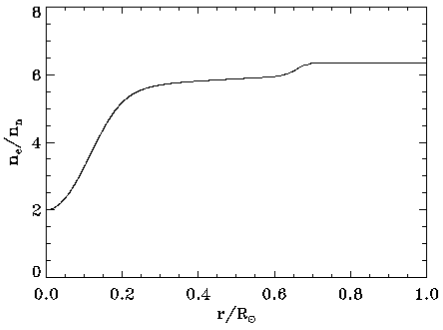

Figure 18. The computed n_e/n_n ratio as a function of distance from solar centre, from [COU02].

matter effects. In the former strong spectral distortions are expected while in the latter case spectral distortions can still occur due to a resonance, which is energy dependent, caused by the density of the solar matter. The Earth's matter density can also affect the conversion probability: in fact a "regeneration" of "disappeared" ν_e's during the night is possible: the flux during N-time (Earth crossing) and D-time (no Earth crossing) should be different.

LMA solution predicts rapid oscillations in Earth and a rather flat distribution in zenith angle. LOW solution corresponds to the matter dominated regime of oscillations and predicts a structure of peaks in the zenith distribution, [BAL88, GON01d]. The D-N asymmetry is detectable for the LMA solution only at E$\geq$ 5 MeV; moreover, its value increases with E. LOW solution shows the opposite behaviour.

LMA predicts a small reduction of the p-p $\nu_\odot$ flux, a strong depletion of the ^{7}Be $\nu_\odot$ contribution and an energy independent reduction of the ^{8}B $\nu_\odot$ component.

SMA solution requires an almost complete suppression of ^{7}Be component, a reduction of the ^{8}B term with deformation on the energy spectrum and no practically effect on p-p $\nu_\odot$'s, [HAT94b].

LMA and LOW solutions predict an increase of the survival probability at low

energies (below the SK and SNO thresholds). The LMA solution does not foresees the matter resonance inside the Sun at low energy so that the probability increases up to the averaged vacuum oscillation value; on the contrary in the LOW solution the survival probability raises its value because of the Earth matter effect. These values are different so that experiments sensitive to low energy $\nu_\odot$'s can check the right solution. The shape of the spectrum for LOW solution shows a weak positive slope.

- **Just So^2.** An early solution, called Just So, was proposed in 1987 to describe vacuum oscillations in vacuum with a mass value, $\sim 10^{-11}$ (eV)^2, which reduces the ^{8}B contribution to Cl experiment; this is an *ad hoc* solution, [GLA87]. Recently, this approach has been renewed but new mass value of $\sim 10^{-12}$ (eV)^2 and a ^{8}B $\nu_\odot$ flux at a level as great as half of the SMs predictions are required, [RAG95, KRA96, LIU97, BAH00b, FOG00].
- **Resonance Spin Flavour Precession** (RSFP). If lepton flavour is not conserved, ν's must have flavour-off-diagonal (transition) magnetic moments, which applies either to Dirac and Majorana ν's and trasversal magnetic field will produce a simultaneous rotation of ν spin and flavour, a spin-flavour precession which can be resonantly enhanced in matter in a very similar way to the MSW effect, [CIS71, SCH81b, SCH82, VOL86a, VOL86b, AKH88, AKH88a, LIM88, AKH95, LIM95, AKH01]. For Majorana ν's the resulting $\overline{\nu}$ can still be detected in electron scattering experiments, while in the Dirac case the final state remains undetectable. The conversion mechanism is dependent on ν energy. RSFP requires either $B_\odot \sim 100$ kG and $\mu_\nu \sim 10^{-11}\mu_B$, a value not experimentally excluded but hard to achieve in a simplest extension of the standard particle model. The available information on $B_\odot$ is presently limited; a large field in the convective zone may not be possible, since it would show up as an 11 year cycle in the SK data which is known not to be the case. Instead a large $B_\odot$ in the lower radiative zone and the core where most $\nu_\odot$'s are produced has been proposed. It remains unclear however whether the sunspots cycle effect extends down to the bottom of the convective zone. Altogether, radiative zone and core field profiles on one hand and convective zone ones on the other are equally favoured by the data: a strong central $B_\odot$ with a rapid decrease thereafter is preferred. The shape of these profiles follows a dipole structure centered at the solar centre and closely resembles the solar density profile. Furthermore RSFP provides a close relationship between the energy shape of the survival probability and $B_\odot$ profile: the most suppressed $\nu_\odot$'s have their resonance located in the region where $B_\odot$ is the strongest. Specific time signatures of the RSFP mechanism may be related with the possible non-axially symmetric character of $B_\odot$ or the inclination of the Earth's orbit. In the first case a time dependence would appear as a variation of the event rate with a period of 28 days, while in the second the possible polar angle dependence of $B_\odot$ would cause a seasonal variation of the rate. Since only the product of μ_ν and $B_\odot$ enters in the ν evolution equation, the analysis can be applied to any other value of μ_ν provided

that $B_\odot$ is rescaled accordingly.
It is assumed that ν's have Majorana-like transition magnetic moments μ_ν which cause the transitions $\nu_{eL} \rightarrow \bar{\nu}_{\mu R}$ or $\nu_{eL} \rightarrow \bar{\nu}_{\tau R}$ in the solar magnetic field, (the Majorana ν gives a better fit of $\nu_\odot$ data than the Dirac ν does). The transition probability depends crucially on the shape and on the $B_\odot$ strength which are essentially unknown. Many $B_\odot$ profiles were proposed but the most part of them in general allows marginal fits of experimental data: at present only few profiles enables fits in agreement with experiments; we mention profiles 1 and 6 from [PUL00], and profile 4 from [PUL01]. The RSFP solution of the SNP is hard to establish experimentally. Except for predicting reduced $\nu_\odot$ flux, it has negative signatures: no time variations beyond the usual d^{-2} variation due to the eccentricity of the Earth's orbit ($B_\odot$ does not vary with time); no D-N effect; no significant distortions of the energy spectrum. In [MIR01] it has been shown that even a non-resonant SFP should be able to reproduce the experimental data.

- Non-standard interactions inducing ν oscillations were suggested, [VAL87, GUZ91, ROU91, BAR91, BER00, GUZ01]. The Hamiltonian in evolutionary equations shows the usual structure: the diagonal term depends either on fermion and electron density radial profiles and on a phenomenological parameter characterizing the strength of the ν interaction. The off-diagonal term, which has the same action of the mixing term in standard MSW solution, is strictly related to the fermion density and to a second parameter responsible for flavour changing. In this approach the conversion probability is energy independent but it is possible to reproduce the detected spectra because the production distributions for $\nu_\odot$'s are different so that a resonant conversion does occur in solar interior.
- The violation of the weak equivalence principle (VEP) of the general relativity has been proposed as mechanism inducing flavour oscillation even if ν's are massless, [GAS88, HAL91, PAN93, GAG00a, GAG00b, GAG01, NUN01b]. In this case ν mixing and flavour oscillation are due to different gravitational interactions so that a violation to the general relativity is needed. Weak and gravitational interacting eigenstates differ so that a mixing angle θ_G is introduced as in the ν mixing in vacuum due to the mass. The evolution equations, describing degenerate mass propagating through gravitational potential, show similar components both in diagonal and off-diagonal terms: they are depending on the energy, on the difference of the gravitational interaction and on the gravitational potential. The mixing term, which depends on $\sin 2\theta_G$, is linearly related to the energy so that the oscillation length is inversely proportional to the ν energy. Two different mechanisms are possible: VEP resonant conversion (a MSW-like process), which badly reproduces experimental data, [PAN00], and VEP vacuum conversion which better agrees with measurements, [GAG00b, GAG01, RAY02].
- Other suggested mechanisms foresee neutrino decay, [CHO01b, CHO01c, CHO02], and CP and T violation, [KUO87, DER99, DIC99, ARA97, BIL98]. In the latter

only appearance experiments should be able to observe this effect which is beyond the presently available technical capabilities. Even neutrino decay in vacuum followed by an oscillatory *scenario* was proposed, [LIN01], but present experimental results do not support this suggestion. In [BAR00] correlations between ν properties and extra dimensions have been analysed.

7.3. The pre-SNO situation.

Complete analyses of SNP in terms of ν flavour mixing were done by many authors, [FOG00, GIU00, GON01a, GON01b, GON01d, GON01f, SCH01] and quoted references. Let us underline that slightly different assumptions can be adopted and consequently results are similar but not equal. Ga experimental results can be separately inserted instead of their average value; KAMIOKANDE results are usually excluded; energy spectra from SK are sometimes added to SK flux but these values are not independent from the SK rate; D-N or zenithal energy spectra are included, sometimes the constraints given by CHOOZ experiment are added.
Let us remember that the total event rate gives information on average oscillation probability while the energy spectrum specifies the dependence of the probability from energy, oscillation length and time. If only fluxes and interaction rates from different experiments are used the "RATES" analysis is given while "GLOBAL SOLUTION" occurs when all parameters concerning $\nu_\odot$ flux are included. SK experiment gives a dominant contribution due to its large, statistics and zenith angle distribution combined with energy spectra.

7.3.1. Two flavour analysis. In terms of 2 flavour mixing the standard procedure uses least-squares analysis so that the authors calculated the allowed regions in $(\Delta m^2, \theta)$ plane, see [FOG96, BAH98c]. This is an approximation of rigorous frequentist methods, [CRE01, GAR01, GAR02a, GAR02b], which can offer results even different from the standard least-squares approach. We underline that several frequentist analyses are available so that it is not easy to select the right procedure.
In the case of active-active ν oscillation different regions are possible for the GLOBAL fit in $(\Delta m^2, \theta)$ plot: SMA, LMA, LOW, VAC and Just So^2; solutions into sterile ν's are also allowed (SMA,VAC and Just So^2). D-N asymmetry is small and the survival probability at higher energy, with the exception of VAC solution, assumes a practically flat dependence. The Earth regeneration effects are relevant only within the mass range 10^{-5} - 10^{-7} (eV)^2. An analytical approach, following [MIK86, KAN87, TOS87, ITO88a, ITO88b, KRA88a, KRA88b, PET88], is usually adopted.
At the beginning of 2001, when SK measurements based on 1258 days of data taking were available, the conclusions quoted in [SMY00, SUZ01a] were:

(i) The ^{8}B spectrum, which does not show a strong suppression at large energies as expected in MSW adiabatic solutions, seems to be undisturbed, even if the uncertainties are large. The low-energy part of the spectrum plays a crucial role

therefore a lowering of the threshold down to 4.0 MeV seems to be necessary (but impossible after the incident occurred in late 2001).

(ii) SK D-N spectrum and the total flux define an enlarged LMA region; the LOW region extends down to the VAC one. LMA solution is the favoured one at 95% C.L. because of the flatness of energy distribution and of the smallness of the D-N effect which takes long time to obtain positive evidence, if any. It is hard to distinguish between LMA and LOW solutions. SMA, Just So solutions and Sterile neutrinos are disfavoured at 95%.

(iii) Measurements of NC interactions are needed.

LMA, SMA and LOW solutions in the case of active ν's and SMA sterile solution were estimated in [BAH01b] as relatively robust solutions, while the VAC solution was classified as fragile. The Just So^2 solution, which is allowed both for active and sterile ν's, showed a relative robustness: in fact it did not well reproduce the Cl rate, otherwise it was in a very good agreement with Ga and SK data.
The results obtained in GLOBAL analysis before SNO data can be summarized in this way:

- The LMA solution gave the best fit, mainly thanks to the constraints done by SK data on D-N and the flatness of the energy spectrum.
- The LOW solution, which is connected with Q-VAC region at 99% CL and extends into the second octant, well described the spectrum data, but it was weaker than LMA because of the rates.
- The SMA solution showed worst results due to its difficulty in the spectrum analysis and the conclusions were similar for sterile solutions.

In practice all these solutions were allowed but LMA was slightly preferred, see fig. 19. We remember that the LMA solution was shown to be the best oscillation solution for the first time in [GON00].
In fig. 20 the NC/CC ratio expected in SNO is shown while in fig. 21 the predictions concerning seasonal difference are drawn.

7.3.2. Three flavour analysis. A more general description is needed when atmospheric, reactor and solar neutrino results are analysed: oscillations occur among three flavours and the unitary matrix relating flavours and masses contains 2 mass differences, 3 mixing angles and 1 or 3 CP violating phases, depending on Dirac or Majorana nature of ν's, [FOG00, GON01a, GON01f]. The CP phases produce effects not accessible to the present experiments so that their contributions are usually excluded from the results. The transition probability has 2 oscillation lengths and shows an oscillatory behaviour. Usually, a hierarchy $\Delta m^2_{atm} \gg \Delta m^2_{\odot}$ is present. The analysis of $\nu_{\odot}$ data constrains 3 parameters (Δm^2 and two mixing angles) while ν_{atm} results pose boundaries on the remaining mass difference and on 2 mixing angles. Only a parameter is common, the θ_{13}

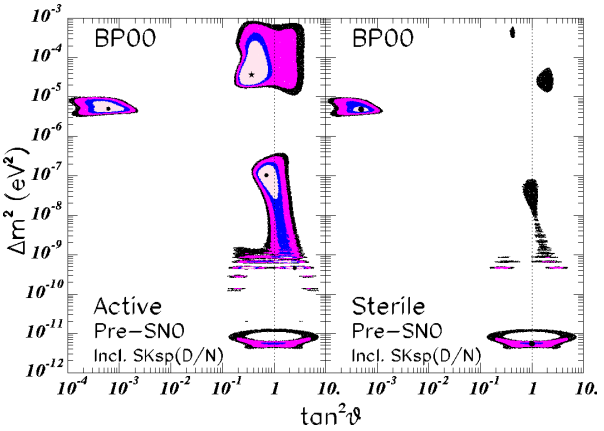

Figure 19. GLOBAL analysis solutions at the beginning of 2001: input data include the total rates from the Cl and Ga averaged experiments, the recoil electron D and N energy spectrum measured by SK. The C.L. contours are 90%, 95%, 99%, and 99.73% (3σ). The allowed regions are limited by the CHOOZ reactor measurements, $\sim$ 7-8 $\cdot 10^{-4}$ (eV)^2. The local best-fit points are marked by dark circles. The theoretical errors for $\nu_\odot$ fluxes from [BAH01a] are included, from [BAH01c].

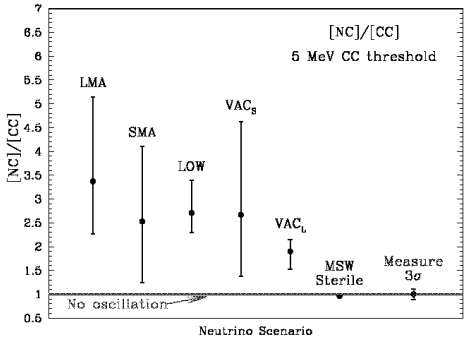

Figure 20. The NC/CC double ratio predictions in SNO at E$\geq$ 5 MeV for different oscillation solutions (the standard model foresees 1.0). The solid error bars represent the 99% C.L. for the allowed regions. The dashed error bar labeled "Measure 3σ" represents the uncertainty in interpreting the measurements, from [BAH00a].

mixing angle, which is strongly constrained by CHOOZ reactor experiment, [APO99]. Its final result suggests $\theta_{13} < 15^\circ$ at 99 % CL; furthermore, oscillations down to $\Delta\, m^2 \sim 7{\cdot}10^{-4}$ (eV)^2 for full mixing are excluded. As $\tan^2\theta_{13}$ increases, all the allowed regions in the (Δm^2,$\tan^2\theta_{12}$) plot disappear so that an upper bound to $\tan^2\theta_{13}$ is present. Moreover, no $\overline{\nu_e} \leftrightarrow \overline{\nu_\mu}$ oscillations were found by PALO VERDE reactor experiment; the ratio between observed and calculated rate is $R = 1.01 \pm 0.024(stat.) \pm 0.053(syst.)$ for $\Delta\, m^2 \geq 1.1 \cdot 10^{-3}$ (eV)^2 at full mixing and $\sin^2 2\theta \geq 0.27$ at large $\Delta\, m^2$, [BOE01]. Other parameters do not influence the mixing matrix elements.
The results can be summarized in this way:

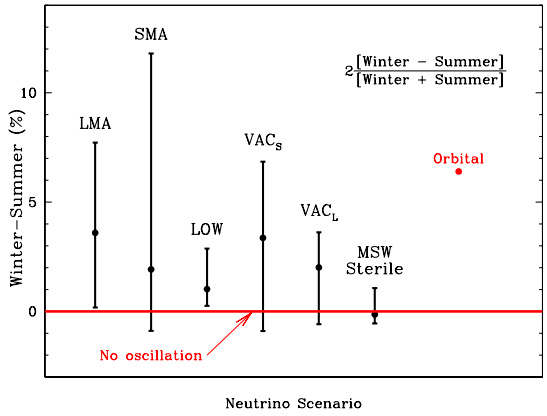

Figure 21. The figure shows for different oscillation solutions the difference (%) between the predicted CC rate in SNO, at E≥ 5 MeV, for a 45 day interval during winter and summer. "Orbital" represents the 45 day winter-summer difference due to the Earth's motion around the sun; the amplitude of this orbital motion has been removed from the neutrino oscillation points. The error bars represent the 99% C.L. for the allowed regions, from [BAH00a].

- LMA is the preferred solution; SMA and LOW solutions are less favoured even if LOW is more acceptable and can provide maximal mixing (θ_{12}= $\pi/4$) for non-zero θ_{13}. Some interesting perspectives survive for VAC solution.
- CHOOZ provides an upper limit on $\sin^2\theta_{13}$ and Δm^2; solar experimental results prefer $\sin^2\theta_{13}$ ∼0 in a good agreement with CHOOZ, but there it no reason for it to be zero.
- Unambiguous selection of ONE solution will not be possible in SK data for several years. Much higher statistics is needed for instance in the spectrum.

7.3.3. Four flavour analysis. More complicated analyses are needed when LSND results are included: ν fields are connected to 4 mass eigenstates *via* a 4x4 unitary mixing matrix containing 6 mixing angles (in any case the CP violating phases are disregarded), [DOO00, GIU00, GON01e].

The reason usually adopted to introduce a new ν flavour is the appearance probability in LSND experiment: three oscillations are needed to explain all the available experimental data. The presently detected ν flavours are three with two independent oscillations, therefore a new flavour has to be added. It is useful to remember that the invisible width of Z-boson as measured at LEP poses a strong limit to weakly interacting neutrino number (3 flavours) so that the new neutrino is supposed to be "sterile", or without interactions with matter. In fact, if $\nu_4 \simeq \nu_e$ then $P(\nu_\odot) \simeq 1$ but the $\nu_\odot$ flux deficit is incompatible; if $\nu_4 \simeq \nu_\mu$ then $P(\nu_{atm}) \simeq 1$ but atmospheric results from SK, MACRO, Soudan rule out this solution; if $\nu_4 \simeq \nu_\tau$ then for the atmospheric sector $\nu_\mu \rightarrow \nu_e + \nu_s$ with strong matter effect never detected. Therefore, $\nu_4 = \nu_s$ is the only viable solution. There are 6 schemes compatible with solar, atmospheric and LSND results: in the so

called "3+1" schemes 3 ν masses are similar, the remaining one is separated by a gap of ~ 1 (eV)^2; otherwise "2+2" schemes with the same energy gap are foreseen. The analyses are strongly model dependent and the experimental data do not give sure indications on the right solution.
The main conclusions were, [GON01e], see also fig. 22:

- The analysis of $\nu_\odot$ data with 4 flavours was the same as in 2 flavour case but a 3-D parameter space was required. Physical space was described if θ_{12}, θ_{23} and θ_{24} vary within the $(0,\pi/2)$ interval, the last two angles entering only by the combination $\cos^2\theta_{23}\cos^2\theta_{24}$.
- A simultaneous analysis of active-sterile and active-active solutions was allowed.
- LMA, LOW and Q-VAC solutions disappeared with increasing values of mixing parameter $\cos^2\theta_{23}\cos^2\theta_{24}$.
- LMA solution was allowed at 95 % if $\cos^2\theta_{23}\cos^2\theta_{24} = 0.5$; each solution was estimated possible at 99% for the maximal mixing case.

7.4. 2001: After SNO (I).

Since first results concerning CC and ES interactions in SNO were available, [AHM01], and a common energy threshold for SK and SNO experiments was computed, new and more complete analyses became possible, [BAN01, FOG01, BAH02c, BAN02a, BAR02a, FOG02a, FOG02b, KRA02].
In summer 2001 the main conclusions were:

- There is a deficit in ν_e flux with respect to the SMs predictions; moreover, there is an evidence that a ν_e conversion into $\nu_{\mu,\tau}$ does occur.
- No astrophysical solution of SNP seemed to be viable.
- Solutions based on pure active-sterile conversion were strongly depressed.
- At $E \sim 6$ MeV the ν_e survival probability is less than 0.5 (from [AHM01] one finds $P = 0.334 \pm 0.22$ in the case of pure active transition). An even smaller value was found when sterile components were included.

The combination of SNO and SK results suggested that the $\nu_\odot$ flux depletion is due to the particle physics sector or, in other words, not only $\nu_{\odot,e}$'s interact inside terrestrial detectors. It seemed therefore (highly) probable that ν_e's produced in solar core undergo flavour conversion, but with an unknown mechanism.
The most part of published papers searched for an answer to the SNP within a flavour oscillation solutions. Let us underline again that if the same input data and analysis are used, different authors obtain essentially identical results, but when different strategies are adopted the predictions are not fully coincident, see for instance [BAH02c, KRA02] for a comparison. The most restricted regions are obtained when all available rates are combined with SK D-N energy spectra, while the largest areas are present if ^{8}B $\nu_\odot$ flux (or even Hep component) is treated as a free parameter, while SK rates are excluded

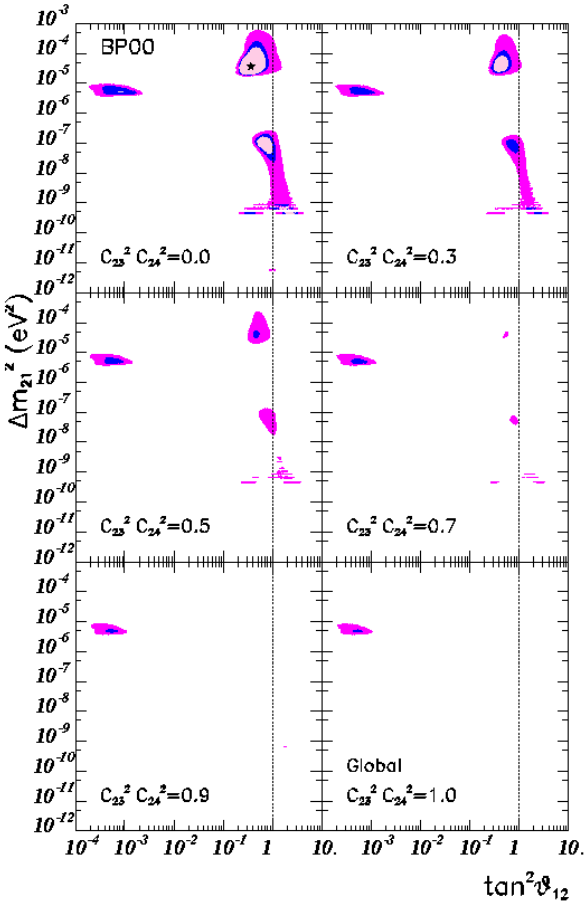

Figure 22. Results of the GLOBAL analysis of $\nu_\odot$ data for the allowed regions in Δm^2_{21} and $\tan^2\theta_{12}$ for the 4 ν description. The different panels represent sections at a given value of the active–sterile admixture $|U_{s1}|^2 + |U_{s2}|^2 = c^2_{23}c^2_{24}$ of the three-dimensional allowed regions at 90%, 95% and 99% CL. The best-fit point in the three parameter space is plotted as a star, from [GON01e].

because of D-N energy spectra.
We show in table 21 the best-fit GLOBAL solution parameters as done in [BAH02c, KRA02]; details concerning the strategy adopted in the analysis are shown in captions.

The main conclusions the GLOBAL analyses put in evidence were, see [KRA02]:

- The LMA solution foresaw as ratio between CC interactions rate and the value predicted in [BAH01a] R_{CC} = 0.20-0.41; the best theoretical values was slightly lower than the SNO mean value, 1 σ. This solution reproduced the physical observables at a level of (or better than) 1 σ, the largest deviation occurring in Cl flux calculations, 1.4 σ higher. SNO measurements shifted the LMA solution region to higher mixing angle values where the survival probability is greater. A slightly higher ^{8}B $\nu_\odot$ flux was allowed (by a factor of 1.1).
- The LOW solution predicted R_{CC} = 0.36-0.42, 2 σ above the SNO result. There

Table 21. *Best-fit GLOBAL analysis oscillation parameters with all solar neutrino data. Best-fit values of the parameters Δm^2, $\tan^2\theta$; f_B and f_{Hep} are the factors multiplying the ^8B and Hep $\nu_\odot$ fluxes as given in [BAH01a]. (s) in the first column means sterile solution. The first 5 columns show results quoted in [KRA02]. The number of degrees of freedom is 38: 4 rates (Homestake, SAGE, GALLEX+GNO, SNO) + 38 SK spectra points - 4 parameters. Last 3 columns are concerning results from [BAH02c]. The number of degrees of freedom is 39 [38 SK spectra + 3 rates - 2 parameters (Δm^2,θ)]. The best-fit fluxes and their estimated errors from [BAH01a, BAH02c] are included. Interaction rates from the GALLEX+GNO and SAGE experiments provide a unique data point.*

	$\Delta m^2(\mathrm{eV})^2$	$\tan^2\theta$	f_B	f_{Hep}	χ^2_{min}	$\Delta m^2(\mathrm{eV})^2$	$\tan^2\theta$	χ^2_{min}
LMA	$4.8\cdot10^{-5}$	0.35	1.12	4	29.2	$3.7\cdot10^{-5}$	0.37	34.5
VAC	$1.4\cdot10^{-10}$	0.40 (2.5)	0.53	6	32.0	$4.6\cdot10^{-10}$	2.5	42.3
LOW	$1.1\cdot10^{-7}$	0.66	0.88	2	34.3	$1.0\cdot10^{-7}$	0.67	40.8
SMA	$6.0\cdot10^{-6}$	0.0019	1.12	4	40.9	$5.2\cdot10^{-6}$	0.0018	49.9
J.So^2	$5.5\cdot10^{-12}$	1.0	0.44	0	45.8	$5.5\cdot10^{-12}$	0.61	52.1
VAC(s)	$1.4\cdot10^{-10}$	0.38 (2.6)	0.54	9	35.1	$4.7\cdot10^{-10}$	3.0	49.1
J.So^2(s)	$5.5\cdot10^{-12}$	1.0	0.44	0	46.2	$5.5\cdot10^{-12}$	0.61	52.1
SMA(s)	$3.8\cdot10^{-6}$	0.00042	0.52	0.2	48.2	$4.6\cdot10^{-6}$	0.00034	52.3
LMA(s)	$1.0\cdot10^{-4}$	0.33	1.14	0	49.0	–	–	–
LOW(s)	$2.0\cdot10^{-8}$	1.05	0.83	0	49.2	–	–	–

was a shift of allowed region toward smaller mixing angles corresponding to smaller survival probability.

- R_{CC} = 0.33-0.42 was the estimated value for the VAC solution, a 1 σ higher mean value while VAC oscillations to ν_s indicated R_{CC}= 0.36-0.41.
- Remaining solutions, in particular SMA, were less probable because of their high R_{CC} value (0.37-0.50). Moreover, the suppression showed an energy dependence of opposite sign with respect to the SNO data. The Just-So^2 (active), SMA (sterile) and Just-So^2 (sterile) were strongly depressed because they foresee the same rate in SK as in SNO.

The SK and SNO results were well within the region where an oscillation from ν_e to $\nu_{\mu,\tau}$ does occur, independently from any sterile component, [FOG01, FOG02a]. The ν_e survival probability took the lowest value allowed by pre-SNO results. Assuming a purely active oscillation, all the main predictions given by SMs were confirmed and the ν_e survival probability was found to be $\sim 1/3$ in the SK-SNO energy range, see fig. 23. The allowed solutions before SNO data, see fig. 19, were still present at level greater than 3 σ; the best-fit values are in LMA region but remaining solutions (LOW, VAC, Q-VAC) were not excluded. In fig. 24 experimental energy spectrum is fitted by using different oscillation solutions.

The LMA region was enlarged: SNO results suggested relatively small values of ν_e

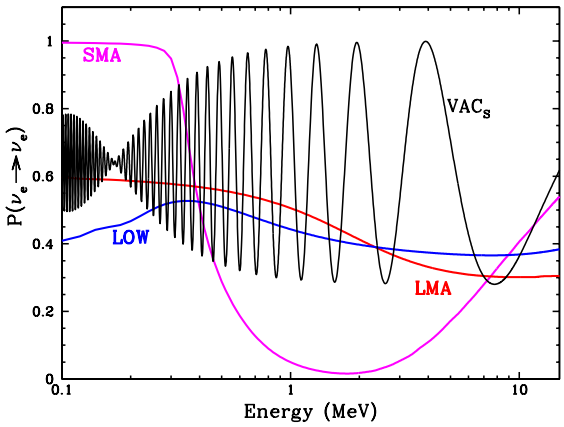

Figure 23. Comparison of survival probabilities for flavour oscillation solutions, a linear energy scale is used, from [BAH00a].

.

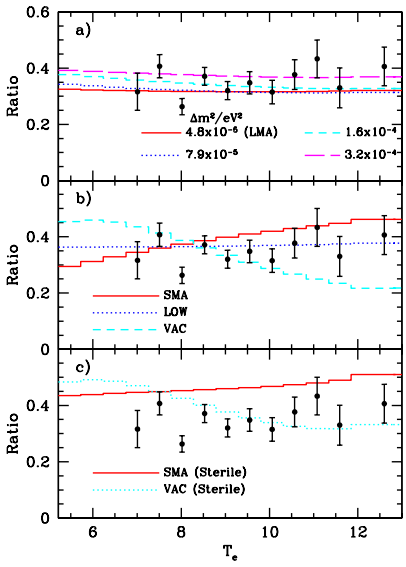

Figure 24. The recoil electron energy spectra of the CC events in SNO for different GLOBAL solutions compared with experimental data, from [AHM01]. Shown are the ratio of the number of events with and without conversion as a function of the electron kinetic energy. In a) LMA solutions for different values of Δm^2 and $\tan^2\theta = 0.35$; in b) SMA, LOW and VAC (active) solutions; in c) SMA(sterile) and VAC(sterile) solutions, from [KRA02].

survival probability consequently LMA solution was favoured in the GLOBAL fit. The SMA solution vanished at level greater than 3 σ when SK D-N spectra were included in the analyses. The LOW solution was less favoured than the LMA due to Ga experiments which supported an increase of the ν_e survival probability at low energy.
SNO results did not modify qualitatively the solution for $\nu_\odot$'s but strengthened the case

for active oscillations with LMA, see fig. 25.

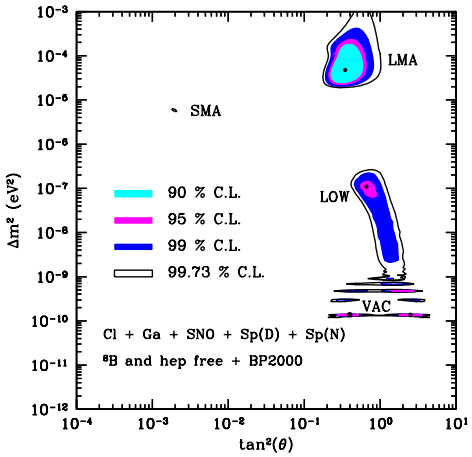

Figure 25. GLOBAL analysis solutions with ^{8}B and Hep $\nu_\odot$ fluxes as free parameters. The best fit points are marked by dark circles. The absolute minimum of the χ^2 is in the LMA region. The allowed regions are shown at 90%, 95%, 99% and 99.73% C.L. with respect to the minimum in the LMA region, from [KRA02].

Many authors discussed the possibility of bi-maximal neutrino oscillations ($\tan^2\theta = 1$), [MIN97, BAR98, XIN00, CHO01a, GHO01]: this option was not favoured by LMA solution at a level ranging from 98.95% C.L. to 99.95% C.L., depending on the adopted strategy.
When the temperature scaling of the nuclear reactions giving rise to ^{7}Be and ^{8}B $\nu_\odot$'s was imposed as an external condition on the fitting procedure, the assumption of no-oscillation is excluded at 7.4 σ, [BAH01c] see also [BAH02a, BAH02b].
We underline that in 4 flavour oscillation analysis, [GON01c], the minimum was found to be in the LMA region, with $\cos^2\theta_{23}\cos^2\theta_{24}= 0.$, $\tan^2\theta_{21}= 0.41$, Δm^2_{21}=$4.1\cdot 10^{-5}(eV)^2$, see also fig. 26.

7.4.1. Waiting for Neutral Current results. We report in this section a short chronicle through the predictions before the longed for SNO results on NC interactions. In table 22 and table 23 the expected $\nu_\odot$ fluxes provided by different GLOBAL analysis solutions are shown, from [BAH02c, KRA02].

In [GAR01], Bayesian and standard least-squares techniques were applied in a GLOBAL analysis context. The χ^2 minimum value was in LMA region if only transition into an active ν is considered, see fig. 27, in VAC region when transition into sterile ν's were allowed. SMA solution was strongly disfavoured and only a small region was allowed for

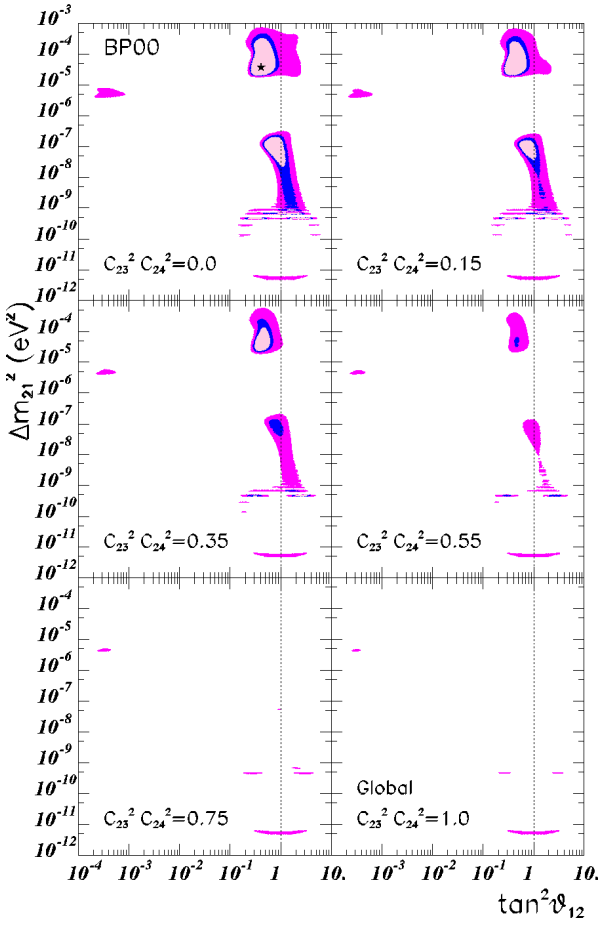

Figure 26. GLOBAL analysis solutions with 4 ν's as in fig. 22 but SNO data, from [AHM01], are included, from [GON01c].

VAC solution. As a marginal conclusion, the authors deduced that the likelihood ratio is a more powerful test in the analysis with respect to the usually adopted "goodness of the fit".
When Bayesian method was applied, either in RATES only or in GLOBAL case, the allowed regions were larger than in the standard analysis: in any case, LMA solution gave the best result and was strongly suggested to be the right solution, the LOW solution was marginally acceptable, see fig. 28. VAC and SMA solutions were in practice excluded, see also [CRE01] for further analyses based on Bayesian approach.
In table 24 predictions concerning the expected interaction rates in different detectors based on RSFP solution to the SNP as computed in [AKH02] are shown.

In [GAG02], different standard and non-standard solutions were analysed. In a first step a RATES analysis with the usual least-squares method was done: for RSFP and non-standard ν interaction solutions a high confidence level was found, even if a very strong $B_{\odot}$ is required ($\sim$ 100 kG); VAC oscillation gave the best result among standard solutions. When energy spectrum and zenithal dependence were included

Table 22. *Interaction rates (in SNU for Cl and Ga experiments, in $10^6\,\nu\,cm^{-2}s^{-1}$ for SK and SNO detectors) as expected for three different flavour oscillation solutions. The first 3 columns are concerning Cl values, in the remaining ones Ga rates are shown. The rates are computed for the best-fit values of the allowed solutions by using the astrophysical factor as quoted in [JUN02] , adapted from [BAH02c]. See table 8, table 12 and table 20 for a comparison with SMs predictions and experimental results.*

Source	LMA	LOW	VAC	LMA	LOW	VAC
p-p	0.00	0.00	0.00	41.80	38.70	44.30
p-e-p	0.12	0.11	0.16	1.49	1.35	1.95
Hep	0.01	0.02	0.03	0.02	0.03	0.04
^{7}Be	0.62	0.58	0.54	18.70	17.50	16.40
^{8}B	2.05	2.94	3.95	4.27	6.13	8.33
^{13}N	0.05	0.04	0.05	1.80	1.69	2.01
^{15}O	0.17	0.16	0.20	2.77	2.64	3.29
^{17}F	0.00	0.00	0.00	0.03	0.03	0.04
Total	3.02±0.3	3.85±0.5	4.93±0.6	70.9±2.6	68.1±2.8	76.4 ±3.2
SK	$2.39^{+0.33}_{-0.36}$	$3.02^{+0.42}_{-0.45}$	$3.81^{+0.53}_{-0.57}$	–	–	–
SNO(CC)	$1.72^{+0.24}_{-0.26}$	$2.50^{+0.35}_{-0.38}$	$3.26^{+0.46}_{-0.49}$	–	–	–

Table 23. *Predictions for Cl, Ga, SK and SNO experiments in the best fit points of GLOBAL solutions found in the free flux analysis. For SK and SNO detectors the fraction (in percent) with respect to the value quoted in [BAH01a] is given, adapted from [KRA02].*

	Cl(SNU)	Ga(SNU)	SK (%)	SNO (%)
LMA	2.89	71.3	45.2	32.3
SMA	2.26	74.4	46.3	39.6
LOW	3.12	68.5	44.6	36.8
VAC	3.13	70.2	42.3	36.4
Just So^2	3.00	70.8	43.4	43.4
SMA(s)	2.93	75.5	43.5	44.5
VAC(s)	3.24	69.9	41.4	38.1
Just So^2 (s)	3.01	70.9	43.4	43.5

and a GLOBAL analysis was done, then LMA, RSFP and non-standard ν interactions provided the same confidence level, see table 25 where results computed in [MIR01] concerning resonant and non-resonant SFP solutions are added in the last raws. Flavour oscillation solutions and RFSP approach provided results explaining to the solar, atmospheric and accelerator data, see fig. 29 and fig. 30.

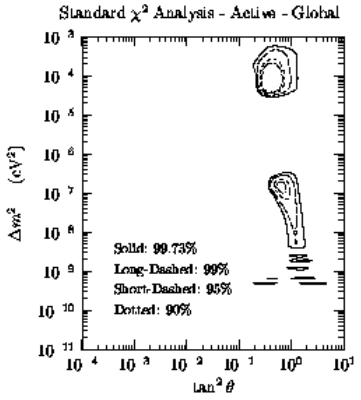

Figure 27. Allowed regions for active transitions in standard analyses including Cl, Ga averaged, SNO rates, SK D and N electron energy spectra and CHOOZ result, from [GAR01].

The main conclusions based on the latest SK data (1496 days of running time) were, [SMY02a]:

- SMA and VAC solutions were excluded: in fact ^{8}B $\nu_\odot$ spectrum seemed to be without distortions. A smaller D-N asymmetry and a slightly flatter recoil energy spectrum produced a small reduction in the lower-mass region of the LMA solution and in the upper-mass region of the LOW solution, see also[BAH02c].
- SK rate required a ^{8}B $\nu_\odot$ flux larger than Cl rate allows so almost the Q-VAC solutions disappeared: only the upper part of LMA and two very small Q-VAC

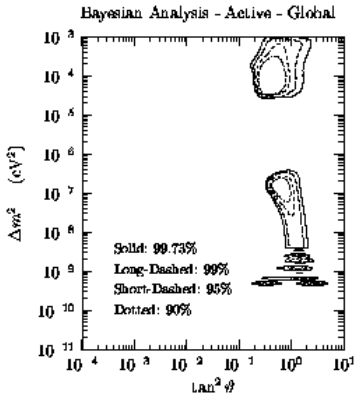

Figure 28. Credible regions obtained with a Bayesian GLOBAL analysis using the same input data as in 27. The drawn lines represent the posterior probability to contain the true values of $\tan^2\theta$ and Δm^2, from [GAR01].

solutions, which better describe SK zenith angle spectrum, survived. The LMA solutions $\Delta\, m^2 \geq 3{\cdot}10^{-5}$ (eV)^2 were found to be the only realistic solution at 95%. In fact Q-VAC solutions were rejected because of the rates of all experiments.

- The excluded areas did not depend on $\nu_\odot$ flux computed with SMs.
- The mixing angle was large but not maximal; moreover, $\Delta m^2 < 10^{-4}$ (eV)^2. In three flavour oscillation solutions the computed mixing angle values were: $\theta_{12} \approx \frac{\pi}{6}$, $\theta_{23} \approx \frac{\pi}{4}$, $\theta_{13} \approx 0$.
- When SK and SNO results were combined the appearance of $\nu_\odot$ flavours other than

Table 24. *The ratio between the expected rates corresponding to best-fit GLOBAL analysis, from [AKH02], and the SSM predictions, from [BAH01a, BAH02c], are shown. In the first column the selected $B_\odot$ profiles: 1 and 6 from [PUL00], 4 from [PUL01]. The values of χ^2_{min} correspond to 39 d.o.f., adapted from [AKH02].*

Profile	R_{Ga}	R_{Cl}	R_{SK}	R_{SNO}	Δm^2 (eV)^2	$B_\odot$ (kG)	χ^2_{min}
1	0.59	0.30	0.41	0.35	$7.65 \cdot 10^{-9}$	45	37.8
6	0.58	0.30	0.39	0.33	$1.60 \cdot 10^{-8}$	113	36.1
4	0.58	0.30	0.40	0.33	$1.48 \cdot 10^{-8}$	101	35.5

Table 25. *Comparison of existing solutions to the SNP when total rates, energy spectrum and zenithal dependence are used. For each one of the indicated mechanisms the best fit values of the relevant parameters are shown, the corresponding χ^2_{min} and C.L. level, adapted from [MIR01, GAG02].*

			χ^2_{min}	C.L.
NO OSC.			100.0 (48 d.o.f)	$1.6 \cdot 10^{-5}$
	Δm^2(eV)^2	$\tan^2\theta$		
LMA	$6.15 \cdot 10^{-5}$	0.349	38.7	75%
VAC	$4.65 \cdot 10^{-10}$	1.89	46.1	47%
LOW	$1.01 \cdot 10^{-7}$	0.783	45.0	38%
SMA	$4.93 \cdot 10^{-6}$	$4.35 \cdot 10^{-4}$	61.5	6.3%
RSFP	Δm^2 (eV)^2	$B_{\odot,max}$ (kG)		
	$1.22 \cdot 10^{-8}$	440	38.4	78%
Non-standard Int.	ϵ'	ϵ		
d-quarks	0.599	$3.23 \cdot 10^{-3}$	37.9	80%
u-quarks	0.428	$1.40 \cdot 10^{-3}$	37.9	80%
VEP	$\lvert\phi\Delta\gamma\rvert$	$\sin^2 2\theta_G$		
	$1.59 \cdot 10^{-24}$	1.0	42.9	60%
	Δm^2 (eV)^2	$\tan^2\theta$		$B_\perp$ (kG)
Non-Resonant SFP	$4.0 \cdot 10^{-9}$	$3.5 \cdot 10^3$	3.83(4 d.o.f.)	84
RSFP	$8.9 \cdot 10^{-9}$	$1.1 \cdot 10^{-3}$	2.98(4 d.o.f.)	84

electronic one was strengthened.

In [FRI02] $\overline{\nu}_\mu$ and $\overline{\nu}_\tau$ components were proposed to be present in $\nu_\odot$ flux, as predicted under spin flavour flip assumption. This process could be induced by a strong relic $B_\odot$ acting in the radiative zone: its strenght should be lower than 0.55 MGauss, mainly due to helioseismological constraints.

Values of quantities measurable by different experiments were newly computed: we report in table 26 [NC]/[CC] ratio and D-N asymmetries, both for ES and CC interactions, [BAH02c], see also fig. 31, fig. 32 and fig. 33. We remark that

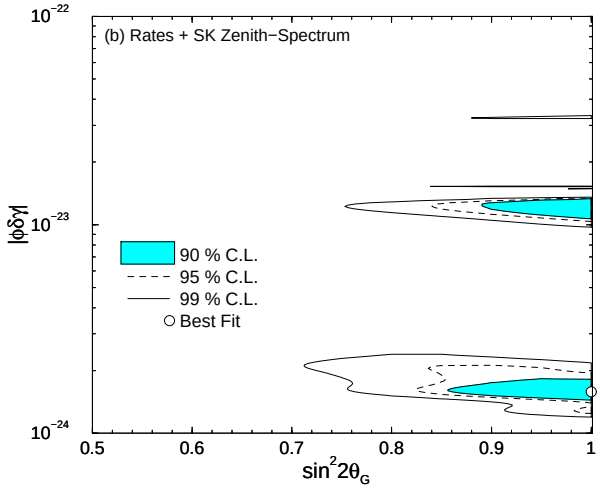

Figure 29. GLOBAL analysis best-fit solution in violation of equivalence principle description as a function of parameters entering the mixing matrix, from [GAG02].

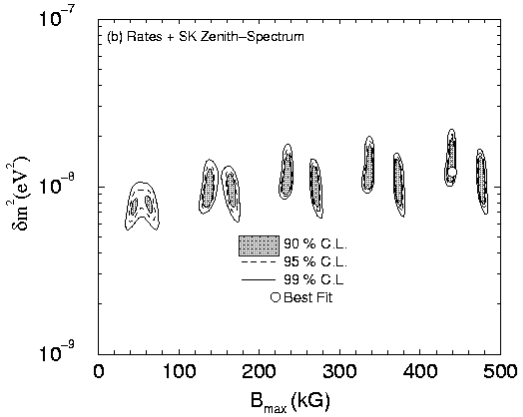

Figure 30. GLOBAL analysis best-fit solution within a RSFP description. On the X-axis the magnetic solar field intensity is shown, from [GAG02].

the predictions concerning the D-N asymmetry for ES interactions in SK and SNO experiments are very similar.

Table 26. *Predictions for NC/CC double ratio, D-N asymmetry for CC and ES events in SNO. Two different thresholds of the recoil electron kinetic energy are used: 4.5 MeV and 6.75 MeV. The 3σ regions are obtained within a GLOBAL analysis using modified ^8B $\nu_\odot$ flux, adapted from [BAH02c].*

	4.5 MeV	6.75 MeV
	[NC]/[CC]	[NC]/[CC]
LMA	3.44 (1.79,5.28)	3.45 (1.82,5.28)
LOW	2.39 (1.71,3.22)	2.37 (1.71,3.20)
VAC	1.76 (1.43,2.06)	1.82 (1.46,2.17)
	A_{D-N}^{CC}	A_{D-N}^{CC}
LMA (%)	7.4 (0.0,+19.5)	8.3 (0.0,+21.4)
LOW (%)	4.3 (0.0,+10.4)	3.7 (0.0,+9.5)
VAC (%)	0.1 (-0.2,+0.3)	0.2 (-0.3,+0.5)
	A_{D-N}^{ES}	A_{D-N}^{ES}
LMA (%)	4.1 (0.0,+10.1)	4.7 (0.0,+11.4)
LOW (%)	3.3 (0.0,+7.8)	2.9 (0.0,+7.1)
VAC (%)	0.0 (-0.1,+0.1)	0.1 (-0.2,+0.3)

7.5. 2002: After SNO (II).

After the SNO results on NC interactions and D-N asymmetry, a lot of new articles was prepared. A great part of published papers involves only active ν transitions; in [BAH02e] the possible contribution of a ν sterile component is also analysed. Usually, the standard least-square technique approximation for the definition of the allowed regions with a given confidence level has been applied.

SNO collaboration has presented results for the CC, NC, and ES fluxes under the assumption that the CC and ES recoil energy spectra are undistorted by ν oscillations or any other new physics. This hypothesis is a good approximation for the LMA and LOW solutions but is less accurate for the remaining ones.

In [ALI02a, ALI02b, BAH02f, DEH02, FOG02c, KRA02], results and predictions obtained within a GLOBAL analysis approach are exposed (it has to be underlined that used techniques are slightly different).

In [BAH02f], the energy dependence and correlations of the errors in the ν absorption cross-sections for the Cl and Ga experiments as computed in [BAH02e], the latest data from SAGE, [ABD02], zenith angle-recoil energy spectrum data from SK after 1496 days, [SMY02a], the predictions and the uncertainties from [BAH01a], different strategies in

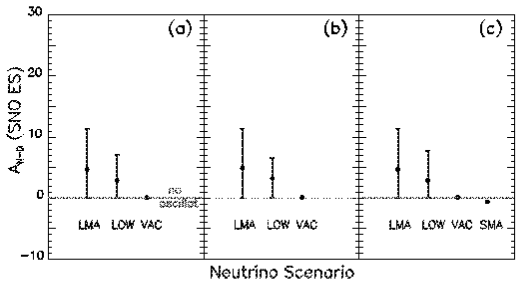

Figure 31. Predictions for SNO experiment: the percentage differences between D and N ES interactions (for flavour oscillation solutions allowed at 3σ C.L.). The recoil electron kinetic energy threshold is 6.75 MeV. The three panels refer to results for different analysis strategies: in a) modified ^{8}B flux is used, [BAH02c], in b) SK event rate is also included, in c) the ^{8}B ν flux is a free parameter, from [BAH02c].

analyses are used.

The strategy (a) selects $\nu_\odot$ fluxes from [BAH01a] (with the exception of ^{8}B component which is a free parameter), the experimental rates (with the exception of SK total rate), the zenith angle-recoil energy spectrum data for SK, fluxes and asymmetries from SNO. On the contrary, strategy (b) includes the predictions concerning ^{8}B $\nu_\odot$ flux and uncertainty from [BAH01a] while in strategy (c) the total SK rate is included together with a free normalization factor for the zenith angle-recoil energy spectrum of the recoil electrons. Strategy (b) allows a slightly larger region for the LOW solution mainly due to the uncertainty for the ^{8}B $\nu_\odot$ flux, see also fig. 34. The comments from [BAH02f] are based on strategy (a).

In [DEH02], the rates measured by Homestake, SAGE, GALLEX+GNO are separately introduced in computations. The SK values, based on 1496 days of data taking, include 8 energy bins with 7 zenith angles bins in each, except for the first and the last energy bins (44 points). The experimental errors and systematic uncertainties treatment is respectively from [SMY02a] and from [GAG02]. In [FOG02c] 81 observables (Cl and Ga

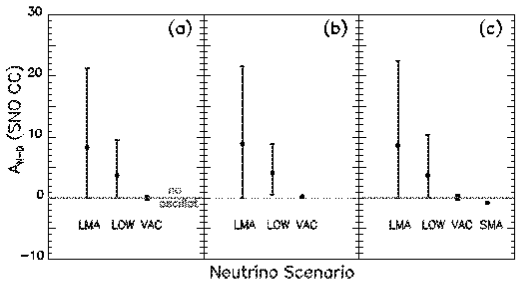

Figure 32. Predictions for SNO experiment: as in fig. 31 but for CC interactions in SNO (for flavour oscillation solutions allowed at 3σ C.L.). The recoil electron kinetic energy threshold is 6.75 MeV. The three panels refer to results for different analysis strategies: in a) modified ^{8}B flux is used, [BAH02c], in b) SK event rate is also included, in c) the ^{8}B ν flux is a free parameter, from [BAH02c].

average rates, winter-summer difference from GALLEX+GNO, 44 absolute event rates for the energy-nadir differential spectrum of electrons from SK, 34 D-N energy spectrum bins from SNO experiment) and 31 sources of correlated systematics (12 uncertainties related to SSM input, the ^{8}B ν shape uncertainty, 11 SK error sources and 7 SNO sources) are considered in χ^2 modified analysis.

(i) SNO results have reduced the area for the LMA and LOW solutions, see fig. 35, which are allowed at 3σ C.L. (for VAC solution 2.1 σ, but SNO coll. does not find this solution at the 3σ level in its analysis, see fig. 36). If $\nu_\odot$ fluxes quoted in [AHM02a, AHM02b] are introduced in computations with the assumptions of undisturbed recoil energy spectrum and without statistical correlations, VAC solution is not allowed at 3.1σ, [BAH02f].

(ii) Latest results from SAGE and GNO experiments lower the averaged Ga rate, [ABD02, KIR02], but these values are consistent (for instance the latest GNO results are 1.5σ below the previous GALLEX data). It has to be recalled that troubles in acquisition are reported from SAGE coll. so that an "*a posteriori*"

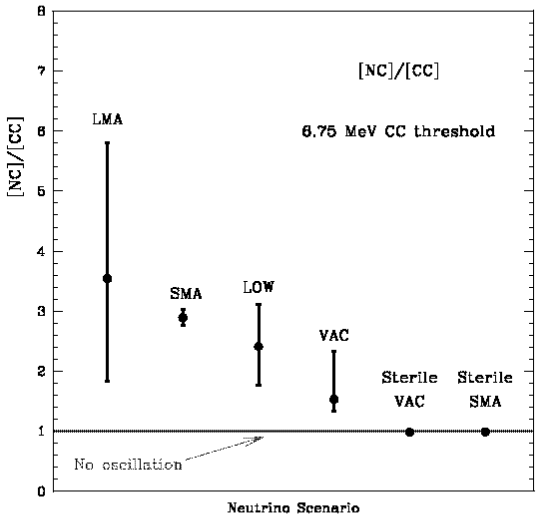

Figure 33. The NC/CC ratio in the best-fit points of the GLOBAL analysis solutions with free fluxes analysis: the error bars show the intervals of NC/CC which correspond to the 3σ allowed regions, from [KRA02].

corrective factor is applied to 1996-1999 measurements while GNO experiment has a completely new electronic setup and a different data acquisition and a lower background is obtained. Both the experiments have improved their systematics: consequently the statistical errors are larger while the systematic ones are reduced. In any case, lower rates in Ga experiments reinforce the LOW solution, [STR02].

(iii) For MSW solutions the energy dependence of the survival probability is weak at high energy, see fig. 37 : SK results do not show statistically significant distortion of the recoil energy spectrum. SNO and SK data have provided a survival probability $P(\nu_e \rightarrow \nu_e) \approx 1/3$; at $E \leq 1$ MeV this value should be $\sim 1/2$, but there are no experimental measurements. The results from SNO have modified at a small level solutions having a survival probability not strongly dependent upon energy (LMA and LOW), while their impact is large on SMA and VAC solutions. A shift of the predicted central values for CC and NC interaction rates is also present, [BAH02f]. SK and SNO results do not suggest any statistical significant hint for Earth matter effect or for modifications in ^{8}B $\nu_\odot$ spectra; both LMA and LOW solutions can fit the D-N asymmetry but different energy values and zenith-angle

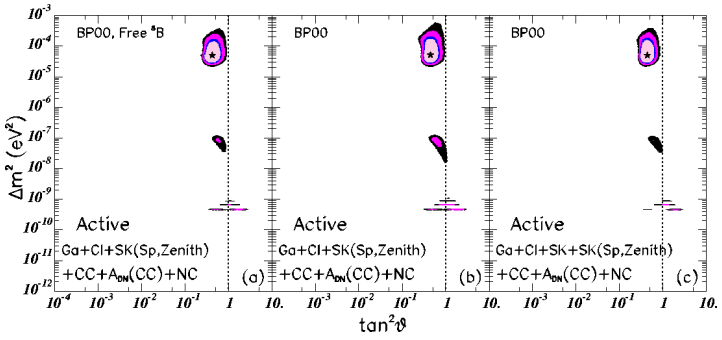

Figure 34. GLOBAL analysis solutions for three different strategies. The input data include the $\nu_\odot$ fluxes and uncertainties predicted by [BAH01a], the total measured CC and NC event rates and the D-N asymmetry from SNO, the Cl and Ga averaged rates, the zenith angle-recoil energy spectrum from SK The C.L. contours shown in the figure are 90%, 95%, 99%, and 99.73% (3σ). The GLOBAL analysis best-fit points are marked by a star.
In a) ^{8}B $\nu_\odot$ flux is a free parameter to be determined by the experimental data together with Δm^2 and $\tan^2\theta$. In b) and c) the theoretical uncertainty in the ^{8}B $\nu_\odot$ flux is included in analysis; in b) the total SK rate is included explicitly together with a free normalization factor for the zenith angle-recoil energy spectrum of the electrons, from [BAH02f].

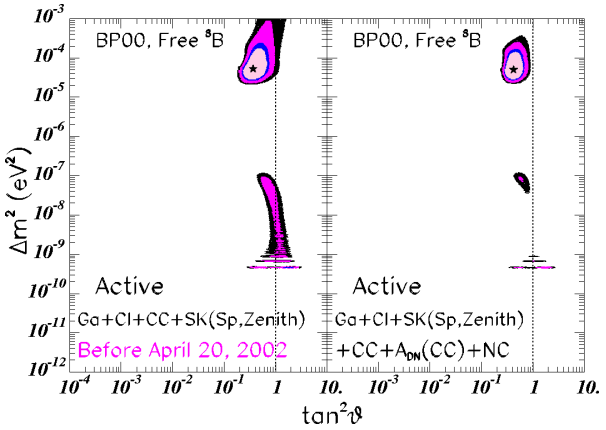

Figure 35. GLOBAL analysis solutions results within a free ^{8}B $\nu_\odot$ flux strategy before and after SNO data concerning NC events and D-N asymmetry. In the left panel, the LOW solution is allowed at 97.4%; on the contrary in the right one LOW is allowed at the 98.8%, from [BAH02f].

spectra are predicted. At present, SK spectral data suggest LMA as favoured solution, [STR02].

(iv) The allowed regions obtained in VAC and Q-VAC solutions depend upon details of the analysis: if the anti-correlation between statistical errors of NC and CC interaction rates is not included, VAC solution is disfavoured at 3σ level, [BAH02f].

(v) Present 3σ upper limits for $\Delta\, m^2$ in LMA solution are: $\Delta m^2 < 3.7 \cdot 10^{-4} (eV)^2$ (3.6 in [DEH02], 2.3 in [BAR02b]). The LMA region does not reach the upper bound

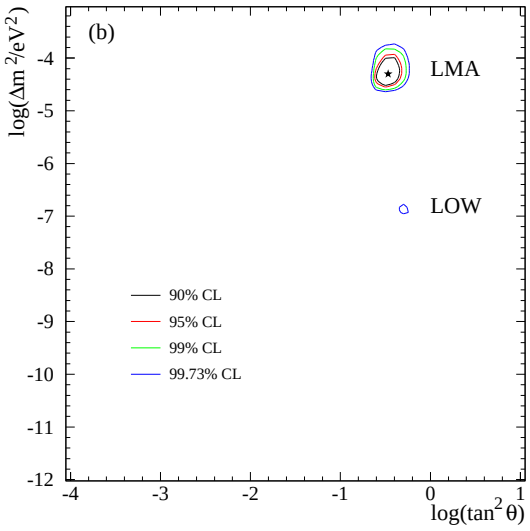

Figure 36. GLOBAL analysis solutions as computed by SNO coll.; the star indicates the best fit value, from [AHM02b].

imposed by the CHOOZ reactor data ($\Delta m^2 \leq 8 \cdot 10^{-4}$ (eV)^2), [BAH02f].

(vi) If one admits oscillations into either active and sterile ν's, the total ^{8}B $\nu_\odot$ flux has to be increased. If a ^{8}B factor is defined:

$$f_B = \frac{\Phi(^8B)_{exp}}{\Phi(^8B)_{SSM}} \tag{71}$$

the SNO collaboration experimentally deduces $f_B = 1.01 \pm 0.12$. Its best-fit in LMA region is obtained with $f_B = 1.07 \pm 0.08$ (LOW solution gives $f_B = 0.91^{+0.03}_{-0.02}$), [BAH02f] and similar values in [DEH02].
According to SMs, the ^{8}B $\nu_\odot$ flux is proportional to $S_{17}(0)$. Latest values deduced from measurements on cross-sections entering this parameter do not fully agree. The choice is relevant in analyses including ν_s's, [BAH02f, BAR02b, CRE02].
Since ^{7}Be and ^{8}B $\nu_\odot$'s are generated by different processes involving ^{7}Be, the agreement between the predictions of SMs and the value deduced from SNO results suggests (but does not imply) a ^{7}Be $\nu_\odot$ flux also in agreement with SMs, [CRE02].

(vii) Bi-maximal mixing solution ($\tan^2\theta = 1$) is disfavoured for LMA (3.3σ C.L.), LOW (3.2σ C.L.) and VAC (2.8σ C.L.) solutions. On the contrary, approximate bi-maximal mixing solution is favoured: at 3σ level LMA solution admits $0.24 < \tan^2\theta < 0.89$ (for LOW solution $0.43 < \tan^2\theta < 0.86$), [BAH02f].

(viii) Among the MSW solutions, the situation has also been clarified: LMA solution is the only viable solution at a level of 2.5σ; LOW solution is excluded at the 98.8% C.L., SMA solution at more than 3.7σ, pure sterile oscillations at 5.4σ, [BAH02f]. If sterile ν's are still included, VAC solution has the best-fit but it is excluded at 5.4σ C.L. (for 3 d.o.f.) while SMA sterile solution was acceptable at 3.6σ before results from SNO, [BAH02f].

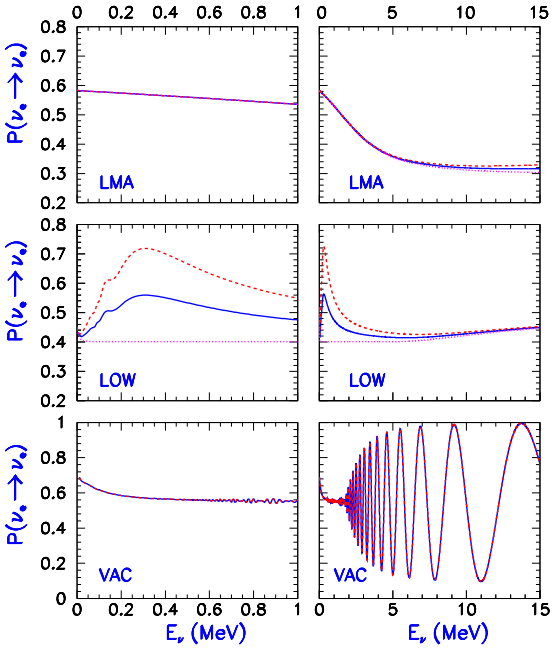

Figure 37. Survival probabilities (yearly-averaged) computed within a free flux analysis for a ν_e produced in the solar centre: average survival probabilities with regeneration in the Earth (full line); D-time probabilities, without regeneration effect (dotted line); N-time probabilities (dashed line). The regeneration effects are computed for SNO (right hand panels) and for LNGS (left side panels) detectors; in any case the differences among SK, SNO and LNGS are very small. LOW solutions in the right-hand panel are averaged over a small energy band (0.1 MeV) to suppress rapid oscillations because of the sensitive dependence upon the Earth-Sun distance. VAC solutions are averaged over an energy band of $\pm$ 0.05 MeV, [BAH02f].

(ix) Assuming no spectral distortion in ^{8}B $\nu_\odot$ component, NC and CC results exclude the case of no oscillations at a level of 5.1σ, or, in other words, SNO data show a 5.1σ evidence for $\nu_{\mu,\tau}$ appearance even if this value slows down to 3σ when generic spectral distortions are allowed. SK data forbids significant spectral distortions while SMA sterile solution predicts this effect: SNO results increase the $\nu_{\mu,\tau}$ appearance consequently sterile solutions are excluded in two different ways, [CRE02].

(x) Sterile ν's can generate solar, atmospheric and LSND oscillations. Atmospheric data give a 6σ evidence for $\nu_\mu \to \nu_\tau$ versus $\nu_\mu \to \nu_s$. "2+2" schemes predict that the fraction of ν_s in $\nu_\odot$ and ν_{atm} oscillations adds to one but both $\nu_\odot$ and ν_{atm} measurements do not require ν_s, [CRE02].

(xi) In [DEH02], oscillations with three flavours are analysed. The number of degrees of freedom is the same as in the 2-ν analysis. The fit parameters are $\tan^2\theta_{12}$, $\sin\theta_{13}$, Δm^2_{12} and f_B. Following the CHOOZ results $\sin\theta_{13} \simeq 0.04$ therefore the survival

probability is:

$$P^{(3)} \approx (1 - 2sin^2\theta_{13})P^{(2)} \tag{72}$$

where $P^{(2)}$ is the 2-flavour computed probability. The main effect of this angle is an overall suppression of the survival probability. The best fit point is in LMA region (for comparison two flavour analysis result is quoted):

$$3\nu\ \Delta m^2 = 6.8 \cdot 10^{-5}(eV)^2\ \tan^2\theta = 0.41\ f_B = 1.09\ \chi^2 = 66.2$$
$$2\nu\ \Delta m^2 = 6.15 \cdot 10^{-5}(eV)^2\ \tan^2\theta = 0.41\ f_B = 1.05\ \chi^2 = 65.2$$

The solution requires slightly higher value of the ^{8}B $\nu_\odot$ flux. The changes are small: an increase of θ_{13} worsens the 2 flavour results. For LOW and SMA solutions an increase of θ_{13} leads to a slight improvement of the fit.

(xii) In [DOL02, RAF02] implications of LMA and other flavour oscillation solutions on cosmology and astrophysics and *viceversa* constraints on oscillation analysis deduced from astrophysical data are nicely analysed.

(xiii) In [FOG02c], a quasi-independent analysis is proposed in the context of active ν's oscillations. The best-fit parameters are in LMA region while Q-VAC and LOW solutions are still acceptable at the 99% and 99.73% C.L., respectively; SMA solution is practically ruled out. LMA bounds appear to be more conservative than in analyses done by remaining authors. In particular, (at the 99.73% C.L.), maximal mixing is marginally allowed in LMA region. The inclusion of the winter-summer difference from GALLEX+GNO results decreases the likelihood of LOW solution because of the smallness of the measured value. Furthermore, probable changes in solar T_c values induced by each $\nu_\odot$ component have been estimated in the case of LMA and LOW solutions.
In [FOG02d] a GLOBAL analysis in term of three flavour oscillation is presented. Upgraded solar experimental results, including winter-summer difference from both the Ga experiments and the latest SK complete data, are combined with CHOOZ, SK atmospheric and K2K measurements. It has to be underlined that terrestrial experiments pose a strong upper limit to the mass value. The figures 38 and 39 show the main results in usual plots as a function of increasing value of $sin^2\theta_{13}$ parameter. The best fit point is in the same LMA point as for the two flavour analysis but LOW and Q-VAC solutions become less disfavoured when $sin^2\theta_{13}$ goes up. Similar conclusions have been obtained in [DEH02]. These analyses have been done under the hypothesis of direct ν mass spectrum hierarchy, but negligible variations are present when inverse hierarchy is used.

(xiv) Experimental measurements strongly suggest $\theta_{12} \simeq 30^\circ$, $\theta_{23} \simeq 45^\circ$ and $\theta_{13} < 10^\circ$.

(xv) The four flavour oscillation solution still appears to be highly disfavoured. In a context including ν_e disappearance results (from reactor experiments) and ν_μ disappearance searches (accelerators), there is a strong conflict (at a level of 3σ) with LSND appearance results in "3+1" schemes. If "2+2" schemes are taken

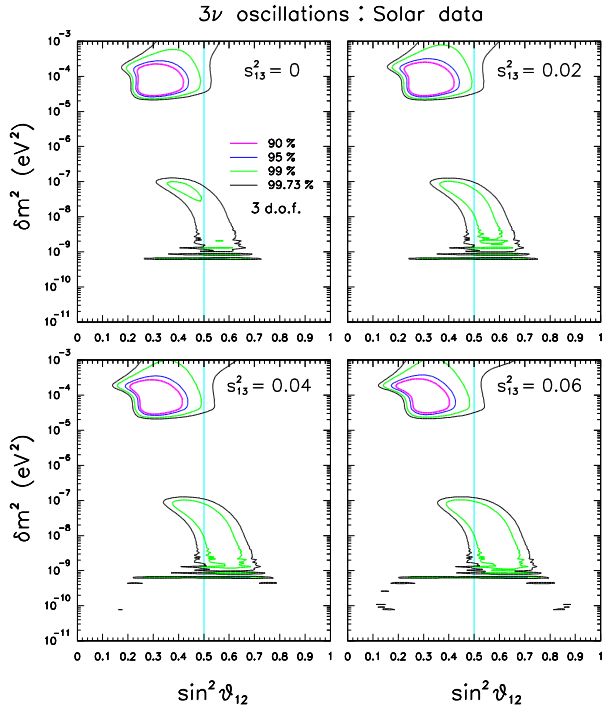

Figure 38. Three flavour GLOBAL analysis of $\nu_\odot$ data: all experimental rates combined with winter-summer difference from Ga experiments, energy and zenith spectra and D-N asymmetry. Sections are concerning different value of $s^2_{13} = \sin^2\theta_{13}$ parameter. C.L. contours are shown: 90% C.L.(full line), 95% (thick dot line), 99% (gray line), 99.73% (thin dot line); from [FOG02d].

into account, including mixed active+sterile oscillation, atmospheric data strongly support a pure $\nu_\mu \rightarrow \nu_\tau$ oscillation; on the contrary solar measurements prefer a pure $\nu_\mu \rightarrow \nu_s$ solution. These results are clearly incompatible. For a detailed analysis see [MAL02].

In table 27 and table 28 the parameters corresponding to several GLOBAL solutions as computed by different authors are shown. In table 29 the expected interaction rates for Cl and Ga experiments are also reported.

7.6. Summary.

Previously shown analyses and results introduce assumptions and solutions beyond the particle standard model. A question arises: is this model ruled out by astrophysical neutrino experimental results?

Accelerator experiments give negative answers: they do not show violation to the particle standard model predictions, see for instance KARMEN, [EIT00, ARM02]: 15 events have been detected while 15.8±0.5 events were expected. On the contrary, LSND's latest

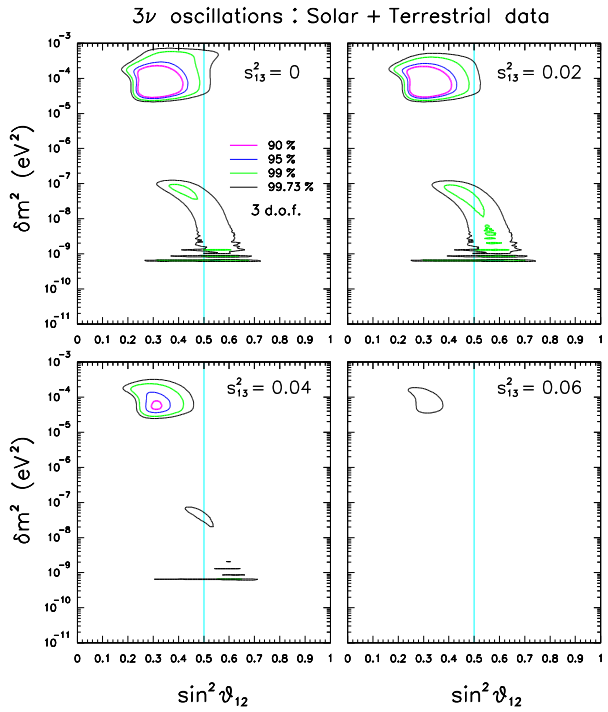

Figure 39. As in fig. 38 but the constraints from CHOOZ, SK atmospheric and K2K ν are added, from [FOG02d].

Table 27. *Best-fit GLOBAL analysis oscillation parameters with all solar neutrino data. f_B is the "corrective" factor with respect to the ^8B $\nu_\odot$ flux predicted in [BAH01a]. (s) means sterile solution. The number of degrees of freedom is 46 [44 (zenith spectrum) + 4 (rates) + 1 ($A_{DN}(CC)$) −3 (parameters: Δm^2, θ, and f_B)]. Solutions having $\chi^2_{min} \geq 45.2 + 11.8 = 57.0$ are not allowed at the 3σ C.L., adapted from [BAH02f].*

	Δm^2 (eV)^2	$\tan^2(\theta)$	f_B	χ^2_{min}
LMA	$5.0 \cdot 10^{-5}$	0.42	1.07	45.5
LOW	$7.9 \cdot 10^{-8}$	0.61	0.91	54.3
VAC	$4.6 \cdot 10^{-10}$	1.8	0.77	52.0
SMA	$5.0 \cdot 10^{-6}$	0.0015	0.89	62.7
Just So^2	$5.8 \cdot 10^{-12}$	1.0	0.46	86.3
VAC (s)	$4.6 \cdot 10^{-10}$	2.3	0.81	81.6
Just So^2 (s)	$5.8 \cdot 10^{-12}$	1.0	0.46	87.1
SMA (s)	$3.7 \cdot 10^{-6}$	0.0047	0.55	89.3

result, [AGU01], confirms the previous measurements, [ATH98a, ATH98b], indicating an excess of 87.9± 22.4± 6.0 events: this implies an oscillation probability for ν's of $0.264 \pm 0.067 \pm 0.045$ %.

Interesting results have been obtained in Japan by using KEK and SK facilities. K2K is a long baseline experiment aiming to establish ν oscillation in the ν_μ-disappearance

Table 28. *The same as in table 27 but the quoted results are: upper part, left side from [BAR02b] (72 degrees of freedom), right side from [BAN02b] free rate analysis; lower part, left side from [DEH02] (78 degrees of freedom), right side from [FOG02c] (79 degrees of freedom)*

	Δm^2 (eV)^2	$\tan^2\theta$	f_B	χ^2_{min}	Δm^2 (eV)^2	$\tan^2\theta$	χ^2_{min}
LMA	$5.6 \cdot 10^{-5}$	0.39	1.09	50.7	$6.07 \cdot 10^{-5}$	0.41	40.57
LOW	$1.1 \cdot 10^{-7}$	0.46	1.03	59.9	$1.02 \cdot 10^{-7}$	0.60	50.62
VAC	$1.6 \cdot 10^{-10}$	0.25 (3.98)	2.46	76.3	$4.43 \cdot 10^{-10}$	1.1	56.11
SMA	$7.9 \cdot 10^{-6}$	0.002	4.85	108	$5.05 \cdot 10^{-6}$	0.0017	70.97
LMA	$6.15 \cdot 10^{-5}$	0.41	1.05	65.2	$5.5 \cdot 10^{-5}$	0.42	73.4
LOW	$9.3 \cdot 10^{-8}$	0.63	0.91	77.6	$7.3 \cdot 10^{-8}$	0.67	83.8
VAC	$4.5 \cdot 10^{-10}$	2.1	0.75	74.9	$6.5 \cdot 10^{-10}$	1.33	81.2
SMA	$4.6 \cdot 10^{-6}$	0.0005	0.57	99.7	$5.2 \cdot 10^{-6}$	0.0011	96.9

Table 29. *Interaction rates and flux variations as expected for different oscillation solutions: Cl experiment (left) and Ga experiments (middle), adapted from [BAH02f]; the right part shows the fractional variation (%) with respect to the values quoted in [BAH01a] is shown, adapted from [FOG02c]. See table 12, table 16, table 20, table 22, table 23 for a comparison with SMs predictions, experimental results and predictions based on previous oscillation analyses.*

	LMA	LOW	VAC	LMA	LOW	VAC	LMA	LOW	VAC	SMA
	SNU	SNU	SNU	SNU	SNU	SNU	%	%	%	
hline p-p	0.0	0.0	0.0	40.4	38.2	40.3	0.0	+0.5	+1.1	+0.9
p-e-p	0.1	0.10	0.15	1.51	1.25	1.82	0.0	+0.8	+1.6	+1.3
Hep	0.01	0.02	0.02	0.02	0.03	0.04	-0.8	0.0	-1.8	+1.8
^{7}Be	0.62	0.53	0.46	18.6	16.0	14.0	+0.5	-5.5	-11.5	-9.9
^{8}B	2.05	2.26	2.34	4.35	4.72	5.00	+5.2	-12.2	-22.2	-24.2
^{13}N	0.04	0.04	0.05	1.79	1.56	1.83	-1.0	-8.3	-15.1	-11.4
^{15}O	0.15	0.15	0.18	2.83	2.44	3.01	-1.2	-8.3	-17.0	-12.8
^{17}F	0.00	0.00	0.00	0.03	0.03	0.04	–	–	–	–
Total	3.03	3.11	3.21	69.6	64.2	66.0	–	–	–	–

and ν_e-appearance mode with a well known flight distance, [HIL01, HAS02]. A beam of ν_μ is produced at KEK, by 12 GeV/c protons incident on aluminium target of 3 cm diameter and 66 cm length; its purity is at the level of 98.2 % of ν_μ. At a distance of 300 m, a set of detectors (a 1 kton water-Čerenkov detector, a scintillating fiber tracker with a water target, lead-glass counters and a muon range detector) analyses the main characteristics of the ν beam, whose direction is within 0.01 mrad from the direction to

SK, which is 250 km far, [AHN01]. The beam-line was aligned by GPS position survey. $80.6^{+7.3}_{-8.0}$ events were expected in the case of no oscillation but 56 fully contained events have been observed, [ISH02]: more precisely 24 multi-ring events (expected 32.2± 5.3) and 32 1-ring events (expected 48.4± 6.8) have been detected. Under the hypothesis of 2 flavour mixing and the conditions $\tan^2\theta = 1$ and $\Delta m^2 = 3 \cdot 10^{-3}$ (eV)^2, 52.4 events are predicted.
When SK atmospheric data and K2K results are combined, Δm^2 value is "relatively well" estimated: $2.7 \pm 0.4 \cdot 10^{-3}$ (eV)^2, under the hypothesis of maximal mixing.
The main challenges for particle standard model come from astrophysical measurements: atmospheric, [FUK98b], and solar ν data give results in strong disagreement with the predictions.
Unfortunately, the presently available experimental results do not allow to select with a great confidence "THE" right solution or to rule out definitively the remaining ones: new experimental data are needed.
Coming back to the $\nu_\odot$ physics, the main questions (problems) on fire are:

(i) How great is the deficit for p-p and ^{7}Be $\nu_\odot$ components?

(ii) Is the ratio between ν_e and total $\nu_\odot$ flux, as measured by SNO, an "ultimate" signal for new physics of weak interactions? Is the flavour oscillation, mainly MSW effect with large mixing angle, the correct solution to the SNP?

(iii) Are the solar modulations measurable?

(iv) Are the low-energy interaction cross-sections right? How the nuclear transition calculations (*e.g.* in excited states) are correctly computed?

(v) Could T_c, ρ and their profiles inside the Sun be further constrained as suggested by SMs? Does further upgrading of SMs (or new helioseismology results) avoid the presently used assumptions (spherical symmetry, no effects due to $B_\odot$, no mass-loss, no rotation...) and change the main results on $\nu_\odot$ flux?

8. The incoming future.

8.1. 2002-2003: what news?

At present time (autumn 2002), three detectors are still continuing their data taking: GNO, SNO and SAGE. SNO will offer other interesting features of $\nu_\odot$ flux (but only at high energy) with new results concerning NC interactions. GNO and SAGE will increase their statistics and lower their experimental errors on the Ga interaction rate mainly based on low-energy p-p $\nu_\odot$'s. At the end of 2002, when new PMT's will be installed, SK will run again but with a higher energy threshold.
SK and SNO have shown that the survival probability of ^{8}B $\nu_\odot$'s is energy-independent. The uncertainty of this component in the Ga interaction rate is ± 1.5 SNU, mainly due to the interaction cross-section on Ga. If Hep and F $\nu_\odot$ components are disregarded and when the ^{7}Be $\nu_\odot$ flux will be measured, it will also be possible to estimate the net p-p $\nu_\odot$ flux by difference. This will strongly constrain the solar physics.

Next years could be fundamental to have such an answer: three new detectors (KAMLAND, BOREXINO and ICARUS) will give their experimental results.
KAMLAND (which has started its data taking in January 2002) and BOREXINO will detect ES and CC interactions and they will measure ^{7}Be and CNO $\nu_\odot$ components. Then, a good estimate of p-p $\nu_\odot$ flux will be allowed. These experiments will check also the robustness of different ν oscillation solutions.
The main features of these detectors are reviewed.

8.2. KAMLAND.

This experiment is mainly dedicated to the analysis of $\overline{\nu}$'s emitted by nuclear reactors but the study of terrestrial and solar ν's is also possible, [ALI98]. In the case of reactor emission, the detected reaction is the inverse β-decay, a process having $E_{thr} = 1.804$ MeV and a well known cross-section (the uncertainty being less than 1%).
The experimental setup is homed at Kamioka mine and measures the $\overline{\nu}_e$ flux produced by Japanese nuclear reactors which are far from the detector no more than 350 km. The $\overline{\nu_e}$ flux above E_{thr} is $1.34{\cdot}10^6\,\nu\,cm^{-2}\,s^{-1}$, with an uncertainty of $\sim 1.4\%$; the expected rate is $\sim$ 1100 events per year at an energy ranging from 2 up to 8 MeV. $\overline{\nu_e}$'s are mainly produced from ^{235}U, ^{239}Pu and ^{241}Pu ($\sim$ 90%), the remaining contrubution being associated with ^{238}U.
The detector consists of a spherical tank with a diameter of 18 m filled with a liquid scintillator (1,2,4 trimethylbenzene (20%), paraffin (80%), with addition of PPO as wavelength shifter at a level of 1.5 g/l) having a fast component of 5.4 ns and a slow component of 37.5 ns. The quenching factor is 13.8. The emitted light is collected by 1325 17"-PMT's and 554 20"-PMT's, [PIE01]. The attenuation length is 100 m at 400 nm and 20 m at 450 nm while the light transparency is at a level of 93 % at 400 nm. The expected vertex resolution is better than 10 cm at E = 1 MeV; the energy resolution is $\sim 5\%/\sqrt{E}$. The radiopurity is at a level of few 10^{-16} g/g for U, Th and ^{40}K. The PMT coverage is $\sim$ 32%, [DEB00, PIE01].
The predicted interaction rate for terrestrial $\overline{\nu}_e$'s is $\sim$ 800 events per year (2 events per day) with an estimated background of $\sim$ 40 events per year (0.1 event per day).
The background due to neutrons produced by cosmic rays is suppressed by detector location (a shield of 2700 mwe) and by a cosmic ray veto.
Data taking started in January 2002. If a radiopurity level lower than 10^{-16} g/g will be reached (even by 2 order of magnitude for ^{40}K background) KAMLAND will detect ^{7}Be $\nu_\odot$'s through elastic scattering interactions, the energy window for scattered electrons varying from $\sim$ 300 to 800 keV. The expected interaction rate is $\sim$ 460 events per year. The measured positron energy spectrum should allow a sensitive probe of oscillation effects, [BAR01b], see also [GOU01, GON02, MUR02] for analyses concerning the possible impact of KAMLAND results on SNP.

8.3. BOREXINO.

The detector is under installation in Hall C at LNGS and it is aimed to study purely leptonic $\nu_\odot$ interactions at $E \geq 250$ keV; it will allow to measure the ^{7}Be ν flux, [BEL95, ALI02c]. It consists of a nylon transparent and spherical inner vessel (8.5 m), filled with 321 m^3 of liquid scintillator, pseudocumene as a solvent and PPO at the concentration of 1.5 g/l as solute. The target mass is viewed by $\sim$ 2200 8" PMT's fixed on a supporting structure (13.7 m of diameter) plunged in a water tank (18 m of diameter). The outer detector is a 200 PMT's muon veto system.
The effective light coverage will be at a level of $\sim$ 30%. In such a detector the total energy, the position (with a mean accuracy of $\sim$ 15 cm in X, Y and Z directions) and the time of each event will be measured. The total energy will be estimated with an accuracy ranging from 18 % at 250 keV to 5 % at 1 MeV, [CAL00].
The main sources of the background are the rock and concrete of the laboratory and the radioactive contamination due to the detector materials. The external tank contains water as a shield against gamma rays and neutrons from the surrounding rock. Moreover, the water allows the detection of Čerenkov light emitted by cosmic muons crossing the detector. The expected background in the fiducial volume is $\sim$ 11 counts per day to be compared with the estimated unperturbed $\nu_\odot$ flux of 55 events per day, [ALI02c].
BOREXINO will detect all flavour $\nu_\odot$'s *via* ES interactions. In the electron kinetic energy window T_e = 250 - 800 keV, the major contribution to the signal (78%) is expected from a monochromatic line of ^{7}Be $\nu_\odot$'s with the energy 863 keV, the remaining contributions being from ^{15}O, ^{13}N and p-e-p $\nu_\odot$'s (10%, 7.2% and 3.6% respectively).
Among the big experimental difficulties the BOREXINO coll. had to get over, the scintillator radiopurity required the major effort. A prototype called Counting Test Facility (CTF), with an inner nylon vessel (2 m of diameter), was installed at LNGS and their encouraging results concerning the level of ^{14}C, U and Th, showed the feasibility of such experiment, [BOR98].
At the end of 2002, the vessel will be filled (water and scintillator), then, tests will start; in spring 2003 measurements should begin.
After two years, BOREXINO should give precise measurements concerning ^{7}Be $\nu_\odot$ interaction rate. Owing to the large expected statistics, analyses on seasonal and other temporal variations will be possible. Moreover, BOREXINO would allow searches for $\overline{\nu}_e$ coming from the Sun and from other different cosmic sources, [GIA01, RAN01]. The radiopurity of the detector, at level of 10^{-16} g/g for U and Th, the lowest value presently available, has to be pointed out: the so aquired experiences and high radiopurity techniques should be applied to different sectors, like in $\beta\beta$-decay experiments.

8.4. ICARUS.

Many years ago a technique combining bubble chamber features with an electronic read-out was suggested, [RUB77], then, a 3000 t liquid Ar time projection chamber detector was proposed in 1989, [ICA89, ICA94, ICA95]. Its main feature is the high quality

(similar to that of a heavy liquid chamber) of "images" that can be obtained thanks to its granularity (1 mm). Such a detector is homogeneous and continuously sensitive, so that it is perfectly suitable to estimate the energy of a contained particle. It allows particle identification: proton-decay, atmospheric ν interactions, high energy ν's from accelerator beams and naturally $\nu_\odot$ interactions, [RUB96, MON99].
A 3 t prototype was built at CERN and the experience gained was the technical basis for further projects; at present a 600 tons module was constructed.
This detector should be able to measure $\nu_\odot$ interactions in two ways:

- by neutrino scattering off electron: $\nu_e + e^- \rightarrow \nu_x + e^-$ at $E \geq 5$ MeV;
- by interaction on ^{40}Ar: $\nu_e + ^{40}Ar \rightarrow e^- + ^{40}K^* \rightarrow ^{40}K_{g.s.} + \gamma's$.

The expected number of events per years, under standard assumptions, is ~ 230 by ES interactions (40 events from background) and ~ 1440 by absorption (180 events from background).
This detector will check the ν oscillation hypothesis measuring the ratio between ES and ν_e absorption. This reaction is expected to proceed through two channels: Fermi transition to the 4.38 MeV excited isobaric analogue K^* state or Gamow-Teller transition to the excited levels below the 4.38 MeV K^* state. It will be possible to distinguish between these processes by the energy and multiplicity of γ ray emitted in the de-excitation of the K^* states and by the energy spectrum of the primary electron.
The module T600 has been tested at Pavia and it should be installed in LNGS at the end of 2002; its startup is foreseen in 2003, [ICA00, ICA01a, ICA01b].

8.5. KAMLAND and BOREXINO: is the "final" answer incoming?

KAMLAND and BOREXINO can detect the ^{7}Be $\nu_\odot$ flux and strenghten or weaken the presently proposed solution to the SNP. We shortly summarize in table 30 the available predictions concerning these experiments, as given in [ALI01, STR01b, BAH02c, BAH02f, BAR02b, KRA02], and the quoted comments.

- The predicted ratio for BOREXINO and for CC KAMLAND event rate are not significantly affected by latest SNO results, see fig. 40.
- Only LOW solution predicts a consistent D-N asymmetry; LMA solution foresees a negligible variation while VAC solution has small and negative value due to the Earth-Sun distance and to the longest nights occuring in the Northern hemisphere when the distance diminishes, see fig. 41.
  In KAMLAND and BOREXINO predicted D-N asymmetry are very similar: for LMA solution the values agrees at a level of 0.1%; LOW solution has a maximum value for KAMLAND which is $\sim$ 2% less than for BOREXINO. VAC solution predicts a minimum value of -3.9% for KAMLAND which has to be compared with -4.8% for BOREXINO.
  Fig. 42 shows the computed rate and the distortion of CC interaction spectrum

Table 30. *Best-fit predictions and uncertainties (3σ ranges) by using currently available $\nu_\odot$ data. The threshold of the recoil electron kinetic energy, used in computing the SNO predictions, is 5 MeV. For the BOREXINO experiment, electron recoil energies are between 0.25 and 0.8 MeV. The results for the KAMLAND reactor observables are computed for E_{thr}=1.22 and 2.72 MeV. Columns nr. 2 and 3 show the predicted values before the latest SNO results, columns nr. 4 and 5 include NC events in the analysis. The p-p $\nu_\odot$ scattering on electron ratio, with respect to the [BAH01a] predictions for future real-time detector, is also shown. The analysis allows a ^8B $\nu_\odot$ free flux, adapted from [BAH02f].*

Observable	LMA $\pm$ 3σ	LOW $\pm$ 3σ	LMA $\pm$ 3σ	LOW $\pm$ 3σ
A_{N-D}(SNO CC)(%)	$4.4^{+11.4}_{-4.4}$	$1.3^{+3.9}_{-1.3}$	$4.7^{+9.1}_{-4.7}$	$2.7^{+2.7}_{-2.1}$
[R(^{7}Be)]	$0.66^{+0.09}_{-0.07}$	$0.59^{+0.13}_{-0.06}$	$0.64^{+0.09}_{-0.05}$	0.58$\pm$0.05
A_{N-D}(^{7}Be)(%)	$0.0^{+0.1}_{-0.0}$	15^{+17}_{-15}	$0.0^{+0.1}_{-0.0}$	23^{+10}_{-13}
[CC](KAMLAND)				
(E_{thr}=2.72 MeV)	$0.56^{+0.20}_{-0.34}$	–	$0.49^{+0.25}_{-0.26}$	–
(E_{thr}=1.22 MeV)	$0.57^{+0.16}_{-0.31}$	–	$0.52^{+0.20}_{-0.25}$	–
δE_{vis}(KAMLAND) (%)				
(E_{thr}=2.72 MeV)	-7^{+14}_{-4}	–	-7^{+14}_{-4}	–
(E_{thr}=1.22 MeV)	-7^{+15}_{-7}	–	-9^{+17}_{-5}	–
p-p ν's - e^- scattering				
(T_{thr} = 100 keV)	$0.722^{+0.085}_{-0.067}$	$0.689^{+0.058}_{-0.065}$	$0.705^{+0.073}_{-0.049}$	$0.683^{+0.035}_{-0.042}$
(T_{thr} = 50 keV)	$0.718^{+0.086}_{-0.069}$	$0.689^{+0.058}_{-0.068}$	$0.700^{+0.074}_{-0.050}$	$0.677^{+0.038}_{-0.045}$

in KAMLAND, which can be as large as 20%: its value, if non-zero, will strongly constrain the range of the oscillation parameters.
In practice, the measurement of ES interactions is a critical test either for SMs and for oscillation solutions: a large value for the D-N effect would imply the correctness of the LOW solution.

- VAC solution would be ruled out if a rate depletion or a spectral distortion in the KAMLAND reactor experiment will be observed. Moreover, it predicts a Δm^2 value too small to lead to an observable effect with KAMLAND. A strong signal for VAC solution would be the observation of a large seasonal variation in BOREXINO, with a monthly dependence of the observed rate; a D-N effect at a level of $\pm$8% associated with this seasonal variation is also possible. In BOREXINO the rates predicted by LMA, LOW and VAC solutions are very similar.
- KAMLAND could indicate LMA as a good solution if a consistent deficit in reactor $\overline{\nu}$'s will be detected.
- SMA will be the best solution if BOREXINO will detect no $\nu_\odot$'s; in any case the SK energy spectrum has to be thought as wrong.
- Just So^2 solution will be the right answer if the ratio CC to NC events as measured at SK and SNO will change, indicating no oscillations, and BOREXINO data will

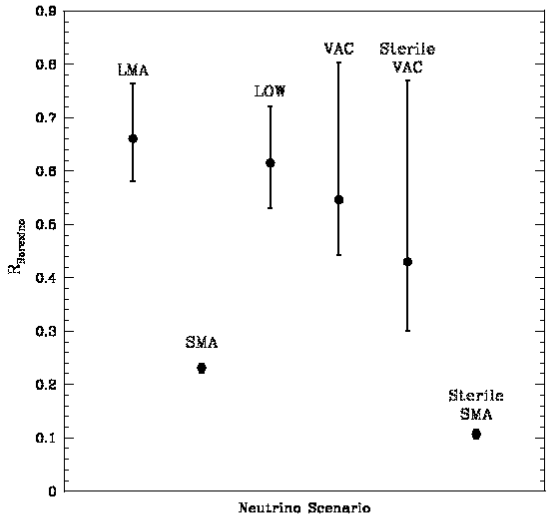

Figure 40. The event rate predictions for BOREXINO experiment. The circles give values of R_{BOR} in the best-fit points of the GLOBAL analysis solutions. The error bars show intervals corresponding to the 3σ allowed regions, from [KRA02].

show a depression in ^{7}Be $\nu_\odot$ flux.

- NO OSCILLATION will be the right solution to the SNP if BOREXINO will find no $\nu_\odot$'s and if the ratio CC/NC in SNO data is incorrect.
- BOREXINO should be able to discriminate among the non-standard solutions to the SNP, [NUN01a]. Except for the possible direct evidence of the LMA solution KAMLAND could provide, BOREXINO is able to distinguish between flavour oscillation solutions and RSFP. When latest SNO and Ga data are included in analyses, also RSFP show a little shift in the best-fit parameter values allowing an even clearer distinction between RSFP and oscillation signatures in BOREXINO predictions. In [CHA02] such a difference for the LMA solution is possible to more than 5.7σ whereas for the LOW solution all predictions are more than 4.5σ. The only possible model dependence of RSFP solution is related to the choice of $B_\odot$ profile, which is constrained by the requirement of fitting all $\nu_\odot$ data. In table 31 the expected interaction rate in BOREXINO as computed in flavour oscillation and RSFP solutions are compared with the prediction in [BAH01a] is shown.
  In $\overline{\nu}_{\mu,\tau}$ scenario no D-N asymmetry is foreseen but 27-day modulation and annual

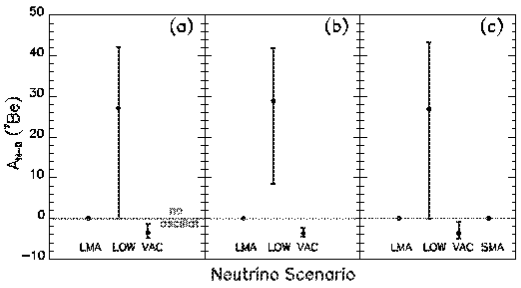

Figure 41. The predicted percentage differences between D and N rates in BOREXINO for recoil electrons with kinetic energies in the range 0.25 - 0.80 MeV. The three panels refer to results for different analysis strategies: in a) modified ^{8}B flux is used, [BAH02c], in b) SK event rate is also included, in c) the ^{8}B ν flux is a free parameter, from [BAH02c].

periodicity having the maximum value in September and March should constitute a signature of such a mechanism. When the new profiles, proposed in [CHA02], are analysed, a reduction factor of ~ 0.45, for strong $B_\odot$ existing in the radiative zone, or of ~ 0.35, if $B_\odot$ is acting in convective zone, is predicted.

Table 31. *The expected interaction rate (events per day) in BOREXINO computed following [BAH01a] and within flavour oscillation and RSFP GLOBAL solutions, see also table 24. The $B_\odot$ profiles (1-6) are from [PUL00], the profile (4) is from [PUL01].*

SSM	LMA	LOW	1	6	4
55.2	35.3	32.0	15.5	22.6	19.3

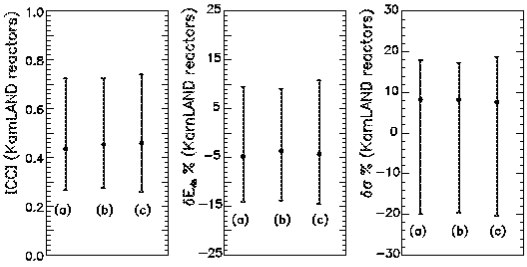

Figure 42. The 3σ predictions concerning KAMLAND experiment for the CC and the first and second moments of the visible energy spectrum with respect to the expectations based upon [BAH01a, BAH02c]. The visible energy threshold is 1.22 MeV. Results based on different analysis strategies are shown: in a) modified ^{8}B flux is used, [BAH02c], in b) SK event rate is also included, in c) the ^{8}B ν flux is a free parameter, from [BAH02c].

9. The next generation of detectors.

The knowledge on $\nu_\odot$ physics has been greatly enhanced by SNO's results; when BOREXINO and KAMLAND data will be available, a more exhaustive answer will be provided. Perhaps, the main questions could have "THE" right way out and only details should remain to be clarified. In any case, only next experimental data will give an answer.

Before latest SNO results, many physicists thought that real-time detectors measuring p-p $\nu_\odot$ flux and spectra were the "ultimate" weapon to solve SNP. Many proposed experiments were based on fascinating techniques, but a lot of difficulties has prevented their construction up to now. The measurement of energy and direction for each event produced by $\nu_\odot$'s should allow the on-line estimation of background and a higher signal to noise ratio, the spectroscopy of $\nu_\odot$'s, the $\nu_\odot$ astronomy, [BAR01b]. We shortly resume, alphabetically ordered, the main features of proposed $\nu_\odot$ detectors, their performance and present status.

9.1. CLEAN.

CLEAN (Cryogenic Low Energy Assay of Neutrinos) experiment, which would detect $\nu_\odot$ elastic scattering off electron, proposes to use of liquid He or Ne as a target for $\nu_\odot$'s in order to have a good real-time spectroscopy, [MCK00, MCK01]. Such a detector should measure the large UV scintillation produced by ionizing radiation; a good transparency, with respect to the emitted light, and a low background levels are required. UV radiation, *via* wave length shifter, should then be converted to optical photons, allowing the detection with PMT's.
A cryogenic scintillator test facility was proposed: a spherical geometry with the external diameter up to 2 m, working temperature of $\sim$ 25 K and a central active region of $\sim$ 100 kg are the main characteristics. Neon purification, internal background evaluation and optical properties of cryogenic scintillator will be attentively analysed. A radiopurity level as low as in BOREXINO should be needed for U, Th, ^{42}Ar and ^{85}Kr, the most serious one.

9.2. GENIUS.

GENIUS project (GErmanium in liquid NItrogen Underground Setup) is based on the powerful capabilities of a set of "naked" Ge detectors merged in liquid N_2: its main goal is to search for dark matter and $\beta\beta$-decay. The minimum external dimension of N_2 tank will be 13 m diameter and 12 m height. An array of 400 detectors of enriched ^{76}Ge as a target, 2.5 kg each, is foreseen, [KLA99, BAU00, KLA01b, KLA01a]. The total target mass of natural Ge corresponds to $3{\cdot}10^{29}$ electrons.
If a background level of 0.001 events per year per kg per keV in the energy region from 0 to 260 keV will be reached, this detector will be able to measure in real-time low-energy component of $\nu_\odot$'s *via* ES interactions. The maximum electron recoil energy is 261 keV for p-p $\nu_\odot$'s, with an expected rate of 1.8 events per day, and 665 keV for ^{7}Be $\nu_\odot$'s, 0.6 events per day; 2.4 events per day is the total prediction while the expected background is of $\sim$ 0.6 events per day. This detector should be installed in LNGS.
The background is due to both external and internal factors; the former comes from to showers, photons, neutrons from rock and direct or secondary cosmic ray muon component. After the reduction of the cosmic ray component, the main part of the background comes from N_2 and Ge themselves. The N_2 must reach a radiopurity as low as in BOREXINO's scintillator for ^{238}U, ^{232}Th, ^{40}K. The Ge presents another challenge, due to the possible cosmogenic activation on Earth's surface: the best solution should be the complete building phase in underground laboratories.
If S/N will be greater than 1, the $\nu_\odot$'s detection will be allowed by spectroscopic analysis only, on the contrary the possible solar signature of each event will be computed.
A test facility was approved in 2001 to check the feasibility of the whole detection technique and its building step will start as soon as possible, [BAU02].

9.3. HELLAZ.

HELLAZ (HELium tpc at Liquid AZote temperature) experiment should detect $\nu_\odot$'s in a pressurized He TPC (Time Projection Chamber) (its volume should be $\sim 2000\, m^3$) having the aim of measuring the purely leptonic interactions at E$\geq$ 100 keV. Owing to the low Z of He, it should be possible to deduce the energy of incoming ν, event by event, and to study the flux and the energy spectrum of the p-p $\nu_\odot$'s with an error of $\sim$ 4 %, [BON94].
The detector should be filled with 7 t of He + CH_4 (95-5 %) added for technical reasons. Different combinations of temperature and pressure were presented: 20 bar/ 300 K, 10 bar/ 140 K, 5 bar/ 77 K [BON01a]. The addition of CH_4 is very dangerous because of a consistent background due to ^{14}C β-decay.
The calculated rate of ES interaction events from p-p and ^{7}Be $\nu_\odot$'s is $\sim$ 10 events per day taking into account the electron threshold energy and the detector fiducial volume. The sensitive volume will be shielded by CO_2 blocks, a steel tank and a thermal insulating material. Ionisation electrons, generated by ionizing particles which cross the active volume, are drifted in an uniform axial electric field and detected by a MW system.
The dominant background is γ-e Compton scattering, its cross-section being 10^{20} times larger than that of ν_e. HELLAZ would allow a rejection rate of $\sim 10^4\,\gamma$ per day mainly thanks to the tracking procedure and to the energy measurement. The future of this project is not completely defined.

9.4. HERON.

HERON (HElium Roton Observation of Neutrinos) experiment, [LAN01], is aiming to realize a real-time detector measuring $\nu_\odot$ elastic scattering off electron with a low energy threshold and a high rate. The target is superfluid He at T= 0.05 K: a mass of $\sim$ 20 tons, with a fiducial mass of $\sim$ 5 tons, would allow an interaction rate of $\sim$ 12 events per day.
When a ν interacts, a single recoil electron is produced and stopped in the liquid. The ^{7}Be $\nu_\odot$'s produce a flat distribution with energy ranging from 0 to 665 keV; on the contrary a p-p $\nu_\odot$'s show a slowly falling down spectrum from 0 to 261 keV. The recoil track in He is shorter than 2 cm and it seems essentially a point source of radiation.
The idea is to measure both phonon and UV photon within same calorimetric device. In short all the detection process: the initial energy loss of a stopping particle is by ionisation; at the ending point, the primary energy is distributed among phonons, rotons, photons and some few long-lived dimers, depending on the primary ionisation along the track.
If phonons/rotons reach the liquid free surface and have an energy greater than the binding energy of He itself ($8{\cdot}10^{-4}$ eV), they should begin a quantum evaporation.
The scintillation UV photons derive from radiative decay of He dimers produced along the track and their energy ranges between 14 and 20 eV, 16 eV being the maximum. A

silicon and sapphire wafer could detect these photons and produce a prompt heat pulse. Photons and phonons could be distinguished by their different arrival times on wafer. A 5 l. prototype with Si or Al_2O_3 readout was built to test the feasibility of this unusual technique and the performance of the detector.
About the background problem:

- The impurities in superfluid He attach to walls or fall to bottom (nothing is soluble in He and all the elements are frozen; moreover, the gravitational energy is greater than thermal energy so that all the particles fall down).
- Long-lived isotopes do not exist and the first excited state is at $\sim$ 20 MeV.
- At E$\leq$ 3 MeV γ-conversions are Compton scatters ($>$ 95 %); this is the most dangerous background.
- Through-going μ's are rejected by pattern recognition and energy deposit ($\sim$ 450 events per day at LNGS and $\sim$ 11000 at Soudan); in any case their interactions in He are negligible.
- There are β-decays in Si-wafers ($\sim$ 30 kg) and 1.28 MeV γ's from ^{22}Na ($\leq$ 3 events per day).
- Photons play the main role because the event location and the consistency with signal topology are used for energy determination and for background rejection.

Technological problems are connected with the requirement of low background in refrigeration systems, cryostat and shielding, in the ^{3}He purification, in the energy threshold of calorimeter and in the SQUID electronic, which will be adapted to large area Si-wafers.
MC simulations, in which the distribution of photon incident on the wafers from a source anywhere in the detector is used to determine the most probable position of an event technique, are in progress. The major sources of background are Compton γ-ray in liquid He from cosmogenically produced isotopes in cryostat materials or in any material which contacts He. A MC analysis including many possible background related parameters combined with different shapes and sizes of fiducial-non fiducial volume is on run.
Other topics under analysis are the single 16 eV photon sensitivity on wafer sensor, the efficiency of the "coded aperture" for event location and background signature reconstruction and the use of a new magnetic calorimeter allowing greater absorbing area. A saphyre readout system with a geometry closer to the final needed version is under construction.

9.5. LENS.

LENS (Low Energy Neutrino Scintillator) project was proposed many years ago aiming to measure p-p and ^{7}Be CC $\nu_\odot$ interaction on isomeric excited states of rare earth nuclei. An important step was the discovery of 3 stable target systems (^{176}Yb, ^{160}Gd, ^{82}Se) for ν capture with isomeric tag, [RAG97]. The decay of these states produces a distinct,

time-delayed γ-ray, located at, or around, the capture side that allow to tag the $\nu_\odot$ interaction in space and time. $\nu_\odot$ interaction produces a transition $0^+ \rightarrow 1^+$ to an excited state in the final nucleus; the emitted γ has E$\sim$ 100 keV while the mean lifetime of the isomeric states is $\sim$ 100 ns.
The estimated interaction rate in a 20 tons of natural Yb detector is $\sim$ 370 events per year: $\sim$ 180 events from p-p $\nu_\odot$'s, 140 from ^{7}Be $\nu_\odot$'s, 10 from p-e-p $\nu_\odot$'s and 40 from NO $\nu_\odot$'s. The reaction is ^{176}Yb (ν_e, e^-) ^{176}Lu at E$\geq$ 301 keV (^{176}Yb has a good isotopic abundance, $\sim$ 13 %). It is also possible a ^{7}Be $\nu_\odot$ NC interaction on ^{173}Yb at E$\geq$ 482 keV, [CRI00].
A 25 tons of Gd should have the same flux, the threshold being E$\geq$ 244 keV.
The ν energy is given by the sum of kinetic energy of electron and the Q value of the reaction. This experiment could have a good energy resolution while the background should be rejected thanks to a good time resolution. Moreover, electron-γ coincidence should help to achieve a background reduction at low energy so that it should allow a measurement of the low-energy part of the $\nu_\odot$ spectrum.
Among different aspects, we underline the influence of the use of extractants in rare earth technology, [RAG00a, RAG00b]. In 2001 an aromatic scintillation solvent loaded with organo-metallic Yb compounds was realized. Background reactions gave serious troubles: many decays produce two signals correlated in space and time as the ν_e tag (^{231}Th, ^{169}Yb, ^{176}Lu). At present time, the great amount of difficulties in electronics and in signal identifications when Yb is used, have stopped the evolution of this project.
Indium liquid scintillator detector was recently proposed, [RAG01]; the first reaction is $\nu_e + ^{115} I \rightarrow ^{115} Sn + e^-$, then ^{115}Sn de-excites (T=4.76 μs) giving rise to a 115.6 keV electron (or γ in 4% of the decays) and to a 497.3 keV γ. The low Q-value (118 keV) allows a practically complete detection of $\nu_\odot$ spectrum. Moreover, the delayed coincidence has strong signature, a relatively high energy ($\sim$ 613 keV) and a high isotopic abundance ($\sim$ 96 %).
The electron can be tagged as a product of ν_e capture by a unique delayed space-time coincidence of radiations de-exciting the isomeric state. In a 4 tons ^{115}In detector, an interactions rate of 1 p-p $\nu_\odot$ per day is foreseen, [RAG76, RAP85].
The only but terrible obstacle is the β decay, with t= $6.4 \cdot 10^{14}$ y, end-point at 495 keV and activity of 0.25 Bq/g, which overlaps the p-p and ^{7}Be $\nu_\odot$ signal. The use of In liquid scintillator with specific solvents and "prompt" and "spatial" coincidences should allow a modular detector with a sufficient efficiency and accurate rejection of impurities and background. Among a lot of technical difficulties, we mention the amount of phototubes having small section, 2 cm x 2 cm, ($\sim$ 10000), and the fine resolution needed to reject background events produced by bremsstrahlung.

9.6. LESNE.

LESNE (Lithium Experiment on Solar Neutrinos) is a radiochemical experiment which should use Li in metallic form as target nucleus; it was proposed by a Russian-Italian

working group, [ZAT97]. A great advantage of this detector is the compactness; for instance technical troubles are due to the required special handling of Li in the melted form. Thanks to the relative low threshold a clear detection of higher energy line from ^{7}Be and from p-e-p $\nu_\odot$ should be allowed. The Li mass adequate to perform precision measurements of seasonal variations is 100 tons. The ^{7}Be $\nu_\odot$ features should be checked by means of a cryogenic microcalorimeter, [GAL97a, GAL97b, KOP02].

9.7. MOON.

MOON (MOlibdenum Observatory of Neutrinos) experiment is based on a detector using ^{100}Mo as a target, the main aim being the search for $\beta\beta$-decay. Among many interesting features, the low energy threshold, 168 keV, the real-time detection and a good spatial resolution are the most promising ones. An event rate of ~ 5 events per day with a 10 tons detector is foreseen, [EJI00a, EJI00b, EJI01b, EJI01a].
The physical process is a ν absorption which induces an inverse β-decay followed by a β-decay to ^{100}Tc with a mean life of 23 s. Two electrons are emitted and the identification of the$\nu_\odot$ production reaction is allowed by the measurement of the energy of the inverse β^-. The time window between the emission of both the electrons allows a rejection of background reactions and accidental $\beta\beta$-decay which is the main background component and the most challenging problem to overcome.
The detector should consist of 34 tons (3.3 tons of ^{100}Mo) purified at a level of 10^{-3} Bq/ton respective of ^{238}U and ^{232}Th (similar level was achieved in SNO but for different materials). A plastic scintillator set of foils is responsible for the electron detection. Wavelength shifter fiber light collectors and PMT's are also present. The energy resolution for ^{7}Be $\nu_\odot$'s would be of about 15%.
The originally proposed detector (6x6x5 m) consisted of Mo foils and plains of scintillator with an expected time resolution of ~ 1 ns but a more compact version (2.5x2.5x1.0 m) enriched in ^{100}Mo up to 85% was recently proposed, [EJI01b], the lower dimensions allowing a gain in energy resolution, in light collection, in cosmogenic background and in signal to noise ratio.

9.8. MUNU.

A TPC detector using CF_4 were proposed [ARP96] with essentially the same goals as HELLAZ. Obviously CF_4 is not as good as He if one takes into account only angular resolution but a smaller number of technical problems is present, i.e. it is not necessary to use a pressurized vessel.
The MUNU collaboration has realized a TPC looking for the ν magnetic moment and the interactions induced by reactor $\overline{\nu}_e$'s: it has published the first measurements of energy and direction of the recoil electron at E$\geq$ 0.3 MeV.
The main characteristics of the detector are:

- The filling gas has high density and relatively low atomic number, so that the multiple scattering is reduced, being the cosmogenic activation of C and F at a low

level.

- It does not contain free protons.

An unexpected background due to α's and electrons, mainly from Rn, was reduced by a factor of $\sim 10^3$ after installation of new components (purifier and cathode). The peak of events from the reactor is starting to come out, [BRO02, BRO01b].
The present central detector is an acrylic cylinder of 0.9 m inner diameter and 1.62 m long filled with CF_4 at 3 bar pressure. This vessel is mounted inside a stainless steel tank filled with a liquid scintillator, used as a cosmic muons veto and anti-Compton, viewed by 48 PMT's.
The MUNU detector could be exploited as a low background prototype for the spectroscopy of $\nu_\odot$'s in the energy region below 1 MeV. It has the great advantage to work at atmospheric pressure and room temperature. In a detectore having a volume of 200 m^3, filled with gas at a pressure of 1 bar, the total target mass being of 740 kg, the expected interaction rate per day is 0.4 events from p-p $\nu_\odot$'s, 0.4 events from ^{7}Be $\nu_\odot$'s and 0.1 events from p-e-p, ^{13}N and ^{15}O $\nu_\odot$'s, [BRO01a]. The energy threshold is 100 keV. The background due to Rn and ^{14}C requires further studies; only a very high radiopurity and a sure signal identification procedure will allow the useful feasibility of such a detector in $\nu_\odot$ physics.

9.9. TPC.

A proposal based on TPC technique has been done by [BON01a, BON01b, BON02b]. It should be a cylinder 20 m long and $\sim$ 20 m in diameter filled with 7-10 tons of gas and separated from the rock by $\sim$ 3 mwe of high purity shielding. The gas should be boil-off He in bulk with a small component of natural gas, He(97%), CH_4(3%) at 10 atm pressure: in this way metals and many radioactive or electronegative gases, from H_2O vapor to Rn, are eliminated. The TPC cylinder, having a slight overpressure, is enclosed in an external pressure vessel. Teflon gaskets are used to seal the juncture of the barrel and endcap. The philosophy is the one of a device having electronic channels and materials coming into contact with the gas as little as possible. The end caps are the detector planes and contain a single set of wires, reconstructing the (x, z) profile of a track, and a single set of strips, giving the (y, z) profile, z being the drift direction. The vertex and energy are reconstructed by combining both track views. More than 30000 electronic FADC channels are needed for TPC. 100 keV tracks are considered the TPC ultimate benchmark. Such a track at 10 atm has a total length of 9 cm and generates 2500 electrons that will drift to the anode while diffusing.
Resolution effects are dominated by angular resolution which depends significantly on multiple scattering: from simulations a value of 15° at 100 keV and 10 Atm, and decreasing like $T^{-0.6}$, T being the electron kinetic energy, has been estimated.
This detector should use MUNU results as starting point for R&D.

9.10. UNO, HYPERKAMIOKANDE, TITANIC.

The philosophy of these proposals is to "enlarge" the SK detector by a large factor, [JUN00], using the same detecting technique (Čerenkov light emission).
Among different proposed geometries for the UNO project (Ultra underground Nucleon decay and neutrino Observatory), the most feasible one is a linear 3-modular detector 60 m large, 60 m high and 180 m long. The best motivations are mainly due to the current PMT pressure stress limit (8 bar for 20"-PMT's) and to the finite light attenuation length in pure water, 80 m at a wavelength of $\sim$ 400 nm. This multi-purpose "swimming pool" would foresee to use only the medium tank to $\nu_\odot$ searches for, the remaining tanks being dedicated to proton-decay and galactic ν's analysis and, at the same time, acting as a lateral shield for $\nu_\odot$ central detector. The fiducial volume should be of $\sim$ 450000 tons.
A great advantage of this proposal detector is obvious: new technique is not needed. The problems seem to be (only) the funding and the location but only higher energy $\nu_\odot$'s should be detected even with an energy threshold maybe lower than in SK experiment (4.0 MeV ?).
HyperKAMIOKANDE is a second gigantic detector, its proposed mass being 1 Megatons. A "linear" modular solution and a "toroidal" version were proposed, [NAK00]. The only presently viable location should be the Kamioka mine, with the advantage of the existing SK facilities.
A further and more ambitious project, TITANIC, foresees a fully merged in sea water, at depth ranging from 100 to 200 m, fourfold modular detector, (50x50x100 m) or (70x70x100 m), with a fiducial mass of $\sim$ 2 million tons, [SUZ00b].

9.11. XMASS.

The experiment XMASS (Xenon MASsive detector for Solar neutrinos) uses liquid Xe, a sufficiently known scintillator without the background problems related to C atoms, [SUZ00a].
The interaction process is based on excitation or ionisation of Xe atoms which then go into excited Xe_2^* states emitting some time later UV photons at 173 nm. The recombination time is variable, depending on exciting particle, from $\sim$ 40 ns in the case of electron down to 3 ns if α's are present. This feature allows a pulse shape discrimination. The attenuation length is not known but depends upon the level of purity. The PMT's can be placed either in the liquid (at a working temperature of 165 K) or outside the detector.
A great technical advantage is due to the possibility of using liquid N_2 to liquefy Xe; furthermore, Xe has both high density and high atomic number and it allows a good self-shielding so that the background problems seem to be not too hard to overcome. As a final advantage Xe produces proportional scintillation by multiplication process in an electric field.
The cosmogenic component of background does not produce long lived Xe-isotopes while

the ^{85}Kr and ^{42}Ar presence is due to their boiling temperatures which are lower than Xe. An absorption column removing this component is under analysis. ^{3}H can be removed *via* chemical process. The U/Th chain should require a contamination level 10 times lower than in CTF-Borexino experiment; the feasibility seems to be related to the pulse shape discrimination. If the detector will be installed at Kamioka mine, a reduction of ~ 4 orders of magnitude of neutron flux is needed. A water shield is possible.
The main difficulties come from the ^{136}Xe 2ν $\beta\beta$-decay: the only possible solution is an isotopic separation, with enrichment or depletion. A "fair" solution should be a $\nu_{\odot}$'s module based on odd Xe enriched sample, an even enriched module for $\beta\beta$ decay while both the components should be used to search for dark matter.
A 3 kg detector viewed by new type 2"-PMT's was built to check the feasibility of such a technique. A 100 kg facility is presently under construction and installation at Kamioka mine: the main goal is to test energy reconstruction, electron/γ separation, neutron background, self-shielding purification, attenuation length and new PMT's.

9.12. Further Proposals.

Other detectors based on different techniques have been recently suggested; among them we mention:

- COBRA, a $\beta\beta$-decay experiment, which would use CdTe semiconductors and measure in real-time $\nu_{\odot}$'s at E$\geq$ 366 keV, [ZUB01, ZUB02].
- SIREN, which should employ Gd as a scintillator: a test module is being designed for installation at Boulby mine in U.K., [AKI02, KUD02].
- An hybrid detector, with I and Cl as a target mass, installed at Homestake mine, when the future of this mine will be clarified.

10. Summary and conclusions.

Solar neutrino physics is presently an active and exciting field of research: in the last years our knowledge has been greatly enhanced but a lot of problems remains unexplained. The available experimental results should require a new theoretical effort because they imply a particle physics beyond standard model (if the flavour oscillation is the right solution to the SNP, then neutrinos do have a mass).
We can try to resume the present status in $\nu_{\odot}$ physics in this way:

(i) The experiments have detected $\nu_{\odot}$'s but a deficit is present when compared to the predictions of SMs, which are reinforced by the helioseismological observations. This deficit is critical mainly for the Ga experiments, which measure low energy component of $\nu_{\odot}$ flux: their interaction rate seems to be lower than the minimum value allowed by $L_{\odot}$ (energy conservation law), which is independent from the adopted SM.

(ii) The ratio among NC, CC and ES interactions has been (finally) measured with high precision by SNO; SK results, which are based on high statistics, show that

the energy spectrum of the ^{8}B component seems to be undisturbed. Being true these results, the $\nu_\odot$ flux deduced from NC measurements at SNO, well agree with the predictions of SMs; on the contrary either spectral distortions or a ν component without interactions enhances the differences. This conclusion is based on data at high energy: no direct individual measurements of components at E$\leq$ 1 MeV ($\sim$ 98% of the total $\nu_\odot$ flux) are presently available.

(iii) It appears very difficult to reproduce the experimental data by changing the solar physics. The preferred solution to the SNP is in term of ν flavour oscillations. If the detected ν flavours are not mass eigenstates but a superposition of mass eigenstates, ν's can change flavour. Solar data are well described in terms of 2 flavour oscillations: different regions in the parameter space (mixing angle θ and mass difference $\Delta\, m^2$) were obtained at the beginning by experimental measurements. Present results seem to be in agreement with predictions given by a solution with resonant oscillation in matter and large mixing angle.

(iv) It has to be remarked that first and strong data suggesting ν flavour oscillations come from observation of atmospheric and solar neutrino interactions; at present time LSND and K2K experiments confirm these signals but other detectors are still starting.

(v) The present detectors (GNO, SAGE, SNO and SK, when operating) will continue their data taking. KAMLAND and BOREXINO will measure the ^{7}Be $\nu_\odot$ flux; at this point, the p-p $\nu_\odot$ net component will be estimated from GNO-SAGE data and a right solution to the SNP will be more evident. Before the end of 2002, KAMLAND measurements concerning $\overline{\nu}_e$ from reactors will constraints, if any, oscillation solutions.

(vi) Real-time low-energy detectors, which should allow even a detailed analysis of time dependence of $\nu_\odot$ flux, were proposed but many technical problems are presently existing (mainly the background estimation and reduction): their feasibility and operativity seem to be far.

(vii) It was proposed, [TUR01b], to transform GNO experiment in a permanent solar observatory, due to its possibility to check the inner solar behaviour by detecting low-energy $\nu_\odot$ component: this should be a return to the beginning of $\nu_\odot$ experimental physics, when Cl experiment was proposed to study the features of the Sun.

(viii) Present SMs well reproduce solar features despite their assumptions. Numerical techniques and self-consistent methods to realize a more refined and complete SM, testable with experimental data, are at their beginning. It is needed to have new low-energy nuclear physics experiments to better understand and estimate nuclear parameters entering the SMs, even if the laboratory conditions are different from the solar plasma.

(ix) In two flavour *scenario* among active neutrinos, an important task is to refine the neutrino squared mass difference and the mixing angle. In order to accomplish this

task more precise measurements and calculations of the ν_e survival probability P_{ee} and of related observable quantities are needed. It is important to stress that improving the statistical analysis and the evaluation of the uncertainties is an important task in $\nu_\odot$ physics. After the observation of the disappearance of atmospheric ν_μ and of solar ν_e and the upcoming tests at long-baseline accelerator and reactor experiments, an era of searches for smaller effects is starting. Moreover, there is no "direct" proof for oscillation patterns in vacuum or in matter.

As a concluding remark it could be useful to remember the final comment to the neutrino "birth":
"...I admit that my expedient may seem rather improbable from the first, because if neutrons (ν, of course) existed they would have been discovered long since. Nevertheless, nothing ventured nothing gained..." (Wolfgang Pauli)
The right philosophy in searching for solutions could be suggested by a Sir A. Conan Doyle's sentence:
"..It is an old maxim of mine that when You have excluded the impossible, whatever remains, however improbable, must be the truth."
Therefore, let us underline the proposal quoted in [OHL02]: if (or when) neutrino oscillation will be the right answer to the SNP, a neutrino oscillation tomography could be in a far future a way to look for the density inside the Earth and, maybe, to discover metals and petroleum.
A worthy conclusion is in our opinion an early prophecy done by L.A.Saeneca in his book "Quaestiones naturales":
"..Veniet tempus quo ista quae nunc latent in lucem dies extrahat et longioris aevi diligentiae.... Veniet tempus quo posteri nostri tam aperta nos nescisse mirentur."

11. Acknowledgements.

We wish to thank many people: among them we mention E.Bellotti, C.Cattadori, G.L.Fogli and E.Lisi for useful discussions, S.Couvidat and S.Turck-Chièze for information on their solar models, C.Broggini, O.Cremonesi, A.Strumia and F.Vissani for their suggestions.
Very special thanks to N.Ferrari, B.Ricci and L.Zanotti for a lot of precious comments during the manuscript preparation.
Thanks again to J.N.Bahcall, E.Bellotti for GNO coll., M.Boulay and S.Oser for SNO coll., C.Giunti, M.C.Gonzalez-Garcia, E.Lisi, O.L.G.Peres, B.Ricci, A.Y.Smirnov, M.B.Smy for SK coll. and S.Turck-Chièze which have authorized the reproduction of plots and figures from their articles.
Figure nr. 1 is reproduced by permission of Elsevier Science.
Figures nr. 2, 3, 4, 5, 6, 7, 8, 9, 10, 11, 12, 17, 18 are reproduced by permission of American Astronomical Society.
Figures nr. 15, 16, 20, 21, 22, 23, 24, 25, 29, 30, 33, 36, 40 are reproduced by permission of American Physical Society.

12. Appendix: WEB pages.

We also list useful web-pages in $\nu_\odot$ physics:

(i) J.N.BAHCALL = www.sns.ias.edu/ jnb
(ii) BAKSAN = www.inr.ac.ru/INR/Baksan
(iii) KAMIOKA = www-sk.icrr.u-tokyo.ac.jp/
(iv) LNGS = www.lngs.infn.it
(v) Neutrino Oscillatory Industry = www.hep.anl.gov/ndk/hypertext/nuindustry
(vi) Neutrino Unbound = www.to.infn.it/ giunti/NU/
(vii) BOREXINO = borex.lngs.infn.it
(viii) EXO = hep.stanford.edu/neutrino/exo
(ix) GALLEX = www.lngs.infn.it/site/exppro/gallex
(x) GENIUS = www.mpi-hd.mpg.de/non_acc
(xi) GNO = www.lngs.infn.it/site/exppro/gno
(xii) HELLAZ = cdfinfo.in2p3.fr/experiences/hellaz
(xiii) HERON = www.physics.brown.edu/research/cme/heron
(xiv) HOMESTAKE = cpt1.dur.ac.uk/scripts/explist
(xv) ICARUS = www.aquila.infn.it/icarus
(xvi) KAMLAND = www.awa.tohoku.ac.jp/kamland
(xvii) LESNE = al20.inr.troitsk.ru/ beril
(xviii) MOON = ewi.npl.washington.edu/moon
(xix) MUNU = www.unine.ch/phys/corpus/munu
(xx) SAGE = ewi.npl/washington/edu/sage
(xxi) SK = www-sk.icrr.u-tokyo.ac.jp
(xxii) SNO = www.sno.phy.queensu.ca
(xxiii) UNO = superk.physics.sunysb.edu/nngroup/uno

13. References.

[ABD94] ABDURASHITOV J.N. *et al.* (SAGE coll.): *Phys. Lett.* B **328**,(1994) 234.
[ABD96] ABDURASHITOV J.N. *et al.* (SAGE coll.): *Phys. Rev. Lett.* **77**,(1996) 4708.
[ABD99a] ABDURASHITOV J.N. *et al.* (SAGE coll.): *Phys. Rev.* C **59**,(1999) 2246.
[ABD99b] ABDURASHITOV J.N. *et al.* (SAGE coll.): *Phys. Rev.* C **60**,(1999) 055801.
[ABD02] ABDURASHITOV J.N. *et al.* (SAGE coll.): hep-ph/0204245 v2 Preprint, 2002; submitted to *JETP*.
[ADE98] ADELBERG E.G. *et al.*: *Rev. Mod. Phys.* **70**,(1998) 1265.
[AGU01] AGUILAR A. *et al.* (LSND coll.): *Phys. Rev.* D **64**,(2001) 112007.
[AHM01] AHMAD Q.R. *et al.* (SNO coll.): *Phys. Rev. Lett.* **87**,(2001) 071301.
[AHM02a] AHMAD Q.R. *et al.* (SNO coll.): *Phys. Rev. Lett.* **89**,(2002) 011301.
[AHM02b] AHMAD Q.R. *et al.* (SNO coll.): *Phys. Rev. Lett.* **89**,(2002) 011302.
[AHN01] AHN S.H. *et al.*: *Phys. Lett.* B **511**,(2001) 178.
[AKH88] AKHMEDOV E.K.: *Phys. Lett.* B **213**,(1988) 64.
[AKH88a] AKHMEDOV E.K.: *Sov. J. Nucl. Phys.* **48**,(1988) 382.
[AKH95] AKHMEDOV E.K. *et al.*: *Phys. Lett.* B **348**,(1995) 124.
[AKH01] AKHMEDOV E.K.: Talk at *Solar neutrinos: where are the oscillations? International Workshop, LNGS 2001.*
[AKH02] AKHMEDOV E.K. AND PULIDO J.: *Phys. Lett.* B **529**,(2002) 193.
[AKI02] AKIMOV D. *et al.*: *Phys. Lett.* B **524**,(2002) 245.
[AKI97] AKIMUNE H. *et al.*: *Phys. Lett.* B **394**,(1997) 23.
[ALE94] ALEXANDER D.R. AND FERGUSON J.W.: *The Astrophys. J.* **437**,(1994) 879.
[ALI01] ALIANI P. *et al.*: hep-ph/0111418 Preprint, 2001.
[ALI02a] ALIANI P. *et al.*: hep-ph/0205053 Preprint, 2002.
[ALI02b] ALIANI P. *et al.*: hep-ph/0206308 Preprint, 2002.
[ALI02c] ALIMONTI G. *et al.* (BOREXINO coll.): *Astropart. Phys.* **16**,(2002) 205.
[ALI98] ALIVISATOS P. *et al.* (KAMLAND coll.): Stanford-HEP-98-03 Preprint, 1998.
[ALT00] ALTMANN M. *et al.*: *Phys. Lett.* B **490**,(2000) 16.
[ALV38] ALVAREZ L.W.: *Phys. Rev.* **54**,(1938) 486.
[ALV49] ALVAREZ L.W.: UCRL-328 Report, 1949.
[ANG99] ANGULO C. *et al.*: *Nucl. Phys.* A **656**,(1999) 3.
[ANS92] ANSELMANN P. *et al.* (GALLEX coll.): *Phys. Lett.* B **285**,(1992) 376.
[ANS95] ANSELMANN P. *et al.* (GALLEX coll.): *Phys. Lett.* B **342**,(1995) 440.
[ANT94] ANTIA H.M. AND BASU S.: *Astron. & Astrophys.* **107**,(1994) 421.
[ANT98] ANTIA H.M. AND CHITRE S.M.: *Astron. & Astrophys.* **339**,(1998) 239.
[ANT00] ANTIA H.M. AND BASU S.: astro-ph/0004355 Preprint, 2000; *The Astrophys. J.* accepted.
[APO99] APOLLONIO M. *et al.* (CHOOZ coll.): *Phys. Lett.* B **466**,(1999) 415.
[ARA97] ARAFUNE J. AND SATO J.: *Phys. Rev.* D **55**,(1997) 1653.
[ARM02] ARMBRUSTER B. *et al.* (KARMEN coll.): *Phys. Rev.* D **65**,(2002) 112001.
[ARP96] ARPESELLA C. *et al.*: *Astropart. Phys.* **4**,(1996) 333.
[ASP00] ASPLUND M.: *Astron. & Astrophys.* **359**,(2000) 755.
[AST20] ASTON F.W.: *Phil. Mag. & J. Sci.* **69**,(1920) 611.
[ATH98a] ATHANASSOPOULOS C. *et al.*: *Phys. Rev.* C **58**,(1998) 2489.
[ATH98b] ATHANASSOPOULOS C. *et al.*: *Phys. Rev. Lett.* **81**,(1998) 1774.
[ATK29] ATKINSON R.D.E. AND HOUTERMANS F.G.: *Z. Phys.* **54**,(1929) 656.
[BAB02] BABA C.V.K. *et al.*: *Phys. Rev.* D **65**,(2002) 073033.
[BAH63] BAHCALL J.N. *et al.*: *The Astrophys. J.* **137**,(1963) 344.
[BAH64] BAHCALL J.N.: *Phys. Rev. Lett.* **12**,(1964) 300.
[BAH68] BAHCALL J.N. *et al.*: *Phys. Rev. Lett.* **20**,(1968) 1209.
[BAH82] BAHCALL J.N. *et al.*: *Rev. Mod. Phys.* **54**,(1982) 767.

[BAH87] BAHCALL J.N. *et al.*: *The Astrophys. J. Lett.* **320**,(1987) L 69.
[BAH88] BAHCALL J.N. AND ULRICH R.K.: *Rev. Mod. Phys.* **60**,(1988) 297.
[BAH89] BAHCALL J.N.: *Neutrino astrophysics*, (Cambridge Univ. Press) 1989.
[BAH90a] BAHCALL J.N. AND BETHE H.A.: *Phys. Rev. Lett.* **65**,(1990) 2233.
[BAH90b] BAHCALL J.N. AND LOEB A.: *The Astrophys. J.* **360**,(1990) 267.
[BAH92] BAHCALL J.N. AND PINSONNEAULT M.H.: *Rev. Mod. Phys.* **64**,(1992) 885.
[BAH94a] BAHCALL J.N. AND GLASNER A.: *The Astrophys. J.* **427**,(1994) 485.
[BAH94b] BAHCALL J.N.: *Phys. Rev.* D **49**,(1994) 3923.
[BAH95] BAHCALL J.N. AND PINSONNEAULT M.H.: *Rev. Mod. Phys.* **67**,(1995) 781.
[BAH96a] BAHCALL J.N. AND ULMER A.: *Phys. Rev.* D **53**,(1996) 4202.
[BAH96b] BAHCALL J.N. AND KRASTEV P.I.: *Phys. Rev.* D **53**,(1996) 4211.
[BAH96c] BAHCALL J.N. *et al.*: *Phys. Rev.* C **54**,(1996) 411.
[BAH96d] BAHCALL J.N. AND LISI E.: *Phys. Rev.* D **54**,(1996) 5417.
[BAH97a] BAHCALL J.N.: *Phys. Rev.* C **56**,(1997) 3391.
[BAH97b] BAHCALL J.N. *et al.*: *The Astrophys. J. Lett.* **485**,(1997) L 91.
[BAH97c] BAHCALL J.N. AND KAMIONKOWSKI M.: *Nucl. Phys.* A **625**,(1997) 893.
[BAH97d] BAHCALL J.N. *et al.*: *Phys. Rev. Lett.* **78**,(1997) 171.
[BAH97e] BAHCALL J.N.: hep-ph/9711358 Preprint, 1997.
[BAH98a] BAHCALL J.N. *et al.*: *Phys. Lett.* B **433**,(1998) 1.
[BAH98b] BAHCALL J.N. AND KRASTEV P.I.: *Phys. Lett.* B **436**,(1998) 243.
[BAH98c] BAHCALL J.N. *et al.*: *Phys. Rev.* D **58**,(1998) 096016.
[BAH00a] BAHCALL J.N. *et al.*: *Phys. Rev.* D **62**,(2000) 093004.
[BAH00b] BAHCALL J.N. *et al.*: *Phys. Lett.* B **477**,(2000) 401.
[BAH01a] BAHCALL J.N. *et al.*: *The Astrophys. J.* **555**,(2001) 990.
[BAH01b] BAHCALL J.N. *et al.*: *J. High Energy Phys.* **0105**,(2001) 015.
[BAH01c] BAHCALL J.N. *et al.*: *J. High Energy Phys.* **0108**,(2001) 014.
[BAH01d] BAHCALL J.N. *et al.*: *Phys. Rev.* D **63**,(2001) 053012.
[BAH02a] BAHCALL J.N.: *Phys. Rev.* C **65**,(2002) 015802.
[BAH02b] BAHCALL J.N.: *Phys. Rev.* C **65**,(2002) 025801.
[BAH02c] BAHCALL J.N. *et al.*: *J. High Energy Phys.* **0204**,(2002) 007.
[BAH02d] BAHCALL J.N. *et al.*: *Astron. & Astrophys.* **383**,(2002) 291.
[BAH02e] BAHCALL J.N. *et al.*: hep-ph/0204194 Preprint, 2002.
[BAH02f] BAHCALL J.N. *et al.*: *J. High Energy Phys.* **0207**,(2002) 054.
[BAL98] BALACHANDRAN S. AND BELL R.A.: *Nature* **392**,(1998) 791.
[BAL88] BALTZ A.J. AND WENESER J.: *Phys. Rev.* D **37**,(1988) 3364.
[BAN01] BANDYOPADHYAY A. *et al.*: *Phys. Lett.* B **519**,(2001) 83.
[BAN02a] BANDYOPADHYAY A. *et al.*: *Phys. Rev.* D **65**,(2002) 073031.
[BAN02b] BANDYOPADHYAY A. *et al.*: *Phys. Lett.* B **540**,(2002) 14.
[BAR00] BARBIERI R. *et al.*: *Nucl. Phys.* B **585**,(2000) 28.
[BAR80] BARGER V. *et al.*: *Phys. Rev.* D **22**,(1980) 2718.
[BAR91] BARGER V. *et al.*: *Phys. Rev.* D **44**,(1991) 1629.
[BAR98] BARGER V. *et al.*: *Phys. Lett.* B **437**,(1998) 107.
[BAR01a] BARGER V. *et al.*: *Phys. Lett.* B **498**,(2001) 53.
[BAR01b] BARGER V. *et al.*: *Phys. Rev.* D **64**,(2001) 073009.
[BAR02a] BARGER V. *et al.*: *Phys. Rev. Lett.* **88**,(2002) 011302.
[BAR02b] BARGER V. *et al.*: *Phys. Lett.* B **537**,(2002) 179.
[BAS96a] BASU S. AND THOMPSON M.J.: *Astron. & Astrophys.* **305**,(1996) 631.
[BAS96b] BASU S. *et al.*: *The Astrophys. J.* **460**,(1996) 1064.
[BAS97] BASU S. AND ANTIA H.M.: *Monthly Not. R.A.S.* **287**,(1997) 189.
[BAS98a] BASU S.: *Monthly Not. R.A.S* **298**,(1998) 719.
[BAS98b] BASU S. *et al.*: astro-ph/9810132 Preprint, 1998.

[BAS00] BASU S. *et al.*: *The Astrophys. J.* **529**,(2000) 1084.
[BAU00] BAUDIS L. AND KLAPDOR-KLEINGROTHAUS H.V.: astro-ph/0003435 Preprint, 2000.
[BAU02] BAUDIS L. *et al.*: *Nucl. Instrum. & Methods* A **481**,(2002) 149.
[BAY11a] von BAYER O. *et al.*: *Phys. Z.* **12**,(1911) 273.
[BAY11b] von BAYER O. *et al.*: *Phys. Z.* **13**,(1911) 273.
[BAY12] von BAYER O. *et al.*: *Phys. Z.* **13**,(1912) 264.
[BEA01] BEACOM J.F. AND PARKE S.J.: *Phys. Rev.* D **64**,(2001) 091302.
[BEL95] BELLINI G.P. *et al.*: *Nucl. Phys.* B (P.S.) **48**,(1996) 363.
[BEL01] BELLOTTI E.: *Nucl. Phys.* B (P.S.) **91**,(2001) 44.
[BER95] BEREZHIANI Z. AND ROSSI A.: *Phys. Rev.* D **51**,(1995) 5229.
[BER94] BEREZINSKY V.: *Comments Nucl. Part. Phys.* **21**,(1994) 249.
[BER00] BERGMANN S.*et al.*: *Phys. Rev.* D **62**,(2000) 073001.
[BET34] BETHE H.A. AND PEIERLS R.: *Nature* **133**,(1934) 532.
[BET36] BETHE H.A. AND BACHER R.F.: *Rev. Mod. Phys.* **8**,(1936) 82.
[BET38a] BETHE H.A. AND CRITCHFIELD C.L.: *Phys. Rev.* **54**,(1938) 248.
[BET38b] BETHE H.A. AND CRITCHFIELD C.L.: *Phys. Rev.* **54**,(1938) 862.
[BET39] BETHE H.A.: *Phys. Rev.* **55**,(1939) 434.
[BET01] BETTINI A.: *Riv. del Nuovo Cimento* Vol. **24** ,n. 11 (2001).
[BIE90] BIEBER J.W. *et al.*: *Nature* **348**,(1990) 407.
[BIL98] BILENKY S.M. *et al.*: *Phys. Rev.* D **58**,(1998) 003001.
[BOE01] BOEHM F. *et al.*: *Phys. Rev.* D **64**,(2001) 112001.
[BOE58] BOEHM-VITENSE E.: *Z. Astrophys.* **46**,(1958) 108.
[BOE87] BOERCKER D.: *The Astrophys. J. Lett.* **316**,(1987) L 95.
[BON01] BONANNO A. *et al.*: *Astron. & Astrophys.* **375**,(2001) 1062.
[BON02a] BONANNO A. *et al.*: astro-ph/0204331 Preprint, 2002; to be published in *Astron. & Astrophys.*
[BON99] BONETTI R. *et al.* (LUNA coll.): *Phys. Rev. Lett.* **82**,(1999) 5205.
[BON94] BONVICINI G.: *Nucl. Phys.* B (P.S.) **35**,(1994) 438.
[BON01a] BONVICINI G. *et al.*: hep-ex/0109032 Preprint, 2001.
[BON01b] BONVICINI G. *et al.*: hep-ph/0109199 Preprint, 2001.
[BON02b] BONVICINI G. AND SCHREINER A.: hep-ex/0203014 Preprint, 2002.
[BOG00] BOGER J. *et al.*: astro-ph/0001482 Preprint, 2000.
[BOO02] BOOTHROYD A.I. AND SACKMANN I.J.: astro-ph/0210127 Preprint, 2002, to be published in *The Astrophys. J.* .
[BOR98] BOREXINO coll.: *Nucl.Instrum.& Methods* A **406**,(1998) 411.
[BRO01a] BROGGINI C.: Proc. *Low energy solar neutrino detection LOWNU2*, edited by Y.SUZUKI, M.NAKAHATA AND S.MORIYAMA (World Scientific) 2001, p. 132.
[BRO01b] BROGGINI C.: hep-ex/0110026 Preprint, Proc. *NO-VE International Workshop, Venezia 2001*, edited by M.Baldo Ceolin (Padoa Univ.) 2001.
[BRO02] BROGGINI C.: *Nucl. Phys.* B (P.S.) **110**,(2002).
[BRO97] BROWN L.S. AND SAWYER R.F.: *Rev. Mod. Phys.* **69**,(1997) 411.
[BRO98] BROWN T.M. AND J.CHRISTENSEN-DALSGAARD: *The Astrophys. J. Lett.* **500**,(1998) L 195.
[BRU98] BRUN A.S. *et al.*: *The Astrophys. J.* **506**,(1998) 913.
[BRU99] BRUN A.S.*et al.*: *The Astrophys. J.* **525**,(1999) 1032.
[BUR57] BURBIDGE E.M. *et al.*: *Rev. Mod. Phys.* **29**,(1957) 547.
[BUT01] BUTLER M. *et al.*: *Phys. Rev.* C **63**,(2001) 035501.
[CAL00] CALAPRICE F.P.: *Nucl. Phys.* B (P.S.) **87**,(2000) 180.
[CAM58a] CAMERON A.*et al.*: *Ann. Rev. Nucl. Sci.* **8**,(1958) 299.
[CAM58b] CAMERON A.: Chalk River Lab-Rep CRL-41 Preprint, 1958.
[CAN91] CANUTO V.M.Canuto AND MAZZITELLI I.: *The Astrophys. J.* **370**,(1991) 295.

[CAR88] CARRARO C. *et al.*: *The Astrophys. J.* **331**,(1988) 565.
[CAS94] CASTELLANI V. *et al.*: *Phys. Lett.* B **324**,(1994) 425.
[CAS97] CASTELLANI V. *et al.*: *Phys. Rep.* **281**,(1997) 309.
[CAS99] CASTELLANI V. *et al.*: *Nucl. Phys.* B (P.S.) **70**,(1999) 301.
[CAT02] CATTADORI C.: *Nucl. Phys.* B (P.S.) **110**,(2002) 311.
[CHA95] CHABOYER B. *et al.*: *The Astrophys. J.* **446**,(1995) 435.
[CHA14] CHADWICK J.: *Verh. d. D. Phys. Ges.* **16**,(1914) 383.
[CHA64] CHANDRASEKHAR S.: *The Astrophys. J.* **139**,(1964) 664.
[CHA99] CHARBONNEAU P. *et al.*: *The Astrophys. J.* **527**,(1999) 445.
[CHA02] CHAUHAN B.C. AND PULIDO J.: hep-ph/0206193 Preprint, 2002.
[CHO01a] CHOI K. *et al.*: *Phys. Rev.* D **64**,(2001) 113013.
[CHO01b] CHOUBEY S. *et al.*: *Phys. Rev.* D **64**,(2001) 053002.
[CHO01c] CHOUBEY S. *et al.*: *Phys. Rev.* D **64**,(2001) 113001.
[CHO02] CHOUBEY S. *et al.*: *Phys. Rev.* D **65**,(2002) 073001.
[CHR91] CHRISTENSEN-DALSGAARD J. *et al.*: *The Astrophys. J.* **378**,(1991) 413.
[CHR92] CHRISTENSEN-DALSGAARD J.: *The Astrophys. J.* **385**,(1992) 354.
[CHR93] CHRISTENSEN-DALSGAARD J. *et al.*: *The Astrophys. J. Lett.* **403**,(1993) L 75.
[CHR96] CHRISTENSEN-DALSGAARD J.: *Nucl. Phys.* B (P.S.) **48**,(1996) 325.
[CHR01] CHRISTENSEN-DALSGAARD J. AND THOMPSON M.J.: astro-ph/0111607 Preprint, in *Dynamic Sun*; edited by B.N.DWIVEDI, (Cambridge Univ.Press) (2001).
[CIS71] CISNEROS A.: *Astrophysics Space Science* **10**,(1971) 87.
[CLA68] CLAYTON D.: *Principles of stellar evolution and nucleosynthesis*, (Mc Graw-Hill) 1968.
[CLE98] CLEVELAND B.T. *et al.*: *The Astrophys. J.* **496**,(1998) 505.
[COR99] CORADDU M. *et al.*: *Brazilian J. Phys.* March **29**,(1999) 153.
[COU02] COUVIDAT S. *et al.*: astro-ph/0203107 Preprint, 2002; submitted to *The Astrophys. J.*
[COX89] COX A.N. *et al.*: *The Astrophys. J.* **342**,(1989) 1187.
[COW53] COWAN C.L. AND REINES F.: *Phys. Rev.* **90**,(1953) 492.
[COW56] COWAN C.L. *et al.*: *Science* **124**,(1956) 103.
[CRA39a] CRANE H.R.: *Phys. Rev.* **55**,(1939) 501.
[CRA39b] CRANE H.R. AND HALPERN J.: *Phys. Rev.* **56**,(1939) 232.
[CRA48] CRANE H.R.: *Rev. Mod. Phys.* **20**,(1948) 748.
[CRE01] CREMINELLI P. *et al.*: *J. High Energy Phys.* **0105**,(2001) 052.
[CRE02] CREMINELLI P. *et al.*: hep-ph/0102234 v3 Preprint, 2002.
[CRE93] CREMONESI O.: *Riv. del Nuovo Cimento*, Vol. **16**,n. 12 (1993).
[CRI00] CRIBIER M.: *Nucl. Phys.* B (P.S.) **87**,(2000) 195.
[CRO96] CROMMELYNCK D. *et al.*: *Geophys. Res. Lett.* **23**,N17,(1996) 2293.
[CUM96] CUMMING A. AND HAXTON W.C.: *Phys. Rev. Lett.* **77**,(1996) 4286.
[DAP88] DAEPPEN W. *et al.*: *The Astrophys. J.* **332**,(1988) 261.
[DAP91] DAEPPEN W. *et al.*: in *Lecture Notes in Physics*, edited by D.O.GOUGH AND J.TOOMRE, 388 (Springer,Heidelberg) 1991, p. 111.
[DAN62] DANBY G. *et al.*: *Phys. Rev. Lett.* **9**,(1962) 36.
[DAR91] DAR A. AND NUSSINOV S.: *Particle World* **2**,(1991) 117.
[DAR96] DAR A. AND SHAVIV G.: *The Astrophys. J.* **468**,(1996) 933.
[DAR98] DAR A.: *Surveys High Ener. Phys.* **15**,(1998) 157.
[DAR99] DAR A. AND SHAVIV G.: *Phys. Rep.* **311**,(1999) 315.
[DAR59] DARWIN C.: *On the Origin of the Species by Natural Selection* or *The Preservation of favoured Races in the Struggle for Life*, (Murray,London) 1859, p. 285.
[DAV01] B.DAVIDS *et al.*: *Phys. Rev. Lett.* **86**,(2001) 2750.
[DAV55] DAVIS R.: *Phys. Rev.* **97**,(1955) 766.
[DAV64] DAVIS R.: *Phys. Rev. Lett.* **12**,(1964) 303.
[DAV68] DAVIS R. *et al.*: *Phys. Rev. Lett.* **20**,(1968) 1205.

[DAV70] DAVIS R.: *Hungaricae Supp.* **4**,29,(1970) 371.
[DAV71] DAVIS R. *et al.*: *Bull. Amer. Phys. Soc.* II,**16**,(1971) 631.
[DAV94] DAVIS R.: Proc. *VI Neutrino Telescopes International Workshop, Venezia 1994*; edited by M. BALDO-CEOLIN (Padoa Univ.Press) 1994, p.165.
[DAV96] DAVIS R.: *Nucl. Phys.* B (P.S.) **48**,(1996) 284.
[DEB00] DE BRAECKLEER L.: *Nucl. Phys.* B (P.S.) **87**,(2000) 312.
[DEG97] DEGL'INNOCENTI S. *et al.*: *Astropart. Phys.* **7**,(1997) 77.
[DEG98a] DEGL'INNOCENTI S. *et al.*: *Phys. Lett.* B **441**,(1998) 291.
[DEG98b] DEGL'INNOCENTI S. *et al.*: *Phys. Lett.* B **416**,(1998) 365.
[DEH02] DEHOLANDA P.C. AND SMIRNOV A.Y.: hep-ph/0205241 v2 Preprint, 2002.
[DEM91] DEMARQUE P. AND GUENTHER D.B.: in *Solar interior and atmosphere*; edited. by A.N.COX, W.C.LIVINGSTON NAD M.S.MATTHEWS, (Univ.Arizona Press,Tucson) 1991, p. 1186.
[DER99] DE RUJULA A. *et al.*: *Nucl. Phys.* B **547**,(1999) 21.
[DIC99] DICK K. *et al.*: *Nucl. Phys.* B **562**,(1999) 29.
[DOL02] DOLGOV A.D. *et al.*: *Nucl. Phys.* B **632**,(1999) 363.
[DOO00] DOOLING D. *et al.*: *Phys. Rev.* D **61**,(2000) 073011.
[DOR91] DORMAN L.I. AND WOLFENDALE A.W.: *J. Phys. G Nucl. Part. Phys.* **17**,(1981) 789.
[DUV93] DUVALL T.L. JR. *et al.*: *Nature* **362**,(1993) 430.
[DUV96] DUVALL T.L. JR. *et al.*: *Nature* **379**,(1996) 235.
[DZI90] DZIEMBOWSKI W.A.*et al.*: *Monthly Not. R.A.S.* **244**,(1990) 542.
[DZI95a] DZIEMBOWSKI W.A.*et al.*: *The Astrophys. J.* **445**,(1995) 509.
[DZI99] DZIEMBOWSKI W.A.*et al.*: *Astron. & Astrophys.* **343**,(1999) 990.
[DZI95b] DZITKO H. *et al.*: *The Astrophys. J.* **447**,(1995) 428.
[EDD20a] EDDINGTON S.A.: *Nature* **106**,(1920) 14.
[EDD20b] EDDINGTON S.A.: *Observatory* **43**,(1920) 353.
[EDD26] EDDINGTON S.A.: *The internal constitution of the Stars*, (Cambridge Univ.Press) 1926.
[EGG73] EGGLETON P.P. *et al.*: *Astron. & Astrophys.* **23**,(1973) 325.
[EGU02] EGUCHI K. *et al.*: hep-ph/0212021 Preprint, 2002; to be published in *Phys. Rev. Lett.*
[EIN05] EINSTEIN A.: *Ann. der Phys.* **17**,(1905) 891.
[EIT00] EITEL K. *et al.*: Proc. *Lake Louise Winter Institute 1999*, edited by A. ASTBURY *et al.*, (World Scientific) 2000, p. 353.
[EJI00a] EJIRI H. *et al.*: *Phys. Rev. Lett.* **85**,(2000) 2917.
[EJI00b] EJIRI H.: Talk at *LOWNU1 International Workshop, Sudbury 2000.*
[EJI01a] EJIRI H.: *Nucl. Phys.* B (P.S.) **91**,(2001) 255.
[EJI01b] EJIRI H.: Proc. *Low energy solar neutrino detection LOWNU2*, edited by Y.SUZUKI, M.NAKAHATA AND S.MORIYAMA (World Scientific) 2001, p. 29.
[ELL96] ELLIOTT J.R.: *Monthly Not. R.A.S.* **280**,(1996) 1244.
[ELL98] ELLIOTT J.R. AND KOSOVICHEV A.G.: *The Astrophys. J. Lett.* **500**,(1998) L 199.
[ELL27] ELLIS C.D. AND WOOSTER W.A.: *Proc. Royal Soc.* A **117**,(1927) 109.
[EME24] EMELEUS K.G.: *Proc. Camb. Phil. Soc.* **22**,(1924) 400.
[ENG92] ENGSTLER S. *et al.*: *Phys. Rev. Lett.* B **279**,(1992) 20.
[EPS50] EPSTEIN R.: *The Astrophys. J.* **112**,(1950) 207.
[EWA92] EWAN G.T. *et al.* (SNO coll.): *Phys. in Canada* **48**,(1992) 112.
[EZE68] EZER D. AND CAMERON A.G.W.: *The Astrophys. J. Lett.* **1**,(1968) 177.
[FER33] FERMI E.: *La Ricerca Scient.* **2**,(1933) 491.
[FER34a] FERMI E.: *Il Nuovo Cimento* **11**,(1934) 1.
[FER34b] FERMI E.: *Z. Phys.* **88**,(1934) 161.
[FER01] FERRARI N.: Proc. *Low energy solar neutrino detection LOWNU2*, edited by Y.SUZUKI, M.NAKAHATA AND S.MORIYAMA (World Scientific) 2001, p. 19.
[FET72] FETYSOV V.N. AND KOPYSOV Y.S.: *Phys. Lett.* B **40**,(1972) 602.

[FIO99a] FIORENTINI G. *et al.*: *Astron. & Astrophys.* **342**,(1999) 492.
[FIO99b] FIORENTINI G. AND RICCI B.: *Comm. Mod. Phys.* E **1**,(1999) 49.
[FIO00] FIORENTINI G. AND RICCI B.: *Nucl. Phys.* B (P.S.) **81**,(2000) 95.
[FIO01a] FIORENTINI G. *et al.*: *Phys. Lett.* B **503**,(2001) 121.
[FIO01b] FIORENTINI G. *et al.*: *Nucl. Phys.* B (P.S.) **95**,(2001) 116.
[FIO01c] FIORENTINI G. *et al.*: hep-ph/0109275 Preprint, 2001.
[FIO02] FIORENTINI G. AND RICCI B.: *Phys. Lett.* B **526**,(2002) 186.
[FOG95] FOGLI G.L. AND LISI E.: *Astropart. Phys.* **3**,(1995) 185.
[FOG96] FOGLI G.L. *et al.*: *Phys. Rev.* D **54**,(1996) 2048.
[FOG00] FOGLI G.L. *et al.*: *Phys. Rev.* D **62**,(2000) 013002.
[FOG01] FOGLI G.L. *et al.*: *Phys. Rev.* D **64**,(2001) 093007.
[FOG02a] FOGLI G.L. *et al.*: *Nucl. Phys.* B (P.S.) **110**,(2002) 268.
[FOG02b] FOGLI G.L. *et al.*: *Phys. Rev.* D **65**,(2002) 117301.
[FOG02c] FOGLI G.L. *et al.*: hep-ph/0206162 Preprint, 2002; to be published in *Phys. Rev. D.*
[FOG02d] FOGLI G.L. *et al.*: hep-ph/0208026 Preprint, 2002.
[FOW58] FOWLER W.A. *et al.*: *The Astrophys. J.* **127**,(1958) 551.
[FOW72] FOWLER W.A.: *Nature* **238**,(1972) 24.
[FOW84] FOWLER W.A.: *Rev. Mod. Phys.* **56**,(1984) 149.
[FRI02] FRIELAND A. AND GRUZINOV A.: hep-ph/0202295 v2 Preprint, 2002.
[FRI53] FRIEMAN E.A. AND MOTZ L.: *Phys. Rev.* **89**,(1953) 648.
[FRO98] FROELICH C. AAND LEON J.: *Geophys. Res. Lett.* **25**,N23,(1998) 4377.
[FUJ96] FUJIWARA M. *et al.*: *Nucl. Phys.* A **599**,(2001) 223.
[FUK01a] FUKUDA S. *et al.*: *Phys. Rev. Lett.* **86**,(2001) 5651.
[FUK01b] FUKUDA S. *et al.*: *Phys. Rev. Lett.* **86**,(2001) 5656.
[FUK02] FUKUDA S. *et al.*: hep-ex/0205075 Preprint, 2002.
[FUK96] FUKUDA Y. *et al.*: *Phys. Rev. Lett.* **77**,(1996) 1683.
[FUK98a] FUKUDA Y. *et al.*: *Phys. Rev. Lett.* **81**,(1998) 1158.
[FUK98b] FUKUDA Y. *et al.*: *Phys. Rev. Lett.* **81**,(1998) 1562.
[FUK98c] FUKUDA Y. *et al.*: *Phys. Rev. Lett.* **81**,(1998) 4279.
[FUK99] FUKUDA Y. *et al.*: *Phys. Rev. Lett.* **82**,(1999) 1810.
[GAG00a] GAGO A.M. *et al.*: *Phys. Rev. Lett.* **84**,(2000) 4035.
[GAG00b] GAGO A.M. *et al.*: *Nucl. Phys.* B (P.S.) **87**,(2000) 215.
[GAG01] GAGO A.M. *et al.*: *Nucl. Phys.* B (P.S.) **100**,(2001) 68.
[GAG02] GAGO A.M. *et al.*: *Phys. Rev.* D **65**,(2002) 073012.
[GAL97a] GALEAZZI M. *et al.*: *Nucl. Instrum.& Methods* A **401**,(1997) 317.
[GAL97b] GALEAZZI M. *et al.*: *Phys. Lett.* B **398**,(1997) 187.
[GAL67] GALITSKII V.M. AND YAKIMETS V.V.: *Sov. Phys. JETP* **24**,(1967) 637.
[GAM28] GAMOW G.: *Z. Phys.* **52**,(1928) 510.
[GAM36] GAMOW G. AND TELLER E.: *Phys. Rev.* **49**,(1936) 895.
[GAR01] GARZELLI M.V. AND GIUNTI C.: *J. High Energy Phys.* **0112**,(2001) 017.
[GAR02a] GARZELLI M.V. AND GIUNTI C.: *Astropart. Phys.* **17**,(2002) 205.
[GAR02b] GARZELLI M.V. AND GIUNTI C.: *Phys. Rev.* D **65**,(2002) 093005.
[GAS88] GASPERINI M.: *Phys. Rev.* D **38**,(1988) 2635.
[GAU97] GAUTIER D. AND MOREL P.: *Astron. & Astrophys.* **323**,(1997) L 9.
[GAV97] GAVRIN V.: Talk at *Solar Neutrinos: News about SNUs International Conference, S.Barbara (USA) 1997.*
[GAV01a] GAVRIN V.: *Nucl. Phys.* B (P.S.) **91**,(2001) 36.
[GAV01b] GAVRIN V.: Communication at *TAUP 2001 International Conference, LNGS, 2001.*
[GEL55] GELL-MANN M. AND PAIS A.: *Phys. Rev.* **97**,(1955) 1387.
[GHO01] GHOSAL A.: *Phys. Rev.* D **62**,(2001) 092001.
[GIA00] GIALANELLA L. *et al.*: *European Phys. J.* A **7**,(2000) 303.

[GIA01] GIAMMARCHI M.: Proc. *Low energy solar neutrino detection LOWNU2*, edited by Y.SUZUKI, M.NAKAHATA AND S.MORIYAMA (World Scientific) 2001, p. 47.
[GIU00] GIUNTI C. *et al.*: *Phys. Rev.* D **62**,(2000) 013005.
[GLA87] GLASHOW S.L. AND KRAUSS L.M.: *Phys. Lett.* B **190**,(1987) 199.
[GOL58] GOLDHABER M. *et al.*: *Phys. Rev.* **109**,(1958) 193.
[GON00] GONZALEZ-GARCIA M.C. *et al.*: *Nucl. Phys.* B **573**,(2000) 3.
[GON01a] GONZALEZ-GARCIA M.C. *et al.*: *Phys. Rev.* D **63**,(2001) 033005.
[GON01b] GONZALEZ-GARCIA M.C.: *Physica Scripta* T **93**,(2001) 26.
[GON01c] GONZALEZ-GARCIA M.C. *et al.*: hep-ph/0108073 v2 Preprint, 2001.
[GON01d] GONZALEZ-GARCIA M.C. *et al.*: *Phys. Rev.* D **63**,(2001) 113004.
[GON01e] GONZALEZ-GARCIA M.C. AND PENA-GARAY C.: *Phys. Rev.* D **64**,(2001) 093001.
[GON01f] GONZALEZ-GARCIA M.C. AND PENA-GARAY C.: *Nucl. Phys.* B (P.S.) **91**,(2001) 80.
[GON02] GONZALEZ-GARCIA M.C. *et al.*: *Phys. Lett.* B **527**,(2002) 199.
[GN096] GNO coll.: INFN/AE-96/27 Preprint, 1996.
[GOO80] GOODMAN C.D. *et al.*: *Phys. Rev. Lett.* **44**,(1980) 1755.
[GOU98] GOUGH D.O. AND MCINTYRE M.E.: *Nature* **394**,(1998) 755.
[GOU90] GOULD A.: *The Astrophys. J.* **362**,(1990) 284.
[GOU00] GOUVEA A. *et al.*: *Phys. Lett.* B **490**,(2000) 125.
[GOU01] GOUVEA A. AND PENA-GARAY C.: *Phys. Rev.* D **64**,(2001) 113011.
[GRE93] GREVESSE N. AND NOELS A.: in *Origin and Evolution of the Elements*, edited by N. PRANTZOS, E. VANGIONI-FLAM AND M. CASSE', (Cambridge Univ.Press) 1993, p. 15.
[GRE96] GREVESSE N.*et al.*: in *Cosmic Abundances*, edited by S.S. HOLT AND G. SONNEBORN, (ASP,C.S.) 1996.
[GRE98] GREVESSE N. AND SAUVAL A.J.: *Space Sci. Rev.* **85**,(1998) 161.
[GRI69] GRIBOV V. AND PONTECORVO B.: *Phys. Lett.* B **28**,(1969) 493.
[GRU97] GRUZINOV A. AND BAHCALL J.N.: *The Astrophys. J.* **490**,(1997) 437.
[GRU98] GRUZINOV A. AND BAHCALL J.N.: *The Astrophys. J.* **504**,(1998) 996.
[GUE92] GUENTHER D.B. *et al.*: *The Astrophys. J.* **387**,(1992) 372.
[GUE97] GUENTHER D.B. AND DEMARQUE P.: *The Astrophys. J.* **484**,(1997) 937.
[GUZ95] GUZIK J.A. AND COX A.N.: *The Astrophys. J.* 448,(1995) 905.
[GUZ91] GUZZO M.M. *et al.*: *Phys. Lett.* B **260**,(1991) 154.
[GUZ01] GUZZO M.M. *et al.*: *Nucl. Phys.* B (P.S.) **100**,(2001) 62.
[HAL91] HALPRIN A. AND LEUNG C.N.: *Phys. Rev. Lett.* **67**,(1991) 1833.
[HAM53] HAMILTON D.R. *et al.*: *Phys. Rev.* **92**,(1953) 1521.
[HAM98a] HAMMACHE F. *et al.*: *Phys. Rev. Lett.* **80**,(1998) 928.
[HAM01] HAMMACHE F. *et al.*: *Phys. Rev. Lett.* **86**,(2001) 3985.
[HAM96] HAMPEL W. *et al.*: *Phys. Lett.* B **388**,(1996) 364.
[HAM98b] HAMPEL W. *et al.*: *Phys. Lett.* B **436**,(1998) 158.
[HAM99] HAMPEL W. *et al.*: *Phys. Lett.* B **447**,(1999) 127.
[HAS02] HASEGAWA K.: *Nucl. Phys.* B (P.S.) **110**,(2002).
[HAS99] HASS M. *et al.*: *Phys. Lett.* B **462**,(1999) 237.
[HAT94a] HATA N. *et al.*: *Phys. Rev.* D **49**,(1994) 3622.
[HAT94b] HATA N. AND LANGACKER P.: *Phys. Rev.* D **50**,(1994) 632.
[HAX99] HAXTON W.C.: *Nucl. Phys.* B (P.S.) **77**,(1999) 73.
[HAX00] HAXTON W.C.: nucl-th/0004052 v2 Preprint, 2000.
[HEE96] HEEGER K.M. AND ROBERTSON R.G.H.: *Phys. Rev. Lett.* **77**,(1996) 3720.
[HEL56] von HELMHOTZ H.: Lecture given in 1854, *Phil. Mag.* **11**(4),(1856) 489.
[HIL01] HILL J.E.: hep-ex/0110034 Preprint, 2001.
[HIR89] HIRATA K.S. *et al.*: *Phys. Rev. Lett.* **63**,(1989) 16.
[HUE77] HUEBNER W.F. *et al.*: Los Alamos Scien. LA-6760-M Report, 1977.
[HUM88] HUMMER D.G. AND MIHALAS D.: *The Astrophys. J.* **331**,(1988) 794.

[ICA89] ICARUS coll.: LNF-89/005(R) Preprint, 1989.
[ICA94] ICARUS coll.: LNGS-94/99 Preprint, 1994.
[ICA95] ICARUS coll.: LNGS-95/10 Preprint, 1995.
[ICA00] ICARUS coll.: *Nucl. Instrum. & Methods* A **455**,(2000) 376.
[ICA01a] ICARUS coll.: *Nucl. Instrum. & Methods* A **461**,(2001) 286.
[ICA01b] ICARUS coll.: *Nucl. Instrum. & Methods* A **471**,(2001) 272.
[IGL91] IGLESIAS C.A. AND ROGERS F.J.: *The Astrophys. J.* **371**,(1991) 408.
[IGL92] IGLESIAS C.A. *et al.*: *The Astrophys. J.* **397**,(1992) 717.
[IGL95] IGLESIAS C.A. AND ROGERS F.J.: *The Astrophys. J.* **443**,(1995) 460.
[IGL96] IGLESIAS C.A. AND ROGERS F.J.: *The Astrophys. J.* **464**,(1996) 943.
[INO01] INOUE K.: Proc. *Low energy solar neutrino detection LOWNU2*, edited by Y.SUZUKI, M.NAKAHATA AND S.MORIYAMA (World Scientific) 2001, p. 57.
[ISH02] ISHII T. (K2K coll.): hep-ex/0206033 Preprint, 2002.
[ITO88a] ITO M. *et al.*: *Prog. Theor. Phys.* **79**,(1988) 13.
[ITO88b] ITO M. *et al.* - Erratum: *Prog. Theor. Phys.* 79,(1988) 555.
[JEF97] JEFFERY C.S. *et al.*: *Observatory* **117**,(1997) 224.
[JOH92] JOHNSON C.W. *et al.*: *The Astrophys. J.* **392**,(1992) 320.
[JOS74] JOSS P.C.: *The Astrophys. J.* **191**,(1974) 771.
[JUN00] JUNG C.K.: hep-ex/0005046 Preprint, 2000.
[JUN02] JUNGHANS A.R. *et al.*: *Phys. Rev. Lett.* **88**,(2002) 041101.
[KAJ94] KAJITA T.: ICRR 332-94-27 Report, 1994.
[KAN87] KANEKO T.: *Prog. Theor. Phys.* **78**,(1987) 532.
[KAN97] KANIADAKIS G. *et al.*: astro-ph/9701118 Preprint, 1997.
[KAN98] KANIADAKIS G. *et al.*: *Physica* A **261**,(1998) 359.
[KEL62] KELVIN W.T.: *MacMillan's Magazine*, **288** March 5,(1862).
[KIR02] KIRSTEN T.: Talk at *Neutrino 2002 Interational Conference, Muenchen 2002.*
[KLA99] KLAPDOR-KLEINGROTHAUS H.V. *et al.*: hep-ph/9910205 Preprint, 1999.
[KLA01a] KLAPDOR-KLEINGROTHAUS H.V. *et al.*: Proc. *DARK 2000 International Conference, Heidelberg 2000*, edited by H.V. KLAPDOR-KLEINGROTHAUS, (Springer,Heidelberg) 2001.
[KLA01b] KLAPDOR-KLEINGROTHAUS H.V.: Proc. *Low energy solar neutrino detection LOWNU2*, edited by Y.SUZUKI, M.NAKAHATA AND S.MORIYAMA (World Scientific) 2001, p. 116.
[KOP02] KOPYLOV A. AND PETUKHOV V.: hep-ph/0201042 v2 Preprint, 2002.
[KOR89] KORZENNIK S.G. AND ULRICH R.K.: *The Astrophys. J.* **339**,(1989) 1144.
[KOS91] KOSOVICHEV A.G. AND FEDOROVA A.V.: *Astron. Zh.* **68**,(1991) 1015.
[KOS96] KOSOVICHEV A.G.: *The Astrophys. J.* **461**,(1996) 55.
[KOS97] KOSOVICHEV A.G. *et al.*: *Solar Phys.* **170**,(1997) 43.
[KOS99] KOSOVICHEV A.G.: *J. Comput. Appl. Math.* **109**,(1999) 1.
[KRA88a] KRASTEV P.I. AND PETCOV S.T.: *Phys. Lett.* B **207**,(1988) 64.
[KRA88b] KRASTEV P.I. AND PETCOV S.T.- Erratum: *Phys. Lett.* B **214**,(1988) 661.
[KRA96] KRASTEV P.I. AND PETCOV S.T.: *Phys. Rev.* D **53**,(1996) 1665.
[KRA02] KRASTEV P.I. AND SMIRNOV A.Y.: *Phys. Rev.*D **65**,(2002) 073022.
[KUD02] KUDRYATSEV V.A. *et al.*: *Astropart. Phys.* **17**,(2002) 401.
[KUO87] KUO T.K. AND PANTALEONE J.: *Phys. Lett.* B **198**,(1987) 406.
[KUO89] KUO T.K. AND PANTALEONE J.: *Rev. Mod. Phys.* **61**,(1989) 937.
[KUR02] KURYLOV A. *et al.*: *Phys. Rev.* C **65**,(2002) 055501.
[KUZ64] KUZMIN V.A.: Lebedev Phys. Inst. Int. A-62 Preprint, 1964.
[KUZ65] KUZMIN V.A.: *Sov. Phys. JETP* **49**,(1965) 1532.
[LAN57] LANDAU L.D.: *Nucl. Phys.* **3**,(1957) 127.
[LAN98] LANDE K. *et al.*: Proc. *IV International Solar Neutrino Conference, Heidelberg 1997*, edited by W.HAMPEL, (M.P.I. fur KernPhysik,Heidelberg) 1998, p. 85.

[LAN52] LANGER L.M. AND MOFFAT J.D.: *Phys. Rev.* **88**,(1952) 689.
[LAN01] LANOU R.: Proc. *Low energy solar neutrino detection LOWNU2*, edited by Y.SUZUKI, M.NAKAHATA AND S.MORIYAMA (World Scientific) 2001, p. 70.
[LAV01] LAVAGNO A. AND QUARATI: *Phys. Lett.* B **498**,(2001) 47.
[LEE56] LEE T.D. AND YANG C.N.: *Phys. Rev.* **104**,(1956) 254.
[LEE57] LEE T.D. AND YANG C.N.: *Phys. Rev.* **105**,(1957) 1671.
[LEI62] LEIGHTON R.B. *et al.*: *The Astrophys. J.* **135**,(1962) 474.
[LEV94] LEVY E.H. AND RUZMAIKINA T.V.: *The Astrophys. J.* **431**,(1994) 881.
[LIM88] LIM C.S. AND MARCIANO W.J.: *Phys. Rev.* D **37**,(1988) 1368.
[LIM95] LIM C.S. AND NUNOKAWA H.: *Astropart. Phys.* **4**,(1995) 63.
[LIN01] LINDNER M. *et al.*: *Nucl. Phys.* B **607**,(2001) 326.
[LIU97] LIU Q.Y. AND PETCOV S.T.: *Phys. Rev.* D **56**,(1997) 7392.
[MAJ37] MAJORANA E.: *Il Nuovo Cimento* **14**,(1937) 170.
[MAK62] MAKI Z. *et al.*: *Prog. Theor. Phys.* **28**,(1962) 870.
[MAL02] MALTONI M. *et al.*: hep-ph/0207157 Preprint, 2002.
[MAR00] MARIS M. AND PETCOV S.T.: *Phys. Rev.* D **62**,(2000) 093006.
[MAS93] MASSETTI S. AND STORINI M.: *Solar Phys.* **148**,(1993) 172.
[MAS95a] MASSETTI S. *et al.*: Proc. *XXIV ICRC, Rome 1995*, edited by N. IUCCI AND E. LAMANNA, Vol. 4, 1995, p. 1243.
[MAS95b] MASSETTI S. *et al.*: Proc. *XXIV ICRC, Rome 1995*, edited by N. IUCCI AND E. LAMANNA, Vol. 4, 1995, p. 1247.
[MAS95c] MASSETTI S.: Proc. *XXIV ICRC, Roma 1995*, edited by N. IUCCI AND E. LAMANNA, Vol. 4, 1995, p. 1251.
[MAS96] MASSETTI S. AND STORINI M.: *The Astrophys. J.* **472**,(1996) 827.
[MCD99] MCDONALD A.: *Nucl. Phys.* B (P.S.) **77**,(1999) 43.
[MCD01] MCDONALD A.: *Nucl. Phys.* B (P.S.) **91**,(2001) 21.
[MCK00] MCKINSEY D.N. AND DOYLE J.M.: *J. Low Temp. Phys.* **118**,(2000) 153.
[MCK01] MCKINSEY D.N.: Proc. *Low energy solar neutrino detection LOWNU2*, edited by Y.SUZUKI, M.NAKAHATA AND S.MORIYAMA (World Scientific) 2001, p. 106.
[MCN95] MCNUTT R.L. JR.: *Science* **270**,(1995) 1635.
[MEI30] MEITNER L. AND ORTHMANN W.: *Z. Phys.* **60**,(1930) 143.
[MIC93] MICHAUD G. AND PROFFITT C.R.: in *Inside the stars*, edited by W.W.WEISS AND A.BAGLIN, IAU 137,(ASP) 1993, p. 246.
[MIH88] MIHALAS D. *et al.*: *The Astrophys. J.* **331**,(1988) 815.
[MIK85] MIKHEYEV S.P. AND SMIRNOV A.Y.: *Sov. J. Nucl. Phys.* **42**,(1985) 913.
[MIK86] MIKHEYEV S.P. AND SMIRNOV A.Y.: *Il Nuovo Cimento* C **19**,(1986) 17.
[MIN97] MINAKATA H. AND YASUDA O.: *Phys. Rev.* D **56**,(1997) 1692.
[MIR01] MIRANDA O.G. *et al.*: *Phys. Lett.* B **521**,(2001) 299.
[MIT77] MITLER H.E.: *The Astrophys. J.* **212**,(1977) 513.
[MON94] MONTALBAN J.: *Astron. & Astrophys.* **281**,(1994) 421.
[MON99] MONTANARI C.: *Nucl. Phys.* B (P.S.) **70**,(1999) 453.
[MOR00] MOREL P. *et al.*: *Astron. & Astrophys.* **353**,(2000) 771.
[MUR02] MURAYAMA H. AND PIERCE A.: *Phys. Rev.* D **65**,(2002) 013012.
[NAK63a] NAKAGAWA M. *et al.*: *Prog. Theor. Phys.* **30**,(1963) 727.
[NAK63b] NAKAGAWA M. *et al.*: *Japan J. Elem. Part. Theor. Group* **27**,(1963) 415.
[NAK00] NAKAMURA K.: Talk at *NOON2000 International Workshop, Tokyo 2000.*
[NAK01] NAKAMURA S. *et al.*: *Phys. Rev.* C **63**,(2001) 034617.
[NAK02] NAKAMURA S. *et al.*: *Nucl. Phys.* A **707**,(2002) 481.
[NUN01a] NUNOKAWA H.: hep-ph/0105027 Preprint, 2001.
[NUN01b] NUNOKAWA H.: Proc. *Low energy solar neutrino detection LOWNU2*, edited by Y.SUZUKI, M.NAKAHATA AND S.MORIYAMA (World Scientific) 2001, p. 9.

[OAK94] OAKLEY D.S. *et al.*: *The Astrophys. J. Lett.* **437**,(1994) L 63.
[OHL00] OHLSSON T. AND SNELLMAN H.: *J. Math. Phys.* **41**,(2000) 2768.
[OHL02] OHLSSON T. AND WINTER W.: hep-ph/0111247 v2 Preprint, 2002.
[OKO63] OKONOGI H. *et al.*: *Jap. J. Elem. Part.& Theor. Group* **27**,(1963) 417.
[ORT00] ORTIZ C.E. *et al.*: *Phys. Rev. Lett.* **85**,(2000) 2909.
[PAN93] PANTALEONE J. *et al.*: *Phys. Rev.* D **47**,(1993) 4199.
[PAN00] PANTALEONE J. *et al.*: *Phys. Rev.* D **61**,(2000) 033011.
[PAR95] PARKE S.: *Phys. Rev. Lett.* **74**,(1995) 839.
[PAU30] PAULI W.: Letter (1930).
[PER33] PERRIN F.: *Comp. Rend. Acad. Sci.* **197**,(1933) 1925.
[PET88] PETCOV S.T.: *Phys. Lett.* B **200**,(1988) 373.
[PIA02] PIAU L. AND TURCK-CHIEZE S.: astro-ph/0111223 Preprint, 2002; to be published in *The Astrophys. J.* .
[PIE01] PIEPKE A.: *Nucl. Phys.* B (P.S.) **91**,(2001) 99.
[PON46] PONTECORVO B.: Chalk River Lab. PD-205 Report, 1946.
[PON57] PONTECORVO B.: *J. Exp. Theor. Phys.* **33**,(1957) 549.
[PON58] PONTECORVO B.: *J. Exp. Theor. Phys.* **34**,(1958) 247.
[PON67] PONTECORVO B.: *J. Exp. Theor. Phys.* **53**,(1967) 1717.
[PRO91] PROFFITT C.R. AND MICHAUD G.: *The Astrophys. J.* **380**,(1991) 238.
[PRO94] PROFFITT C.R.: *The Astrophys. J.* **425**,(1994) 849.
[PUL00] PULIDO J. AND AKHMEDOV E.K.: *Astropart. Phys.* **13**,(2000) 227.
[PUL01] PULIDO J.: hep-ph/0112104 Preprint, 2001.
[RAF96] RAFFELT G.: *Stars as a laboratory for fundamental Physics*, (Univ. Chicago Press) 1996.
[RAF02] RAFFELT G.: hep-ph/0207220 v2 Preprint, 2002.
[RAG76] RAGHAVAN R.: *Phys. Rev. Lett.* **37**,(1976) 259.
[RAG95] RAGHAVAN R.: *Science* **267**,(1995) 45.
[RAG97] RAGHAVAN R.: *Phys. Rev. Lett.* **78**,(1997) 3618.
[RAG00a] RAGHAVAN R.: Talk at *Low energy solar neutrino detection LOWNU1 International Workshop, Sudbury 2000.*
[RAG00b] RAGHAVAN R.: Talk at *Low energy solar neutrino detection LOWNU2 International Workshop, Tokyo 2000.*
[RAG01] RAGHAVAN R.: hep-ex/0106054 (2001) Preprint, 2001; submitted to *Phys. Rev. Lett.*.
[RAN01] RANUCCI G. (BOREXINO coll.): *Nucl. Phys.* B (P.S.) **91**,(2001) 58.
[RAP85] RAPAPORT J.: *Phys. Rev. Lett.* **54**,(1985) 2325.
[RAY02] RAYCHAUDHURI A. AND SIL A.: *Phys. Rev.* D **65**,(2002) 073035.
[REI53] REINES F. AND COWAN C.: *Phys. Rev.* **92**,(1953) 830.
[RIC97] RICCI B. *et al.*: *Phys. Lett.* B **407**,(1997) 155.
[RIC99] RICCI B. *et al.*: *Phys. Lett.* B **456**,(1999) 214.
[RIC00] RICCI B. AND VILLANTE F.: *Phys. Lett.* B **488**,(2000) 123.
[RIC96] RICHARD O. *et al.*: *Astron. & Astrophys.* **312**,(1996) 1000.
[ROG92] ROGERS F.J. AND IGLESIAS C.A.: *The Astrophys. J.* Supp.Series **79**,(1992) 507.
[ROG95] ROGERS F.J. AND IGLESIAS C.A.: in *Astrophysical application of powerful new database*; edited by S.J.ADELMAN AND W.L.WIESSE, Conf. Series Vol.78 (ASP) 1995, p. 31.
[ROG96a] ROGERS F.J. *et al.*: *The Astrophys. J.* **456**,(1996) 902.
[ROG96b] ROGERS F.J. AND IGLESIAS C.A.: *American Astron. Soc. Meeting*, **188**, 1996.
[ROG01] ROGERS F.J.: *Contrib. Plasma Physics* **41**,(2001) 179.
[ROL88] ROLFS C. AND RODNEY W.S.: *Cauldrons in the Cosmos*, (Cambridge Univ.Press) 1988.
[ROU91] ROULET E.: *Phys. Rev.* D **44**,(1991) 935.
[RUB77] RUBBIA C.: CERN-EP/77-08 Preprint, 1977.
[RUB96] RUBBIA C.: *Nucl. Phys.* B (P.S.) **48**,(1996) 172.
[RUS19] RUSSELL H.N.: *Pub. Astr. Soc. Pacific* August (1919).

[SAG99] SAGE coll.: *Phys. Rev. Lett.* **83**,(1999) 4686.
[SAK42] SAKATA S. AND INOUE K.: *J. Japan Soc. Math. Phys.* **16**,(1942) 232.
[SAK46] SAKATA S. AND INOUE K.: *Prog. Theor. Phys.* **1**,(1946) 143.
[SAL57a] SALAM A.: *Il Nuovo Cimento* **5**,(1957) 299.
[SAL52] SALPETER E.E.: *Phys. Rev.* **88**,(1952) 547.
[SAL54] SALPETER E.E.: *Austral. J. Phys.* **7**,(1954) 373.
[SAL57b] SALPETER E.E.: *Rev. Mod. Phys.* **29**,(1957) 244.
[SCH81a] SCHATZMAN E. AND MAEDER A.: *Astron. & Astrophys.* **96**,(1981) 1.
[SCH81b] SCHECHTER J. AND VALLE J.W.F.: *Phys. Rev.* **24**,(1981) 1883.
[SCH82] SCHECHTER J.AND VALLE J.W.F.: *Phys. Rev.* **25**,(1982) 283.
[SCH99] SCHLATTL H. AND WEISS A.: *Astron. & Astrophys.* **347**,(1999) 272.
[SCH01] SCHLATTL H.: *Phys. Rev.* D **64**,(2001) 013009.
[SCH97] SCHOU J. *et al.*: *The Astrophys. J. Lett.* **489**,(1997) L 197.
[SCH06] SCHWARZSCHILD K.: *Nachr. Koenigl. Ges. Wissen.* Goettingen **195**,(1906) 41.
[SCI96] A.A.V.V.: *Science* **272**,(1996).
[SEA64] SEARS R.L.: *The Astrophys. J.* **140**,(1964) 477.
[SEA94] SEATON M.J. *et al.*: *Monthly Not. R.A.S.* **266**,(1994) 805.
[SHA96] SHAVIV N. AND SHAVIV G.: *The Astrophys. J.* **468**,(1996) 433.
[SHA00] SHAVIV N.: astro-ph/0010152 Preprint, 2000.
[SHI96] SHIBAHASHI H. AND TAKATA M.: *Publ. Astron. Soc. Japan* **48**,(1996) 377.
[SMY00] SMY M.B: Talk at *NOON2000 International Workshop, Tokyo 2000.*
[SMY02a] SMY M.B.: hep-ex/0202020 Preprint, 2002.
[SMY02b] SMY M.B.: Talk at *Neutrino 2002 International Conference, Muenchen 2002.*
[SMY02c] SMY M.B.: hep-ex/0206016 Preprint, 2002.
[SMY02d] SMY M.B.: hep-ex/0208004 Preprint, 2002.
[SNO87] SNO coll.: *Phys. Lett.* B **194**,(1987) 321.
[SNO00] SNO coll.: *Nucl. Instrum. & Methods* A **449**,(2000) 172.
[SNO01] SNO coll.: hep-ex/0111040 Preprint, 2001.
[SPI90] SPIRO M. AND VIGNAUD D.: *Phys. Lett.* B **242**,(1990) 279.
[STA00] STAROSTIN A.N. *et al.*: *Phys. Lett.* A **274**,(2000) 64.
[STR89] STRANIERO O. AND CHIEFFI M.: *The Astrophys. J. Supp. Ser.* **71**,(1989) 47.
[STR01a] STRIEDER F. *et al.*: *Nucl. Phys.* A **696**(1-2),(2001) 219.
[STR01b] STRUMIA A. AND VISSANI F.: *J. High Energy Phys.* **0111**,(2001) 048.
[STR02] STRUMIA A. *et al.*: hep-ph/0205261 Preprint, 2002.
[STU99] STURROCK P.A. *et al.*: hep-ph/9904278 Preprint, 1999.
[STU01] STURROCK P.A. AND SCARGLE J.N.: *The Astrophys. J. Lett.* **550**,(2001) L 101.
[STU02] STURROCK P.A. AND WEBER M.A.: *The Astrophys. J.* **565**,(2002) 1366.
[SUZ95] SUZUKI Y.: *Nucl. Phys.* B (P.S.) **38**,(1995) 54.
[SUZ97] SUZUKI Y.: Proc. *IV International Solar Neutrino Conference, Heidelberg 1997*, edited by W.HAMPEL, (M.P.I. fur KernPhysik,Heidelberg) 1997.
[SUZ00a] SUZUKI Y.: hep-ph/0008296 Preprint, 2000.
[SUZ00b] SUZUKI Y.: Talk at *NOON2000 International Workshop, Tokyo 2000.*
[SUZ01a] SUZUKI Y.: *Nucl. Phys.* B (P.S.) **91**,(2001) 29.
[SUZ01b] SUZUKI Y.: Proc. *Low energy solar neutrino detection LOWNU2*, edited by Y.SUZUKI, M.NAKAHATA AND S.MORIYAMA (World Scientific) 2001, p. 81.
[TAK98] TAKATA M. AND SHIBAHASHI H.: Proc. *Structure and dynamics of the Sun and Sun-like Stars* ESA SP-418, edited by S.G.KORZENNIK AND A.WILSON; (Noordwijk,ESA) 1998, p. 548.
[THO94] THOUL A.A. *et al.*: *The Astrophys. J.* **421**,(1994) 828.
[TOS87] TOSHEV S.: *Phys. Lett.* B **196**,(1987) 170.
[TRI97] TRIPATHY S.C. *et al.*: in *IAU Symp. 181: Sounding solar and stellar interiors*; edited by F.PROVOST AND X.SCHMIEDER (Kluwer) 1997, p. 129.

[TSA88] TSALLIS C.: *J. Stat. Phys.* **52**,(1988) 479.
[TSY95] TSYTOVICH V.N. *et al.*: *Phys. Lett.* A **205**,(1995) 199.
[TSY00] TSYTOVICH V.N.: *Astron. & Astrophys. Lett.* **356**,(2000) L 57.
[TUR93] TURCK-CHIEZE S. *et al.*: *Phys. Rep.* **230**,(1993) 57.
[TUR98a] TURCK-CHIEZE S. *et al.*: Proc. *Structure and dynamics of the Sun and Sun-like Stars*, ESA SP-418, edited by S.G.KORZENNIK AND A.WILSON; (Noordwijk,ESA) 1998, p. 555.
[TUR00] TURCK-CHIEZE S.: *Nucl. Phys.* B (P.S.) **87**,(2000) 162.
[TUR01a] TURCK-CHIEZE S.: *Nucl. Phys.* B (P.S.) **91**,(2001) 73.
[TUR01b] TURCK-CHIEZE S.: Talk at *Solar neutrinos: where are the oscillations? International Workshop, LNGS 2001.*
[TUR01c] TURCK-CHIEZE S. *et al.*: *The Astrophys. J. Lett.* **555**,(2001) L 69.
[TUR01d] TURCK-CHIEZE S. *et al.* - *Solar Phys.* **200**,(2001) 323.
[TUR98b] TURCOTTE S. *et al.*: *The Astrophys. J.* **504**,(1998) 539.
[ULR82] ULRICH R.K.: *The Astrophys. J.* **258**,(1982) 404.
[VAL87] VALLE J.F.W.: *Phys. Lett.* B **199**,(1987) 432.
[VIR00] VIRTUE C.J.: *Nucl. Phys.* B (P.S.) **87**,(2000) 183.
[VOL86a] VOLOSHIN M.B. *et al.*: *Sov. J. Nucl. Phys.* **44**,(1986) 440.
[VOL86b] VOLOSHIN M.B.*et al.*: *Sov. J. JETP* **64**,(1986) 446.
[XIN00] XING Z.: *Phys. Rev.* D **61**,(2000) 057301.
[YIN92] YING H.S. *et al.*: *Phys. Rev.* C **45**,(1992) 1982.
[WAT01] WATANABE S. AND SHIBAHASHI H.: *Pub. Astron. Soc. Japan* **53**,(2001) 565.
[WEI01] WEISS A. *et al.*: astro-ph/0102353 Preprint, 2001; to be published in *Astron. & Astrophys.*.
[WEI37] von WEIZSAECKER C.F.: *Phys. Z.* **38**,(1937) 176.
[WEI38] von WEIZSAECKER C.F.: *Phys. Z.* **39**,(1938) 633.
[WIN93] WINK R. *et al.*: *Nucl. Instrum. & Methods* A **329**,(1993) 541.
[WIN01] WINNICK R.A. *et al.*: astro-ph/0111096 v2 Preprint, 2001; to be published in *The Astrophys. J.*
[WOL78] WOLFENSTEIN L.: *Phys. Rev.* D **17**,(1978) 2369.
[WOL79] WOLFENSTEIN L.: *Phys. Rev.* D **20**,(1979) 2634.
[WUC57] WU C.S. *et al.*: *Phys. Rev.* **105**,(1957) 1413.
[ZAH92] ZAHN J.P.: *Astron. & Astrophys.* **265**,(1992) 115.
[ZAT97] ZATSEPIN G.T. AND KOPYLOV A.V.: *The measurement of the flux of solar neutrinos of medium energy by lithium radiochemical detector* - Letter of Intent, March 1997.
[ZUB01] ZUBER K.: *Phys. Lett.* B **519**,(2001) 1.
[ZUB02] ZUBER K.: astro-ph/0206340 Preprint, 2002.